

**DNA-binding protein-A promotes kidney
ischemia/reperfusion injury and participates in
mitochondrial function**

Dissertation

zur Erlangung des akademischen Grades

doctor rerum naturalium (Dr. rer. nat.)

genehmigt durch die Fakultät für Naturwissenschaften der Otto-von-Guericke-Universität
Magdeburg

von M.Sc. Charlotte Reichardt

geb. am 28.04.1994 in Gera

Gutachter: Prof. Dr. med. Peter R. Mertens

Prof. Dr. Christian Kurts

eingereicht am: 16.08.2024

verteidigt am: 30.04.2025

Table of contents

Tables	6
Figures	7
Preamble.....	9
Publications.....	10
Conference contributions.....	12
Abbreviations	13
Abstract	20
Zusammenfassung.....	21
1 Introduction.....	22
1.1 Cold shock proteins (CSPs): Nucleic acid guardians with pleiotropic functions	22
1.1.1 Essential roles and compensation dynamics of CSPs during embryogenesis	22
1.1.2 DbpA isoforms: Structural variants and nucleic acid binding dynamics	22
1.1.3 DbpA in renal dynamics: Junctional regulation, nuclear translocation and protein interactions	23
1.1.4 Importance of CSPs in kidney diseases and therapeutic perspectives.....	24
1.2 Renal physiology: Orchestrating vital functions and nephron complexity	26
1.3 Acute kidney injury (AKI): Clinical complexities, global impact and emerging insights into molecular pathogenesis	27
1.3.1 Clinical relevance of AKI.....	27
1.3.2 Diverse etiology of AKI.....	28
1.3.3 Renal IRI dynamics, vascular implications and long-term consequences.....	29
1.4 Mitochondrial dynamics and functionality in the kidney	30
1.4.1 Mitochondrial turnover	31
1.4.2 Mitochondrial bioenergetics	32
1.4.3 Mitochondrial dynamics	33
1.5 Mitochondrial damage in AKI	33
1.6 Mitochondria-targeted therapeutics.....	35
1.7 Aims of the thesis	36
2 Material.....	37

2.1	Devices.....	37
2.2	Consumables.....	38
2.3	PCR primers	38
2.4	Antibodies.....	39
2.5	Kits	40
2.6	Chemicals and Reagents.....	40
2.7	Buffers and solutions	42
2.8	Software	43
3	Methods.....	45
3.1	Animals.....	45
3.2	Genotyping	45
3.3	Renal ischemia/reperfusion injury (IRI) model.....	45
3.4	Organ perfusion.....	46
3.5	Blood and plasma analyses	46
3.6	Urine measurements	46
3.7	Transcutaneous measurement of glomerular filtration rate (GFR).....	46
3.8	Tissue lysate preparation and Western blot analysis	47
3.9	Immunohistochemistry.....	47
3.10	Periodic acid-Schiff (PAS) staining and Picro Sirius Red staining	48
3.11	Transmission electron microscopy.....	48
3.12	Flow cytometry	48
3.13	Isolation of total RNA and quantitative PCR.....	48
3.14	Transcriptome analysis using RNA-seq	49
3.15	Bioinformatic analysis	49
3.16	Isolation of primary TECs from mice	49
3.17	Isolation of primary bone marrow-derived macrophages (BMDMs) from mice	50
3.18	<i>In vitro</i> hypoxia/reoxygenation (HR) and ferroptosis model.....	50
3.19	Immunofluorescence staining of cells on glass slides	50
3.20	Metabolism assays	50
3.21	Mitochondria fractionation and transfer	51

3.22	Cell death assay using time-lapse microscopy.....	52
3.23	Knockdown of DbpA by lentiviral transduction	52
3.24	Microarray data.....	52
3.25	Statistical Analysis	52
4	Results	53
4.1	Phenotyping of <i>Ybx3</i> ^{+/+} , <i>Ybx3</i> ^{+/-} and <i>Ybx3</i> ^{-/-} mice	53
4.1.1	Phenotyping and long-term survival of mice with genetic <i>Ybx3</i> deletion.....	53
4.1.2	DbpA is expressed in tubular structures of healthy kidneys	54
4.1.3	DbpA is dispensable for kidney development, function and tissue homeostasis under healthy conditions	56
4.2	Tubular expression of DbpA inversely correlates with metabolic processes.....	58
4.2.1	Mitochondrial transfer equalizes respiratory capacity of TECs	61
4.2.2	An increase in mitochondrial activity can be induced via a lentiviral knockdown of DbpA	62
4.2.3	DbpA co-localizes with mitochondrial marker proteins	63
4.2.4	DbpA fulfills tubular cell-specific metabolic functions	65
4.3	DbpA mediates tubular cell damage in AKI and the absence of the protein is linked with cell protection	66
4.3.1	Following IRI upregulated DbpA expression confers acute tubular cell damage	66
4.3.2	<i>Ybx3</i> ^{-/-} animals do not develop an inflammatory response following induced hypoxic stress.....	70
4.3.3	Long-term analysis following IRI revealed an attenuated fibrotic response in kidneys of <i>Ybx3</i> ^{-/-} animals	72
4.3.4	Deletion of DbpA leads to minor ferroptotic cell death following IRI	74
4.3.5	Increased antioxidant activity provides the basis for the protective mechanism after induced hypoxia conditions.....	75
5	Discussion	78
5.1	Challenges and strategies in the comprehensive detection and characterization of DbpA	78
5.2	Unveiling the protective mechanisms of DbpA in IRI and tubular cell adaptation	78

5.3	Mitochondrial-ER interactions and cold shock proteins in renal stress resistance and fibrosis prevention.....	79
5.4	Mitochondrial transfer as a new technique for the prevention and therapy of kidney disease	80
5.5	Protective mechanisms against ferroptosis in <i>Ybx3</i> knockout TECs following IRI ...	81
5.6	AKI as a global public health concern	82
5.6.1	Animal models of AKI	82
5.6.2	DbpA as a promising therapeutic targeting protein in the context of AKI	83
5.7	Limitations and future directions in studying DbpA's role in kidney IRI	83
	References.....	84
	Declaration of Honor	107

Tables

Table 1. Protein/protein interactions of DbpA.	24
Table 2. KDIGO AKI stages.....	28
Table 3. Devices.....	37
Table 4. Consumables.....	38
Table 5. Polymerase chain reaction (PCR) primer sequences.....	38
Table 6. Primary and secondary antibodies used for Western blot	39
Table 7. Primary and secondary antibodies used for immunohistochemistry	39
Table 8. Antibodies used for flow cytometry	40
Table 9. Kits	40
Table 10. Chemicals and reagents	40
Table 11. Buffers and solutions	42
Table 12. Software	43

Figures

Figure 1. Structure of human and murine cold shock proteins DbpA_a and DbpA_b.....23

Figure 2. Anatomical overview of the kidney and nephron.....26

Figure 3. Causes of AKI divided into prerenal, intrinsic renal and postrenal.....29

Figure 4. Cellular metabolism.....30

Figure 5. Mitochondrial health and dysfunction.....34

Figure 6. Mitochondria as promising targets for kidney disease.....36

Figure 7. Phenotyping and long-term survival of mice with genetic *Ybx3* deletion.53

Figure 8. DbpA is expressed in healthy kidneys and liver.....55

Figure 9. Kidney function is preserved despite genetic deletion of DbpA.....56

Figure 10. Tubular cell composition with ion and water transporter expression in wild type and genetically modified animals lacking DbpA.....57

Figure 11. Tubular expression of DbpA inversely correlates with lipid metabolic processes. 58

Figure 12. Tubular expression of DbpA inversely correlates with the mitochondrial oxygen consumption rate and glycolysis.....60

Figure 13. Mitochondrial transfer equalizes respiratory capacity of wild type TECs.61

Figure 14. Lentiviral DbpA knockdown leads to increased mitochondrial respiration.62

Figure 15. DbpA co-localizes with mitochondrial marker proteins.....64

Figure 16. Mitochondrial analyses of primary BMDMs.....65

Figure 17. *Ybx3* expression is upregulated following acute IRI.....67

Figure 18. DbpA expression confers acute tubular cell damage.....69

Figure 19. *Ybx3*^{-/-} animals do not develop an inflammatory response following induced hypoxic stress.70

Figure 20. Kidneys with genetic *Ybx3* deletion demonstrated decreased ER stress following ischemia.....71

Figure 21. *Ybx3*^{-/-} animals showed a decreased activation of matrisome-related proteins..72

Figure 22. Following IRI fibrotic response was attenuated in kidneys of *Ybx3*^{-/-} animals.73

Figure 23. Deletion of DbpA leads to minor ferroptotic cell death following IRI.74

Figure 24. Increased antioxidant activity provides the basis for the protective mechanism *in vivo*.....75

Figure 25. Increased antioxidant activity protects *Ybx3*^{-/-} TECs from ferroptotic cell death *in vitro*.76

Figure 26. Visualization of mitochondria enrichment by electron microscopy.....80

Figure 27. Protective mechanisms against ferroptosis in *Ybx3* knockout TECs.81

Preamble

Parts of the present thesis are published in:

Reichardt C, Brandt S, Bernhardt A, Krause A, Lindquist JA, Weinert S, Geffers R, Franz T, Kahlfuss S, Dudeck A, Mathew A, Rana R, Isermann B, Mertens PR. DNA-binding protein-A promotes kidney ischemia/reperfusion injury and participates in mitochondrial function. *Kidney Int.* 2024 Aug;106(2):241-257. doi: 10.1016/j.kint.2024.05.009. Epub 2024 May 29. PMID: 38821446.

Publications

Publications during the PhD:

Reichardt C, Brandt S, Bernhardt A, Krause A, Lindquist JA, Weinert S, Geffers R, Franz T, Kahlfuss S, Dudeck A, Mathew A, Rana R, Isermann B, Mertens PR. DNA-binding protein-A promotes kidney ischemia/reperfusion injury and participates in mitochondrial function. *Kidney Int.* 2024 Aug;106(2):241-257. doi: 10.1016/j.kint.2024.05.009. Epub 2024 May 29. PMID: 38821446.

Brandt S, Bernhardt A, Häberer S, Wolters K, Gehringer F, **Reichardt C**, Krause A, Geffers R, Kahlfuß S, Jeron A, Bruder D, Lindquist JA, Isermann B, Mertens PR. Comparative Analysis of Acute Kidney Injury Models and Related Fibrogenic Responses: Convergence on Methylation Patterns Regulated by Cold Shock Protein. *Cells.* 2024 Feb 20;13(5):367. doi: 10.3390/cells13050367. PMID: 38474331; PMCID: PMC10930537.

Bernhardt A, Krause A, **Reichardt C**, Steffen H, Isermann B, Völker U, Hammer E, Geffers R, Philipson L, Dhjamandi K, Ahmad S, Brandt S, Lindquist JA, Mertens PR. Excessive sodium chloride ingestion promotes inflammation and kidney fibrosis in aging mice. *Am J Physiol Cell Physiol.* 2023 Aug 1;325(2):C456-C470. doi: 10.1152/ajpcell.00230.2023. Epub 2023 Jul 3. PMID: 37399499.

Lindquist JA, Bernhardt A, **Reichardt C**, Sauter E, Brandt S, Rana R, Lindenmeyer MT, Philipson L, Isermann B, Zhu C, Mertens PR. Cold Shock Domain Protein DbpA Orchestrates Tubular Cell Damage and Interstitial Fibrosis in Inflammatory Kidney Disease. *Cells.* 2023 May 19;12(10):1426. doi: 10.3390/cells12101426. PMID: 37408260; PMCID: PMC10217384.

Abdi Sarabi M, Shiri A, Aghapour M, **Reichardt C**, Brandt S, Mertens PR, Medunjanin S, Bruder D, Braun-Dullaeus RC, Weinert S. Normoxic HIF-1 α Stabilization Caused by Local Inflammatory Factors and Its Consequences in Human Coronary Artery Endothelial Cells. *Cells.* 2022 Dec 1;11(23):3878. doi: 10.3390/cells11233878. PMID: 36497143; PMCID: PMC9737288.

Bernhardt A, Häberer S, Xu J, Damerau H, Steffen J, **Reichardt C**, Wolters K, Steffen H, Isermann B, Borucki K, Artelt N, Endlich N, Kozyraki R, Brandt S, Lindquist JA, Mertens PR. High salt diet-induced proximal tubular phenotypic changes and sodium-glucose cotransporter-2 expression are coordinated by cold shock Y-box binding protein-1. *FASEB J.* 2021 Oct;35(10):e21912. doi: 10.1096/fj.202100667RR. PMID: 34533842.

Brandt S, Ewert L, Scurt FG, **Reichardt C**, Lindquist JA, Gorny X, Isermann B, Mertens PR. Altered monocytic phenotypes are linked with systemic inflammation and may be linked to mortality in dialysis patients. *Sci Rep.* 2019 Dec 13;9(1):19103. doi: 10.1038/s41598-019-55592-y. PMID: 31836803; PMCID: PMC6911068.

Morgenroth R, **Reichardt C**, Steffen J, Busse S, Frank R, Heidecke H, Mertens PR. Autoantibody Formation and Mapping of Immunogenic Epitopes against Cold-Shock-Protein YB-1 in Cancer Patients and Healthy Controls. *Cancers (Basel).* 2020 Nov 25;12(12):3507. doi: 10.3390/cancers12123507. PMID: 33255653; PMCID: PMC7759818.

Conference contributions

Reichardt C, Brandt S, Bernhardt A, Lindquist JA, Ahmad S, Weinert S, Ley TJ, Geffers R, Kahlfuss S, Dudeck A, Isermann B, Mertens PR. DNA binding protein A is a key regulator of mitochondrial function that promotes renal ischemia/reperfusion injury. Presentation. 35th European Renal Cell Study Group (ERCSG) Meeting, Noordwijkerhout, The Netherlands, 2023

Reichardt C, Bernhardt A, Brandt S, Lindquist JA, Sleiman S, Weinert S, Kahlfuss S, Dudeck A, Isermann B, Mertens PR. Tubular expression of cold shock DNA binding protein A negatively regulates mitochondrial biogenesis and thereby the extent of acute hypoxic kidney injury. Poster presentation. 14th Conference of the German Society for Nephrology, Berlin, Germany, 2022

Reichardt C, Bernhardt A, Brandt S, Lindquist JA, Sleiman S, Dudeck A, Isermann B, Mertens PR. Deletion of cold shock protein DbpA protects against acute kidney injury. Presentation. 33rd European Renal Cell Study Group (ERCSG) Meeting, Magdeburg, Germany, 2021

Reichardt C, Sleiman S, Stolze S, Bernhardt A, Brandt S, Lindquist JA, Zhu C, Dudeck A, Isermann B, Mertens PR. Cold shock protein DbpA (DNA binding protein A) influences kidney barrier functions. Poster presentation. 12th Conference of the German Society for Nephrology, Berlin, Germany, 2020

Abbreviations

2-DG	2-deoxy-glucose
2-NBDG	2-(N-(7-Nitrobenz-2-oxa-1,3-diazol-4-yl)Amino)-2-Desoxyglucose
4HNE	4-hydroxynonenal
α SMA	alpha-smooth muscle actin
$\Delta\Psi_m$	mitochondrial membrane potential
ADP	adenosine diphosphate
AE1	anion exchanger 1
AICAR	5-aminoimidazole-4-carboxamide-1- β -d-ribofuranoside
AKI	acute kidney injury
AMPK α	5' adenosine monophosphate-activated protein kinase alpha
APS	ammonium persulfate
Aqp1	aquaporin 1
Aqp2	aquaporin 2
ATF4	activating transcription factor 4
ATP	adenosine triphosphate
ATP5A	ATP synthase lipid-binding protein
Atp6v1b1	ATPase H ⁺ transporting V1 subunit B1
Bax	Bcl-2-associated X protein
Bcl2	B-cell lymphoma 2
BMDMs	bone marrow-derived macrophages
BNIP3	B-cell lymphoma 2/adenovirus E1B 19 kDa protein-interacting protein 3
bp	base pairs
BPA	boronophenylalanine
BSA	bovine serum albumin
BUN	blood urea nitrogen
BUMPT	mouse proximal tubule-derived cell line
C	cortex
CA2	carbonic anhydrase 2
Ca ²⁺	calcium ions
CD	cluster of differentiation
cDNA	complementary deoxyribonucleic acid
CD-PC	collecting duct-principal cell
CKD	chronic kidney disease
Cdk4	Cyclin dependent kinase 4
Cdk5	Cyclin dependent kinase 5
CLDN5	claudin-5

CNT	connecting tubule
CO ₂	carbon dioxide
CoA	coenzyme A
CoQ	ubiquinone/coenzyme Q10
CoQ10	coenzyme Q10 MitoQ (mitochondrial coenzyme Q)
CPT1a	carnitine palmitoyl transferase 1a
CSA	cyclosporine A
CSD	cold shock domain
CSPs	cold shock proteins
CspA	cold shock protein A
cyt c	cytochrome C
d	day(s)
d1	day one
d28	day 28
DAB	diaminobenzidine
DAMPs	damage-associated molecular patterns
DbpA	DNA-binding protein-A
DbpA_a	DNA-binding protein-A isoform a
DbpA_b	DNA-binding protein-A isoform b
DbpC	DNA-binding protein-C
DCT	distal convoluted tubule
DNA	deoxyribonucleic acid
DPBS	Dulbecco's phosphate-buffered saline
DPI	2,4-dihydroxy-5-pyrimidinyl imidothiocarbamate
DRP1	dynamain related protein 1
e ⁻	electron(s)
EC	endothelial cell
ECAR	extracellular acidification rates
EDTA	ethylenediaminetetraacetat
EGF	epidermal growth factor
ECMO	extracorporeal membrane oxygenation
ER	endoplasmic reticulum
ERK 2	extracellular signal-regulated kinase 2
ESRD	end-stage renal disease
ETC	electron transport chain
EtOH	ethanol
Ex/Em	fluorescence excitation/emission

FACS	fluorescence-associated cell sorting
FADH ₂	flavin adenine dinucleotide hydroquinone form
FAO	fatty acid oxidation
FBS	filtrated bovine serum
FCCP	carbonyl cyanide-p-trifluoromethoxyphenylhydrazone
FELASA	Federation of European Laboratory Animal Science Association
FeS	iron-sulfur
FI	fluorescence intensity
Fis1	mitochondrial fission 1
FITC	fluorescein isothiocyanate
FMO	fluorescence minus one
fwd	forward
GAPDH	glyceraldehyde 3-phosphate dehydrogenase
GATM	glycine amidinotransferase
GEF	Guanine nucleotide exchange factor
GFR	glomerular filtration rate
GPX4	glutathione peroxidase 4
GSK3 β	glycogen synthase kinase 3 β
GTPase	guanosintriphosphatase
h	hours
H ⁺	proton(s)
H ₂ O	water
HC	hydrocortisone
HEK Lenti X	human embryonic kidney cells
HIF1 α	hypoxia-inducible factor-1 alpha
HKC-8	human-derived renal proximal tubular cell line
<i>HMOX1</i>	<i>heme oxygenase 1</i>
HO-1	heme oxygenase 1
HR	hypoxia and reoxygenation
IC	intercalated cells
IC-A	intercalated cell type A
IC-B	intercalated cell type B
IgA	immunoglobulin A
IM	inner medulla
IMM	inner mitochondrial membrane
IRI	ischemia/reperfusion injury
ITS	insulin, transferrin, selenious acid

JAK	janus kinase
KDIGO	Kidney Disease: Improving Global Outcomes
LC3	microtubule-associated protein 1 light chain 3 beta
LCFAs	long chain fatty acids
LH(AL)	loop of Henle (ascending loop)
LH(DL)	loop of Henle (descending loop)
M Φ	macrophage
MA-5	mitochonic acid 5
MAMs	mitochondrial-ER-associated membranes
MC	mesangial cell
M-CSF	macrophage colony-stimulating factor
Mdivi-1	mitochondrial division inhibitor 1
MFN	mitofusins
MHC	major histocompatibility complex
min	minutes
miR	microRNAs
MitoQ	mitochondrial coenzyme Q
mPTP	mitochondrial permeability transition pore
mROS	mitochondrial reactive oxygen species
MTCO1	mitochondrially encoded cytochrome c oxidase 1
mtDNA	mitochondrial DNA
MW	molecular weight
N ₂	nitrogen
NAC	N-acetyl-L-cysteine
NADH	nicotinamide adenine dinucleotide hydrogen
NaHCO ₃	sodium hydrogen carbonate
NBR1	neighbor of breast cancer type 1
nDNA	nuclear DNA
NET	neutrophil extracellular trap
NGAL	neutrophil gelatinase-associated lipocalin
NH ₄ Cl	ammonium chloride
nr.	number
NRF1	nuclear respiratory factors 1
NRF2	nuclear respiratory factors 2
O ₂	oxygen
OCR	oxygen consumption rates
OGD	oxygen-glucose deprivation

OM	outer medulla
OMM	outer mitochondrial membrane
OPA1	optical atrophy
OXPPOS	oxidative phosphorylation
pAMPK α	phosphorylated 5' adenosine monophosphate-activated protein kinase alpha
PAS	periodic acid-Schiff
PC	principal cells
PCNA	proliferating cell nuclear antigen
PCR	polymerase chain reaction
PDGF	platelet-derived growth factor
Pen/Strep	penicillin-streptomycin
PFA	paraformaldehyde
PGC-1 α	peroxisome proliferator-activated receptor gamma coactivator 1 alpha
PI	propidium iodide
PINK1	phosphatase and tensin homolog-induced kinase 1
Pod	podocyte
PPAR γ	peroxisome proliferator-activated receptor gamma
PT	proximal tubule
PTEN	phosphatase and tensin homolog
QH ₂	ubiquinol
qPCR	quantitative polymerase chain reaction
RAAS	renin-angiotensin-aldosterone system
RalA	Ras-related protein Ral-A
Rev	reverse
RNA	ribonucleic acid
RNA-seq	ribonucleic acid sequencing
RNS	reactive nitrogen free radicals
ROS	reactive oxygen species
Rot+AA	rotenone + antimycin A
rpm	rounds per minute
rRNA	ribosomal ribonucleic acid
RT	room temperature
SDHB	succinate dehydrogenase complex iron sulfur subunit B
SDS	sodium dodecyl sulfate
sec	seconds
SGLT2	sodium-glucose cotransporter-2

shRNA	small hairpin RNA
SIRT 1	sirtuin-1
SIRT 3	sirtuin-3
SKQR1	10-(6'-plastoquinonyl) decylrhodamine 19
SLC5A4B	solute carrier family 5 (neutral amino acid transporters, system A), member 4b
SLC6A5	solute carrier family 6 member 5
SLC7A13	solute carrier family 7 member 13
SLC7A14	solute carrier family 7 member 14
SLC36A2	solute carrier family 36 member 2
SOD2	superoxide dismutase 2
SPF	specific pathogen-free
SQSTM1	sequestosome-1
SS-20	Szeto-Schiller peptide 20
SS-31	Szeto-Schiller Peptide 31
T3	3,3',5 triiodothyronine
TCA	tricarboxylic acid
TDZD-8	4-benzyl-2-methyl-1,2,4-thiadiazolidine-3,5-dione
TECs	tubular epithelial cells
TEMED	tetramethylethylenediamin
TFAM	mitochondrial transcription factor A
TIM23	translocase of inner mitochondrial membrane 23
TLR9	toll-like receptor 9
TMRE	tetramethylrhodamine, ethyl ester
tRNA	transfer ribonucleic acid
UK	United Kingdom
Ub	ubiquitin
UQCRC2	ubiquinol-cytochrome c reductase core protein 2
UUO	unilateral ureteral obstruction
VDAC1	voltage-dependent anion-selective channel 1
WIF1	WNT inhibitory factor-1
WNT	Wingless/int1
XBP1s	X-box binding protein 1
YB-1	Y-box binding protein-1
<i>Ybx2</i>	<i>Y-box binding protein-2</i>
<i>Ybx3</i>	<i>Y-box binding protein-3</i>
ZO-1	zonula occludens-1

ZO-2	zonula occludens-2
ZO-3	zonula occludens-3
ZONAB	zonula occludens-1-associated nucleic acid-binding protein

Abstract

DNA-binding protein-A (DbpA; gene: *Ybx3*) belongs to the cold shock protein family with known functions in cell cycling, transcription, translation, and tight junction communication. In chronic nephritis, DbpA is upregulated. However, its activities in acute kidney injury models, such as renal ischemia/reperfusion injury (IRI), are unclear.

To study this, mice harboring *Ybx3*^{+/+}, *Ybx3*^{+/-} or *Ybx3*^{-/-} genotype were characterized over 24 months and following experimental kidney IRI. Mitochondrial function, number and integrity were analyzed by mito/glycolysis stress tests, MitoTracker staining, Western blot and electron microscopy. RNA-sequencing, immunohistochemistry, Western blot and flow cytometry were performed to quantify tubular cell damage, tissue scarring and immune cell infiltration.

DbpA was found to be dispensable for kidney development and tissue homeostasis under healthy conditions. Furthermore, endogenous DbpA protein localizes within mitochondria in primary tubular epithelial cells (TECs). Genetic deletion of *Ybx3* elevates the mitochondrial membrane potential, the lipid uptake and metabolism, the oxygen consumption rates (OCR) and glycolytic activities of TECs. *Ybx3*^{-/-} mice demonstrated protection from IRI with less immune cell infiltration, endoplasmic reticulum (ER) stress, tubular cell damage and fibrosis. A presumed protective mechanism was identified via upregulated antioxidant activities and reduced ferroptosis, when *Ybx3* was deleted.

Thus, our studies reveal DbpA acts as a mitochondrial protein with profound adverse effects on cell metabolism and highlights a protective effect against IRI when *Ybx3* is genetically deleted. Hence, preemptive DbpA targeting in situations with expected IRI, such as kidney transplantation or cardiac surgery, may preserve post-procedure kidney function.

Zusammenfassung

Das DNA-bindende Protein-A (DbpA; Gen: *Ybx3*) gehört zur Familie der Kälteschockproteine und hat bekannte Funktionen beim Zellzyklus, der Transkription, der Translation und der *tight junction* Kommunikation. Bei der chronischen Nephritis ist DbpA hochreguliert, jedoch sind die Aktivitäten von DbpA bei akuten Krankheitsmodellen wie der renalen Ischämie/Reperfusion ungeklärt.

Um dies zu untersuchen wurden Mäuse mit dem Genotyp *Ybx3*^{+/+}, *Ybx3*^{+/-} oder *Ybx3*^{-/-} über einen Zeitraum von 24 Monaten und nach einer experimentellen Ischämie/Reperfusion der Nieren charakterisiert. Die mitochondriale Funktion, Anzahl und Integrität wurden durch Mito/Glykolyse-Stress-Tests, *MitoTracker*-Färbung, Western Blot und Elektronenmikroskopie analysiert. RNA-Sequenzierungsanalysen, immunhistochemische Färbung, Western Blot und Durchflusszytometrie wurden durchgeführt, um die Schädigung der Tubuluszellen, die Vernarbung des Gewebes und die Infiltration von Immunzellen zu quantifizieren.

Es wurde festgestellt, dass DbpA für die Nierenentwicklung und die Gewebemöostase unter gesunden Bedingungen entbehrlich ist. Darüber hinaus ist das endogene DbpA-Protein in primären Tubulusepithelzellen in Mitochondrien lokalisiert. Die genetische Deletion von *Ybx3* erhöht das mitochondriale Membranpotenzial, die Lipidaufnahme und den Lipidstoffwechsel, die Sauerstoffverbrauchsrate und die glykolytische Aktivität der primären Tubulusepithelzellen. *Ybx3*^{-/-} Mäuse zeigen einen Schutz vor Ischämie-/Reperfusionsschädigungen der Nieren mit einer geringeren Immunzellinfiltration, Stressantwort des Endoplasmatischen Retikulums, Tubuluszellschädigung und Fibrose. Ein mutmaßlicher Schutzmechanismus wurde durch eine erhöhte antioxidative Aktivität und einer verminderten Ferroptose identifiziert, wenn *Ybx3* deletiert wurde.

Zusammenfassend lässt sich sagen, dass DbpA als mitochondriales Protein fungiert, das tiefgreifende negative Auswirkungen auf die mitochondriale Aktivität hat. Zudem wird eine schützende Wirkung bei Ischämie/Reperfusion hervorgerufen, wenn *Ybx3* genetisch entfernt wird. Daher kann eine präventive DbpA-Fokussierung in Situationen mit zu erwartender IRI, wie z. B. bei Nierentransplantationen oder Herzoperationen, die Nierenfunktion nach dem Eingriff erhalten.

1 Introduction

1.1 Cold shock proteins (CSPs): Nucleic acid guardians with pleiotropic functions

CSPs are evolutionarily conserved, with all members sharing the eponymous cold shock domain (CSD), which have nucleic acid binding properties.^{1,2} This enables these proteins to perform pleiotropic functions, such as regulating transcription, translation and splicing.^{3,4} CSPs were first identified in bacteria, where a drop in temperature (from 37°C to 10°C) triggered an immense increase in the expression of cold shock protein A (CspA) within minutes.^{5,6} This rapid induction is conserved between species.⁷

The predominant group of CSPs is the Y-box protein family.³ This subgroup includes: Y-box binding protein-1 (YB-1, encoded by the gene *Ybx1* on chromosome 1), DNA-binding protein-C (DbpC, encoded by the gene *Ybx2* on chromosome 17) and DNA-binding protein-A (DbpA, encoded by the gene *Ybx3* on chromosome 12).^{1,3}

1.1.1 Essential roles and compensation dynamics of CSPs during embryogenesis

YB-1 is ubiquitously expressed and essential for embryogenesis, as whole body *Ybx1* knockout mice die at embryonic day 18.5.⁸⁻¹⁰ However, an inducible conditional whole body murine knockout of *Ybx1* shows normal lifespan and phenotype.¹¹ In contrast to YB-1, its homolog DbpA is described to be restricted in its expression predominantly during embryogenesis and down-regulated after birth¹², except in smooth muscle cells, heart, skeletal muscle, blood vessels and testis.^{9,13,14} DbpA is dispensable for development and survival, but adult mice have slightly reduced fertility.⁹ Interestingly, embryos with a deficiency of DbpA and YB-1 are not viable and die early on E8.5 to E11.5.⁹ In whole body *Ybx1* knockout embryos, DbpA can compensate the absence of YB-1 in early stages of embryonic development, however, at later time points during embryogenesis, YB-1 is indispensable, which cannot be compensated by DbpA.¹⁵

1.1.2 DbpA isoforms: Structural variants and nucleic acid binding dynamics

DbpA exists in two differential isoforms (DbpA_a, DbpA_b), which differ by an alternatively spliced exon of 69 amino acids (**Figure 1**).^{9,16,17} The DbpA isoforms were first described by Sakura et al., where two cDNAs encoding new DNA-binding proteins have been cloned using a human placenta λ gt11 recombinant cDNA library and DNA fragments as probes.¹⁸

The DbpA isoforms have an N-terminal alanine-proline-rich domain.¹⁵ Common to all CSPs is the presence of one or more CSD, which are highly conserved and identical. These contain two nucleic acid binding motifs, ribonucleoprotein 1 and 2¹⁹, which are responsible for the nucleic acid binding activities of DNA and RNA²⁰⁻²³, to regulate transcription, translation and

cell-cell communication.^{1,24} The extended C-terminal domain contains positively and negatively charged clusters of amino acids.¹⁵

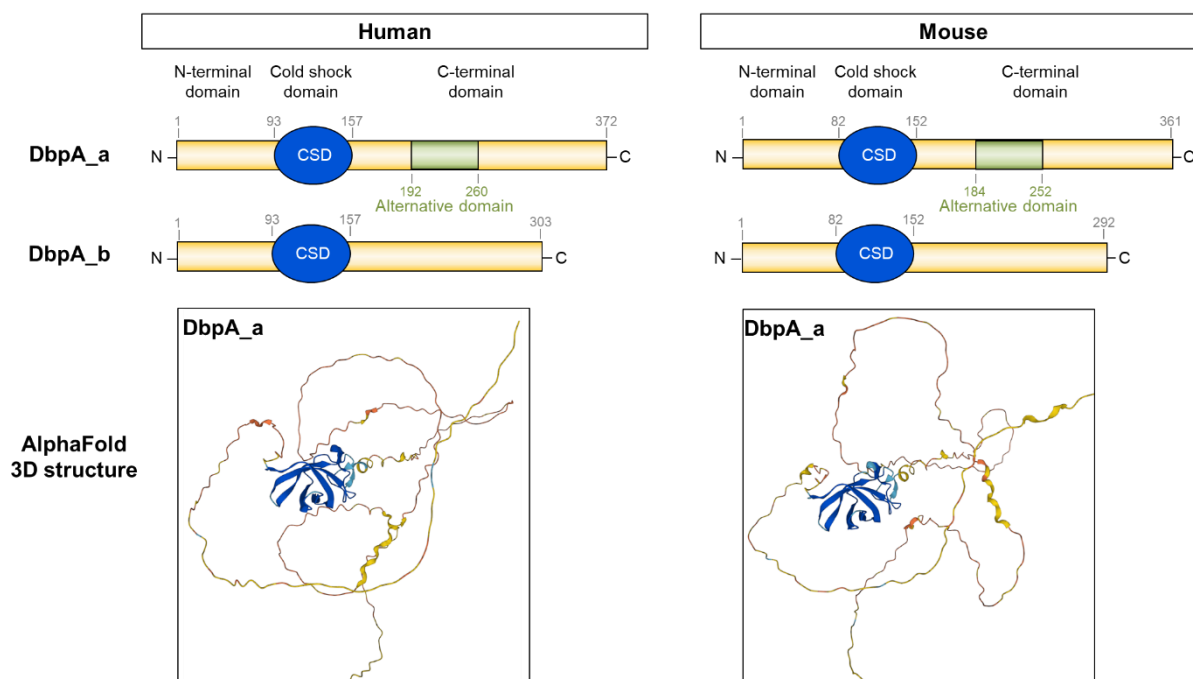


Figure 1. Structure of human and murine cold shock proteins DbpA_a and DbpA_b.

Two isoforms of DbpA exist, due to alternative splicing of a 69 amino acid domain on exon 6 (green). Both DbpA isoforms contain a conserved CSD (blue). The N- and C-terminal domains are mainly unstructured (yellow). The human and murine structures of these proteins are similar, however, there are a few differences in the amino acid sequences. 3D structures were generated by AlphaFold Protein Structure Database (<https://alphafold.ebi.ac.uk/>).

1.1.3 DbpA in renal dynamics: Junctional regulation, nuclear translocation and protein interactions

There is a long tradition of analysis of DbpA in the kidney, which were mainly performed by Maria S. Balda and Karl Matter in the past years. They described DbpA as a component of tight junctions, due to its interaction with the submembrane protein Zonula occludens-1 (ZO-1). Therefore, DbpA is also called ZO-1-associated nucleic acid-binding protein (ZONAB).²⁵ However, the subcellular localization and activity of DbpA are not regulated by ZO-1 alone, but instead the three ZO proteins (ZO-1, ZO-2 and ZO-3) redundantly control the junctional retention and stability of DbpA.²⁶ Interestingly, it was shown, that the stretched conformation of ZO proteins promotes the junctional localization of DbpA.²⁷ When cells lose their cell-cell contacts, DbpA is released from the plasma membrane and translocates to the nucleus, where it initiates cell proliferation via its regulation of proliferating-cell-nuclear-antigen (PCNA) and cyclin D1.²⁸⁻³⁰ DbpA levels are high in the nucleus in proliferating cells when ZO-1 expression is low. An increase of ZO-1 expression levels and cell confluence result in cytoplasmic sequestration and recruitment of DbpA to the tight junctions.²⁸ Furthermore, DbpA also interacts with the small guanosinotriphosphatase (GTPase) Ras-related protein Ral-A (RalA), which localizes along the lateral membrane, including tight junctions. The RalA-DbpA

interaction results in a transcriptional repression of a DbpA-regulated promoter.³¹ Further protein/protein interactions are summarized in **Table 1**.

Table 1. Protein/protein interactions of DbpA.

Interaction partner	Function	Localization within the cell	References
ZO-1	Interaction prevents translocation of DbpA to the nucleus	Tight junctions	²⁵
ZO-1, ZO-2, ZO-3	Control the junctional retention and stability of DbpA	Tight junctions	^{26,27}
RalA	Transcriptional repression of a DbpA-regulated promoter	Tight junctions	³¹
Guanine nucleotide exchange factor (GEF)-H1	Mediation of cyclin D1 promoter activation and expression	Tight junctions	³²
Symplekin	Regulation of transcription, epithelial proliferation and differentiation	Tight junctions or nucleus	^{33,34}
Cyclin dependent kinase 5 (Cdk5) and Cdk4	Cell cycle regulation	Cytoplasm	³⁵
AKT	Positive regulator of proliferation	Cytoplasm	³⁶
Extracellular-signal regulated kinase 2 (ERK2) and glycogen synthase kinase 3 β (GSK3 β)	Repression of the human VEGF promoter	Cytoplasm	³⁷

1.1.4 Importance of CSPs in kidney diseases and therapeutic perspectives

The best known and characterized member of the cold shock protein family is YB-1.³⁸ In the last years, the focus has been on cold shock protein activities within the cancer field involving molecular processes in terms of cell transformation, matrix invasion and excessive proliferation. As a multifunctional oncoprotein in a variety of different cancer forms, YB-1 regulate cancer cell behavior including cell cycle progression, migration, invasion, DNA repair and drug resistance, as summarized recently.³⁹ The molecular functions of YB-1 were analyzed in detail in breast cancer^{40,41}, prostate cancer⁴² and multiple myeloma.⁴³ Recent findings link janus kinase/extracellular signal-regulated kinase (JAK/ERK) signaling with YB-1 in myeloproliferative neoplasia, suggesting YB-1 as a potential therapeutic target in JAK2-mutated neoplasms.⁴⁴

In addition, based on the RNA-binding activities, YB-1 regulates complex inflammatory steps in kidney diseases.²⁴

YB-1 is described to be involved in the progression of diabetic kidney disease⁴⁵, tubulointerstitial fibrosis⁴⁶, glomerulosclerosis⁴⁷⁻⁴⁹, mesangioproliferative glomerulonephritis^{50,51} and AKI (acute kidney injury).^{52,53} Recently it was shown, that YB-1 is a part of the neutrophil extracellular trap (NET) mediation of ischemic kidney damage and cross organ fibrosis.⁵² NET formation and hypoxia trigger the release of YB-1, which subsequently acts as a mediator of kidney tubular damage. Prophylactic administration of neutralizing antibodies against YB-1 in an IRI mouse model significantly reduces tubular damage.⁵²

The expression of cold shock protein YB-1 is an appropriate biomarker for diverse disease.⁵⁴⁻⁵⁶ Therefore, the presence of YB-1 or its fragments can serve for diagnostic purposes.¹ Several intervention strategies for YB-1 are described. For example, HSc025 promotes nuclear translocation of YB-1 and therefore reducing fibrosis by suppressing the gene *collagen type I alpha 2 chain (Col1A2)*.^{57,58} The natural flavonoid fisetin was described to block the AKT-mediated phosphorylation of Serine¹⁰² within the CSD of YB-1 and therefore its nuclear translocation, thus fisetin was identified as an inhibitor of its activation.⁵⁹ Furthermore, successful approaches of targeting YB-1 to alleviate diseases are described for *Uncaria tomentosa*⁶⁰, 2,4-dihydroxy-5-pyrimidinyl imidothiocarbamate (DPI)⁶¹ and neutralizing YB-1 antibodies.⁵²

Due to the sequence homologies and already described similarities in their cellular function, it is important to not only focus on YB-1 alone, but also to give more attention to the cold shock protein DbpA. Unlike YB-1, there is less information on DbpA and its contribution and activity to kidney diseases. Previous work by our group identified DbpA as a key regulator of platelet-derived growth factor (PDGF)-induced mesangial cell proliferation in rodent models of immunoglobulin A (IgA) nephritis.⁶² Furthermore, Festa et al. and Raggi et al. described an involvement of DbpA during lysosomal storage disease such as nephropathic cystinosis and epithelial dysfunction in the kidney. Lysosomal dysfunction results in impaired clearance of damaged mitochondria. The generation of oxidative stress leads to a phosphorylation of ZO-1, which triggers a signal cascade including DbpA, which finally results in cell proliferation and transport defects.^{63,64} It was recently described, that in podocytes a loss of the tight junction integral membrane protein claudin-5 (CLDN5) contributes to kidney disease in a murine diabetic nephropathy model and fibrosis model following unilateral ureteral obstruction (UUO).⁶⁵ A deletion of CLDN5 decreases ZO-1 expression and induces the nuclear translocation of DbpA. There, DbpA leads to a transcriptional downregulation of (Wingless/int1) WNT inhibitory factor-1 (WIF1), resulting in an activation of WNT signaling pathway. In addition, podocyte-derived WIF1 has paracrine functions on tubular epithelial cells. Animals with podocyte-specific deletion of *Cldn5* or *Wif1* demonstrated enhanced kidney fibrosis after

UUO, which can be reversed by systemic administration of WIF1.⁶⁵ Recent findings of our group confirm the data that DbpA orchestrates tubular cell damage and interstitial fibrosis in inflammatory kidney disease.⁶⁶ DbpA expression is induced within the renal interstitium following UUO, whereas kidneys from *Ybx3*-deficient mice are protected from tissue injury with a significant reduction in the number of infiltrating immune cells as well as in extracellular matrix deposition.⁶⁶

These examples clearly demonstrate the up-regulation and contribution of DbpA during chronic kidney disease (CKD), however its activities in AKI models are unclear. In addition, targeting strategies from DbpA are not available so far. The development of targeted therapies requires insights into the pathologies and molecular pathways of the underlying disease.

1.2 Renal physiology: Orchestrating vital functions and nephron complexity

The kidneys consume 10% of the body's oxygen (O_2) to perform their functions.⁶⁷ They consist of multiple cell populations involved in several vital processes, including orchestration of the excretion of metabolic wastes in the blood, regulation and maintenance of acid-base and electrolyte balance, blood pressure regulation, nutrient reabsorption and hormone secretion.⁶⁸ In humans, blood filtration by the kidneys generates on average 1 liter of urine per day.⁶⁸

The human adult kidney consists of approximately 1 million up to 2.5 million nephrons, whose primary functions and structures are divided into a glomerular filtration unit and different tubular segments.^{67,69} The glomerular function is to filter the bloodstream, retaining circulating cells as well as beneficial and valuable macromolecules, resulting in primary urine with a small amount of proteins.⁶⁸ The primary urine is collected in the Bowman's capsule and passes through epithelial tubules: starting from the proximal tubules, the loop of Henle, the distal tubules and the collecting duct. The renal tubules and the collecting ducts express various ion and water channels and transporters to concentrate the composition of the urine by reabsorption and secretion (**Figure 2**).⁶⁸

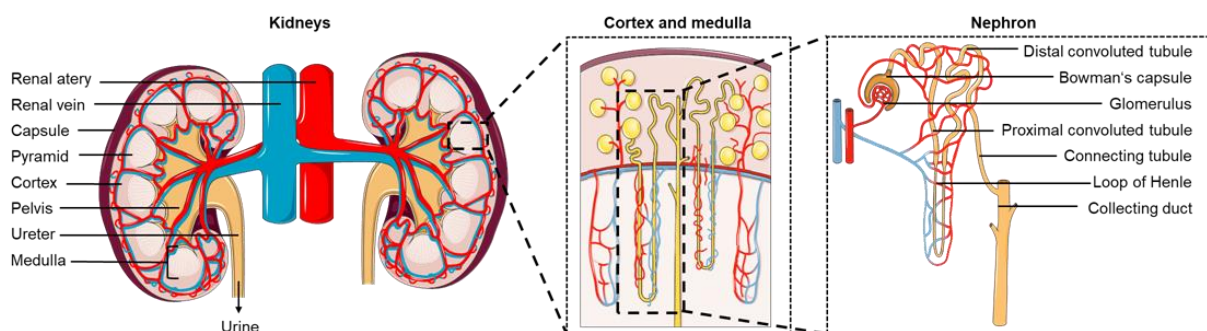


Figure 2. Anatomical overview of the kidney and nephron.

The nephron is the functional unit of the kidney. Blood vessels supply the kidneys with oxygen. The glomerulus and convoluted tubules are located in the kidney cortex, while collecting ducts are located in the pyramids of the medulla. Each nephron is composed of a glomerulus and a tubule. The glomerulus is located at the proximal end and is connected through a series of renal tubules, in which the composition of the urine is refined by reabsorption and secretion. This figure was created using the Servier Medical Art.

Due to the vital roles of the kidneys in body homeostasis, kidney dysfunctions can lead to diseases with systemic complications, which are currently a global health concern.⁷⁰ Kidney diseases are classified into AKI and CKD. Whereas AKI is characterized by rapid renal function impairment, CKD is associated with a gradual loss of kidney function over time.⁷¹

1.3 Acute kidney injury (AKI): Clinical complexities, global impact and emerging insights into molecular pathogenesis

AKI is defined by a rapid renal dysfunction in a variety of clinical contexts.⁷¹ It includes multiple clinical syndromes: specific kidney diseases (acute interstitial nephritis, acute glomerular nephritis, vasculitis), non-kidney specific diseases (IRI, toxic injury), as well as extra-renal diseases (prerenal azotemia, acute postrenal obstructive nephropathy).⁷² It is possible that more than one of these conditions coexist in the same patient. AKI occurs in up to 18% of patients admitted to intensive care units.⁷³ In most cases, recovery of renal function occurs, however, the risk of recurrence of renal impairment is increased.⁷⁴ In addition, with 13.3 million patients per year, AKI is a global public health issue.⁷⁵ Even mild, reversible AKI has significant clinical consequences, including increased costs, morbidity and mortality, with 1.7 million deaths per year.⁷⁵⁻⁷⁷

Long-term outcomes of AKI in patients can include the development of a CKD and end-stage renal disease (ESRD), which are associated with a poor life quality and high costs.^{78,79} Furthermore, in less developed countries, inadequate health care systems and underutilization of diagnostic testing and dialysis further contribute to the underestimation of the prevalence of AKI.⁷⁵ Here, AKI often develops in response to a single illness or infections (e.g. malaria, leptospirosis) and in younger, otherwise healthy individuals. This is in contrast to more developed countries, where AKI occurs predominantly in urban intensive care units and is associated with multiorgan failure, sepsis, high mortality and occurrence in older patients.⁸⁰ Therefore, treatments are needed to reduce morbidity, mortality and costs in context of AKI. However, due to etiology and the variety of clinical causes of AKI, it is challenging to find pharmacological agents.⁷⁷ The underlying pathomechanisms that occur at the molecular level in the kidney during AKI are incompletely understood. However, recent studies using single cell sequencing analysis in mice^{81,82} and human⁸³ show promising insights and results into the molecular and cell-specific pathogenesis of AKI.

1.3.1 Clinical relevance of AKI

From a clinical perspective, AKI is defined as a creatinine increase of at least 50% compared to baseline creatinine value within 7 days, an absolute serum creatinine increase of 0.3 mg/dl above baseline within 48 h, or oliguria (>0.5 ml/kg/h) of at least 6 h.⁸⁴ According to Kidney Disease: Improving Global Outcomes (KDIGO) guidelines, AKI is divided into 3 stages

(Table 2).⁸⁴ The standard AKI-defining parameters are serum creatinine levels and urine output, which are used to assess renal function in the clinic. Disadvantages in their low sensitivity and specificity are well known.⁸⁵ Therefore, a variety of alternative biomarkers have been shown to detect AKI earlier and are more sensitive^{86,87}, but until now these biomarkers are not able to replace serum creatinine levels and urine output in the definition of AKI.

Table 2. KDIGO AKI stages

KDIGO AKI stage	Serum creatinine level	Urine output
1	Increase by ≥ 0.3 mg/dl (26.5 μ mol/l) Increase to 1.5-1.9 times to the baseline level	<0.5 ml/kg/h for 6-12 h
2	Increase to 2-2.9 times to the baseline level	<0.5 ml/kg/h for ≥ 12 h
3	Increase to ≥ 3 times to the baseline level Increase to ≥ 4 mg/dl (353.6 μ mol/l) Initiation of renal replacement therapy In patients younger than 18 years: decrease in eGFR to <35 ml/min/1.73 m ²)	<0.3 ml/kg/h for ≥ 24 h anuria for ≥ 12 h

1.3.2 Diverse etiology of AKI

The main causes of AKI are divided into 3 categories: prerenal, intrinsic renal and postrenal (Figure 3).⁸⁸ Classic triggers of AKI are linked with dehydration or increased water uptake of the patient with an increase or decrease in urine volume. Predisposing factors for AKI may include past or current infections (sepsis), surgeries or pre-existing conditions such as heart failure, hypertension, diabetes mellitus or liver cirrhosis.^{89,90} Clinical contexts in which AKI may occur include autoimmune diseases with renal involvement (collagenoses, glomerulonephrides, vasculitides), urinary calculi, postrenal obstruction or intestinal nephritis.⁹¹ Other causes of AKI are intoxications (alcohol or drugs) or toxic responses to medications such as diuretics, anti-infectives, renin-angiotensin-aldosterone system (RAAS)-inhibitors and chemotherapeutic agents. Toxins like radiocontrast agents or nonsteroidal anti-inflammatory drugs can directly injure renal tissue or cause ischemic injury.⁷⁷

Moreover, AKI and CKD are closely linked. AKI can lead to CKD due to inadequate or maladaptive tissue repair.⁷¹ Hypoxia, mitochondrial dysfunction, cell cycle arrest, chronic inflammation and epigenetic changes may all play a role in the progression of AKI to CKD.^{92,93} Furthermore, also the presence of CKD itself predisposes to the occurrence of AKI.⁹⁴

The most common form of AKI relates to transient oxygen-deficiency with low blood pressure (prerenal AKI) or impaired blood supply (e.g. vasoconstriction following ingestion of non-

steroidal anti-inflammatory drugs; ischemia due to kidney transplantation).⁹⁵ Therefore, it is justified to give high priority to the prophylaxis, detection and treatment of AKI.

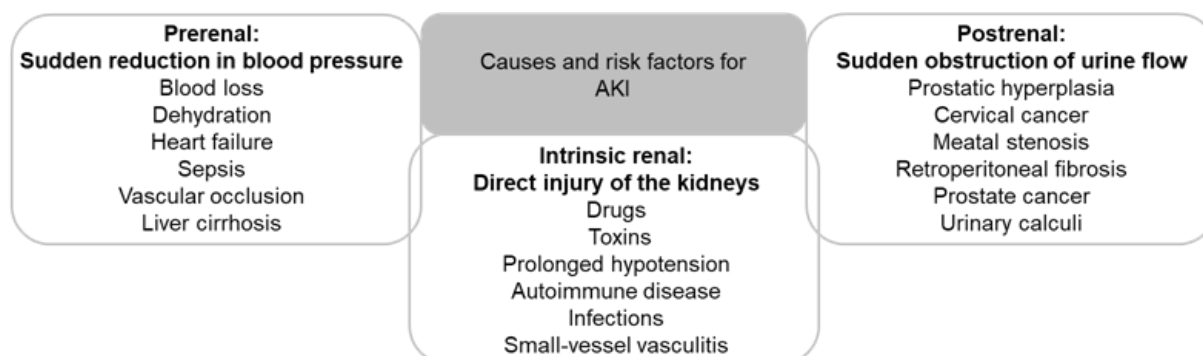


Figure 3. Causes of AKI divided into prerenal, intrinsic renal and postrenal.

Prerenal risk factors for AKI are characterized by a rapid reduction in blood pressure. Direct injuries of the kidneys are called intrinsic renal risk factors, whereas postrenal risk factors are characterized by a sudden obstruction of urine flow. Adapted from Thongprayoon et al.⁹⁶

1.3.3 Renal IRI dynamics, vascular implications and long-term consequences

The renal vasculature system assumes a key function in the pathophysiology of AKI.⁹⁷ The kidneys have a high-energy demand for reabsorption and secretion processes.⁸⁰ However, the oxygen supply to the outer medulla (OM) is quite low and the vascular architecture is highly susceptible to impairment of vascular perfusion and oxygenation.⁹⁸ IRI is characterized by an impaired microcirculation with deficiency of oxygen and nutrients over a certain period of time causing hypoxia, oxidative stress, mitochondrial dysfunction, release of cytochrome C (cyt c) and reactive oxygen species (ROS).⁹⁹

Reperfusion leads to rapid influx of oxygen-rich blood into the ischemic tissue and is characterized by increased epithelial and endothelial cell damage.⁹³ Injury of the vascular endothelium leads to its activation with increased expression of cell surface markers, that promote leukocyte and platelet recruitment, adhesion and immune cell infiltration, resulting in further changes in oxygen supply, epithelial and endothelial cell injury, cell death, vascular permeability and inflammation.¹⁰⁰ Long-term consequences of reduced oxygen supply and vascular injury are a reduction in peritubular capillary density, which contributes to persistent hypoxia and impaired organ function leading to fibrosis.⁷¹ The tubular epithelial cells are directly and especially affected under hypoxic and reperfusion conditions, because of their cellular function and high metabolic activity. These cells undergo programmed cell death, however they have the potential to regenerate from a stem cell pool.^{101,102}

1.4 Mitochondrial dynamics and functionality in the kidney

Mitochondria are especially important in organs with a high metabolic activity, including the heart, muscles and kidneys. These complex, dynamic and heterogeneous cellular power plants are organized within a mitochondrial network and have the essential task of generating the majority of adenosine triphosphate (ATP) through oxidative phosphorylation (OXPHOS), which is required for cellular viability and function.¹⁰³ In addition, mitochondria are substantial in metabolic signaling such as pyrimidine, heme biosynthesis, tricarboxylic acid (TCA) cycle, fatty acid β -oxidation, calcium ion homeostasis, thermogenesis, proliferation and regulating intrinsic apoptotic pathway (**Figure 4**).⁶⁷

The primary energy sources in living cells include glucose, glutamine and fatty acids. The utilization of these fuel reservoirs by mitochondria significantly influences various biological processes.¹⁰⁴ Fatty acid metabolism, also known as lipid metabolism, refers to the processes involved in the synthesis, β -oxidation and modification of fatty acids. During β -oxidation fatty acids are broken down in the mitochondria to generate acetyl coenzyme A (CoA), which enters the TCA cycle for further energy production.¹⁰⁵ Glycolysis is a fundamental metabolic pathway that occurs in the cytoplasm of cells and is crucial for the breakdown of glucose to produce energy.¹⁰⁶ Glutaminolysis is a metabolic process in which the amino acid glutamine is converted into glutamate that enters the TCA cycle.¹⁰⁷ The TCA cycle is the central component of cellular respiration in which acetyl CoA, derived from glycolysis and the β -oxidation, is oxidized to produce energy. The cycle occurs in the mitochondria.¹⁰⁸ OXPHOS is a critical process in cellular respiration where cells generate the majority of their ATP through the electron transport chain (ETC) (**Figure 4**).¹⁰⁴

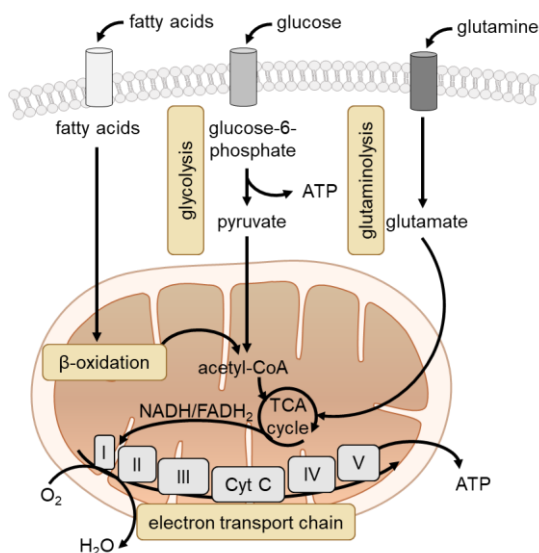


Figure 4. Cellular metabolism.

Cell metabolism refers to the sum of all reactions that occur within a cell to maintain life. These metabolic processes are essential for the growth, maintenance and reproduction of cells. Cells rely on glucose, glutamine and fatty acids as their main sources of energy.

Mitochondrial size, mass, metabolic activity and membrane potential differ for various cell types, due to their dynamics, including permanently changing shape and turnover.^{109,110} Multiphoton imaging reveals significant differences in mitochondrial function, density and

distribution in the various nephron segments. Based on their different energy demands, proximal tubular epithelial cells contain the largest ratio of mitochondrial volume to nuclear volume, to maintain reabsorption and secretion processes.¹¹¹ The differences in comparison to distal tubular epithelial cells may explain the vulnerability of proximal tubular epithelial cells to mitochondrial toxicity or dysfunction.¹¹²

In addition, other epithelial cells in the kidney, the podocytes, are also rich in mitochondria density. These highly differentiated, strongly branched cells form the outer layer of the glomerular filtration barrier.¹¹³ Studies on bioenergetic profiles of mitochondrial function revealed that podocytes are highly susceptible to energy disruption under stress conditions.¹¹⁴ A variety of processes including mitochondrial biogenesis, mitophagy, bioenergetics and dynamics regulate the health and functionality of mitochondria (**Figure 5**).^{67,115}

1.4.1 Mitochondrial turnover

Mitochondrial turnover is dynamic, coordinated process, where damaged or dysfunctional mitochondria are selectively eliminated (mitophagy) and replaced (mitochondrial biogenesis) (**Figure 5**).^{67,115} To maintain an adequate supply of energy, mitochondrial clearance encompasses several steps. First, damaged or excess mitochondria are isolated from the mitochondrial tubular network via fragmentation. The loss of mitochondrial membrane potential ($\Delta\Psi_m$) and the depolarization of the mitochondrial membranes leads to a stabilization of phosphatase and tensin homolog (PTEN)-induced kinase 1 (PINK1) and the recruitment of the E3 ligase Parkin, which attaches ubiquitin (Ub) to proteins of the outer mitochondrial membrane (OMM).¹¹⁶ This enables the recruitment of autophagy adapter proteins (neighbor of breast cancer type 1 (NBR1) or sequestosome-1 (p62/SQSTM1)), which have an Ub binding domain and interacting regions for the microtubule-associated protein 1 light chain 3 beta (LC3) to generate the proximity of autophagosomal membranes and the labeled mitochondria.^{117,118} The damaged mitochondria are encapsulated into autophagosomes, transported, fused and degraded in autolysosomes (**Figure 5 - mitophagy**).^{115,119} The alternative mitophagy pathway involves the direct interaction of B-cell lymphoma 2 (Bcl2) and Bcl2/adenovirus E1B 19 kDa protein-interacting protein 3 (BNIP3) family proteins to prevent ROS accumulation and cell death.¹²⁰

Mitochondrial biogenesis is a coordinated process between nuclear (nuclear DNA, nDNA) and mitochondrial (mitochondrial DNA, mtDNA) genomes to compensate the amount of mitochondria, which were degraded during mitophagy.¹²¹ Peroxisome proliferator-activated receptor gamma (PPAR γ) coactivator 1 alpha (PGC-1 α) is the key regulator of mitochondrial biogenesis. The main modulators of energy metabolism 5' adenosine monophosphate-activated protein kinase (AMPK) and sirtuin-1 (SIRT 1) positively regulate PGC-1 α through posttranslational modification (phosphorylation and deacetylation).⁶⁷ PGC-1 α regulates the

expression of nuclear respiratory factors 1 and 2 (NRF1 and NRF2).¹²² NRF1 and NRF2 are transcription factors that control the expression of transcription factor A, mitochondrial (TFAM), which is responsible for the expression of mitochondrial genes, including transfer ribonucleic acid (tRNA), ribosomal ribonucleic acids (rRNA) and subunits of the respiratory chain (**Figure 5 - biogenesis**).^{115,117}

AMPK helps maintain the energy balance of the cell by stimulating pathways that produce ATP and inhibiting those that consume it.¹²³ Due to its role in regulating metabolic processes such as glucose and lipid homeostasis, AMPK has become a significant therapeutic target for metabolic disorders.¹²⁴ AMPK is composed of an $\alpha\beta\gamma$ heterotrimer and achieves its maximum activity through the phosphorylation of Threonine 172 (Thr¹⁷²) in the activation loop of its kinase domain.¹²⁵

Impairment of mitophagy is associated with the pathogenesis of AKI, as it leads to the release and accumulation of damage-associated molecular patterns (DAMPs) and ROS that contribute to inflammation and pathogenesis.^{115,126} Mitochondrial dysfunction is known to appear long before renal dysfunction is detectable by an increase in serum creatinine levels that occurs approximately 12 h after the onset of AKI.¹²⁷ Therefore, maintaining mitochondrial homeostasis is an important strategy to prevent or cure acute organ failure.¹²⁸

1.4.2 Mitochondrial bioenergetics

More than 90% of the cellular energy production takes place within the mitochondria.¹²⁹ The process of energy production that generates ATP is called OXPHOS (**Figure 5 – OXPHOS bioenergetics**).^{67,115} Furthermore, key enzymes for other metabolic pathways (fatty acid β -oxidation, TCA cycle, urea cycle) are also present within the mitochondria.¹³⁰

The mitochondrial ETC consists of 5 protein complexes, where electrons (e^-) and protons (H^+) are transferred across the inner mitochondrial membrane to generate an electrochemical gradient for ATP synthesis.¹³¹ The enzymatic reactions involved in TCA result in the formation of nicotinamide adenine dinucleotide hydrogen (NADH) and flavin adenine dinucleotide hydroquinone form ($FADH_2$), two important players that are required for the transfer of electrons into the respiratory chain.¹³² The e^- from NADH are passed in complex I (NADH ubiquinone oxidoreductase) to ubiquinone/coenzyme Q10 (CoQ) through a chain of cofactors, followed by seven iron-sulfur (FeS) clusters arranged from low to high potential to enter the Q cycle, in which CoQ is reduced to Ubiquinol (QH_2).¹³³ This induces the pumping of H^+ from the matrix into the intermembrane space of the mitochondria by complex I.¹³⁴ The succinate dehydrogenase (complex II) is a component of the TCA cycle and the ETC, which serves as a link between these two metabolic processes. The e^- from $FADH_2$ are transferred to CoQ via the FeS cluster of complex II, similar to complex I. However, no H^+ were translocated to the intermembrane space.¹³⁵ From the Q cycle, electrons carried by QH_2 are transferred to

complex III, also known as CoQ-cytochrome c reductase and afterwards to cyt c. During this process H^+ are pumped into the intermembrane space.¹³¹ Cyt c transfers single e^- from complex III to complex IV (cytochrome c oxidase), to bind to O_2 and generate H_2O . During this process, H^+ are transferred to the intermembrane space. This oxygen-consuming process is called mitochondrial respiration.¹³⁶ In total 10 H^+ are pumped into the intermembrane space, they accumulate and generate the $\Delta\Psi_m$. Protons from the intermembrane space enter the matrix via complex V (ATP synthase) to break down the proton gradient. The proton movement through the F_0 subunit of the ATP synthase is coupled to a rotation process leading to the addition of a phosphate to adenosine diphosphate (ADP), resulting in the synthesis of ATP at the F_1 subunit.¹³⁷

Notably, during normal electron transfer, < 4% of the oxygen is transformed into superoxide radicals such as ROS and reactive nitrogen free radicals (RNS) via electron leakage.¹³⁸ Furthermore, following ischemia, increased calcium ions (Ca^{2+}) influx into the mitochondria exacerbate ROS production. Reactive radicals lead to modification of DNA and proteins, resulting in lipid peroxidation, the opening of the mitochondrial permeability transition pore (mPTP) and loss of $\Delta\Psi_m$.¹³⁹ In addition, the release of cyt C initiates the cell intrinsic apoptosis pathway.¹⁴⁰

In summary, imbalance of bioenergetics, due to an increased oxidative stress accumulation, can result in mitochondrial dysfunction with an important contribution to the pathogenesis of kidney diseases.

1.4.3 Mitochondrial dynamics

Mitochondria are highly dynamic in changing their size and location. Coordinated fission and fusion enables them to switch between an elongated, connected mitochondrial network and fragmented single mitochondria (**Figure 5 - dynamics**).¹¹⁵ These processes are essential for the maintenance of cellular function and viability.¹⁴¹ Mitochondrial dynamics are regulated by fission proteins (e.g. dynamin related protein 1 (DRP1), mitochondrial fission 1 (Fis1)) and fusion proteins (e.g. mitofusins (MFN), optical atrophy (OPA1)).⁶⁷ The key regulator of mitochondrial dynamics is sirtuin-3 (SIRT3). Through deacetylation and activation of the mitochondrial fusion protein OPA1 the mitochondrial function can be improved under stress conditions of AKI.¹⁴² In addition, an impairment of mitochondrial dynamics leads to dysfunctions and is associated with aging, organ damage and human disease.¹⁴³

1.5 Mitochondrial damage in AKI

Mitochondrial damage and dysfunction is closely related to the pathogenesis of kidney diseases, including AKI. The common link is the generation of ROS or RNS during kidney injury, generated due to impaired mitochondrial biogenesis, ATP energetics, mitophagy or

following hypoxic conditions (**Figure 5**).^{67,115} Stress can change mitochondrial function and dynamics by disrupting the mitochondrial membrane integrity, which leads to a release of pro-apoptotic factors, loss of membrane potential as well as the production and elevated ROS release, which induce cell injury and death.^{144,145} Therefore, extensive investigations of mitochondrial biology and pathology are required to discover effective therapeutic strategies to protect kidneys from AKI, including an improvement of prevention, kidney repair and recovery.

For instance, Suzuki et al. identified mitochonic acid 5 (MA-5) as a kidney cell protective agent in IRI and mutant mice, which carry deleted mtDNA, resulting in a respiration defect. MA-5 is able to increase the ATP production and reduces ROS generation, without decreasing the activity of the ETC.¹⁴⁶ Furthermore, in another AKI model Tsuji et al. demonstrated, that mtDNA is essential for the activation of inflammation and kidney injury during septic AKI via toll-like receptor 9 (TLR9). Therefore, it is suggested, that an extensive removal of damaged mitochondria is an effective therapeutic strategy to prevent and treat AKI.¹⁴⁷ Moreover, mitochondrial dysfunction is described to be involved in the development of kidney fibrosis.¹³⁰ As an example, patients with autosomal dominant renal Fanconi syndrome revealed mutations in the glycine amidinotransferase (*GATM*) gene, which is key mitochondrial enzyme in the creatine biosynthesis pathway in proximal tubular cells. Abnormal *GATM* aggregates-containing mitochondria were elongated, resulting in an increased ROS production and an activation of inflammation, cell death, as well as fibrosis.¹⁴⁸ Therefore, mitochondrial changes initially lead to development of tubular cell damage and later on fibrosis. These studies support the concept, that mitochondria are effective therapeutic targets in regard of AKI.

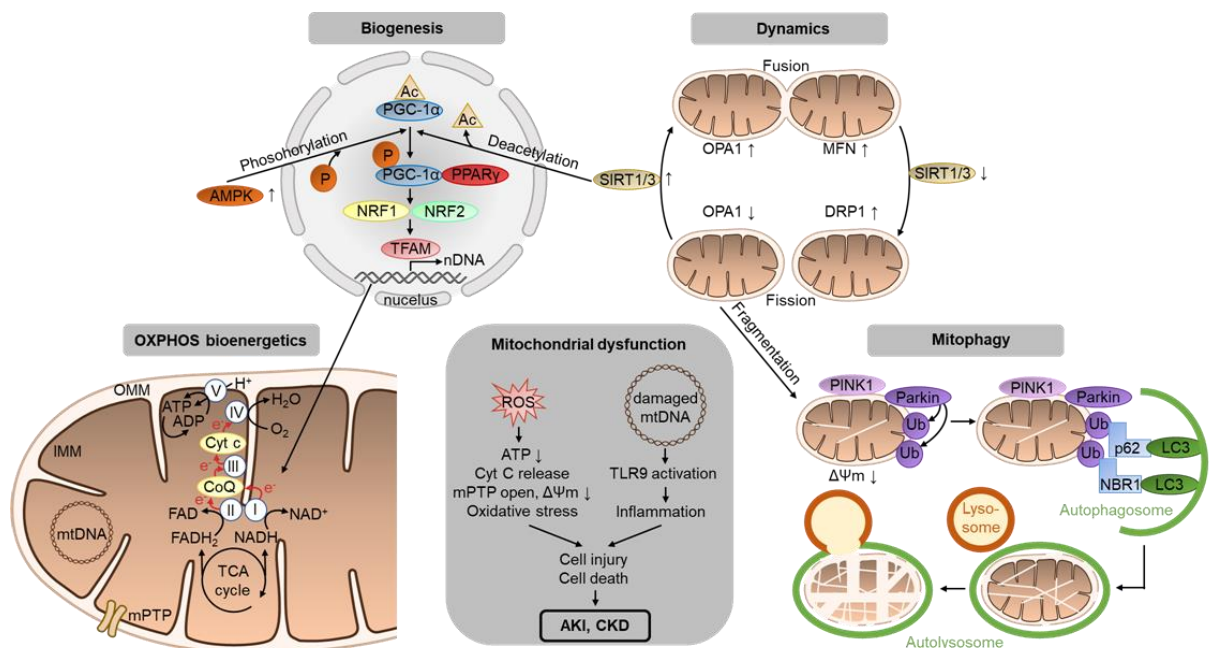


Figure 5. Mitochondrial health and dysfunction.

Several processes regulate the health and disease state of the mitochondria, cells and kidneys. Mitochondrial biogenesis requires the coordinated expression of nDNA, mtDNA, several transcription factors and co-activators.

-Figure legend continued on the next page-

-continued- Mitochondrial dynamics is responsible for the balance between fusion and fission processes. Mitophagy is an important process to clear dysfunctional mitochondria within the cell with the help of lysosomes. During OXPHOS bioenergetics an electrochemical gradient is maintained and ATP is synthesized which depends on the ETC (complexes I–V). Disturbance in any steps of the processes will cause ROS overproduction, decrease in ATP generation, loss of $\Delta\Psi_m$, mPTP opening and cyt c release. The oxidative stress leads to cell injury and death. Damaged mtDNA could stimulate innate immune response through TLR9 and inflammation. Together these mitochondrial dysfunctions can result in AKI or CKD. See text for details/abbreviations. Adapted from Duann et al.¹¹⁵

1.6 Mitochondria-targeted therapeutics

The study of mitochondrial dysfunction has become an extensive new field to find therapies for AKI. Mitochondria-targeting therapeutics to maintain the structure and function have been performed in several AKI models in animals and partly in clinical trials.

A prominent example for this is Szeto-Schiller Peptide 31 (SS-31), also known as MTP-131, Bendavia or Elamipretide. It was revealed, that administration of SS-31 before IRI in rats has protective effects on the kidney.^{149,150} Due to the binding of SS-31 to cardiolipins on the inner mitochondrial membrane (IMM), structural damage and electron leakage are prevented. Therefore, tubular cell death, oxidative stress and inflammation are reduced.^{149,150} Furthermore, regular treatment before the injury decreases peritubular capillary loss, interstitial inflammation and fibrosis 4 weeks after ischemia.¹⁵¹ In addition to ischemic animal models, SS-31 recently shows promising results for a variety of further preclinical kidney disease models.¹⁵²⁻¹⁵⁷ However, the transition into the clinic is still limited, due to an insufficient chemical and physical stability as well as a short circulating plasma half-life.^{158,159} At the moment, 25 clinical trials on SS-31 are running, of which 2 include patients with kidney diseases (NCT02436447: patients with renal impairment; NCT01755858: percutaneous transluminal renal angioplasty.¹⁵⁹) SS-31 is potentially a suitable molecule for patients with kidney disease. Hence, further preclinical and large-scale clinical studies are necessary to reduce particular disadvantages.

Another example for mitochondria-targeted therapeutics is the biogenesis activator and antioxidant resveratrol. In diabetic mice, it decreases renal pathological changes.¹⁶⁰ To prevent potential renal IRI during resuscitation, the treatment of resveratrol revealed enhanced mitochondrial respiration whereas ROS levels and lipid peroxidation was reduced.¹⁶¹ Currently 192 clinical trials, including 6 studies related to kidney diseases (NCT02433925, NCT03352895, NCT03597568, NCT03815786: chronic kidney disease; NCT02704494: diabetic kidney disease; NCT03946176: hemodialysis patients) take place.¹⁵⁹ Unfortunately, only one study has reported their results, which probably means an absence of positive results.¹⁶² Further potential compounds that target mitochondria in relation to AKI and CKD are summarized in **Figure 6**. Although there are several promising findings regarding the effects of mitochondria-targeted therapeutics, additional studies and investigations are required to understand the pathophysiological role of mitochondria in kidney disease and to improve the clinical use.¹⁵⁹

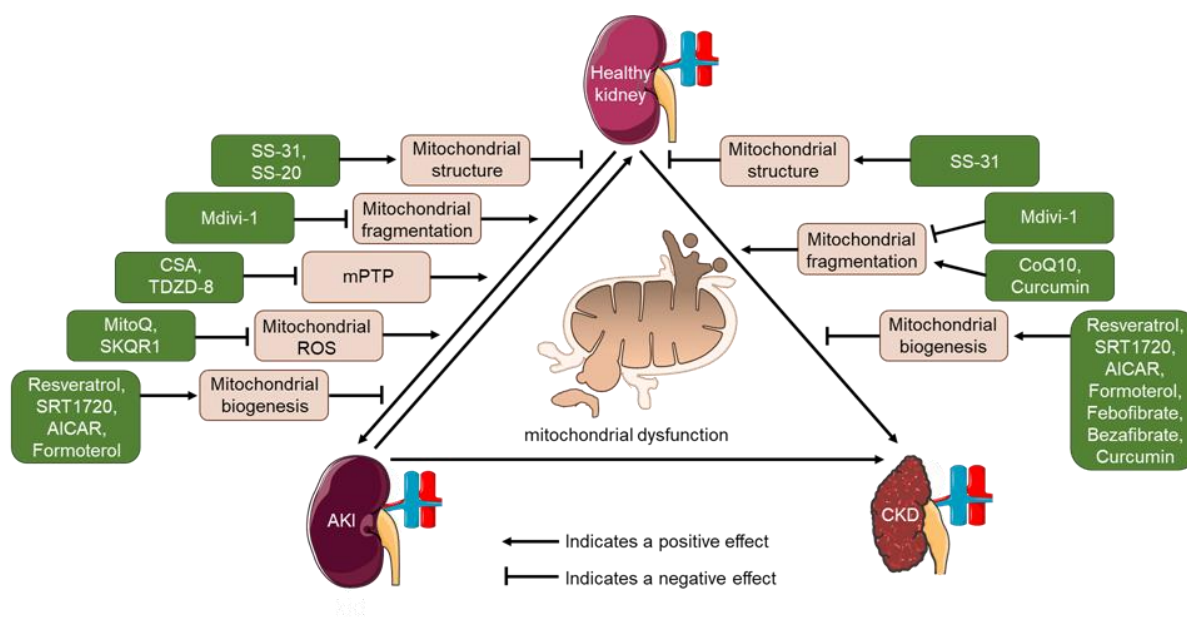


Figure 6. Mitochondria as promising targets for kidney disease.

Potential compounds that target mitochondrial dysfunction in AKI and CKD including mitochondrial structure, fragmentation, biogenesis, mPTP and ROS. Abbreviations: SS-31: Szeto–Schiller peptide 31, SS-20: Szeto–Schiller peptide 20, Mdivi-1: mitochondrial division inhibitor 1, CSA: cyclosporine A, TDZD-8: 4-benzyl-2-methyl-1,2,4-thiadiazolidine-3,5-dione, MitoQ: mitochondrial coenzyme Q, SKQR1: 10-(6'-plastoquinonyl) decylrhodamine 19, AICAR: 5-aminoimidazole-4-carboxamide-1- β -d-ribofuranoside, CoQ10: Coenzyme Q10 MitoQ (mitochondrial coenzyme Q). Adapted from Zhang et al.⁹²

1.7 Aims of the thesis

Given the connection of DbpA with cell cycling and reactivation of developmental cell programs, which are observed during regeneration following tissue damage^{12,62,163}, we hypothesized that DbpA orchestrates tubular cell regenerative responses in AKI. In order to test this hypothesis, 4 specific aims were addressed within this thesis:

1. To phenotype genetically modified animals harboring a homozygous or heterozygous *Ybx3* knockout up to 2 years of age.
2. To determine the cell specific expression and localization of DbpA in kidneys of healthy adult mice.
3. To analyze the mitochondrial structure, mass, number and $\Delta\Psi_m$, as well as the metabolic function and antioxidant activity of primary TECs.
4. To implement a well-defined experimental renal IRI model in genetically modified animals harboring a homozygous or heterozygous *Ybx3* knockout, with comprehensive analyses of short (1 day) and long term (28 days) consequences following IRI.

2 Material

2.1 Devices

Table 3. Devices

Device	Company
-80°C Forma Ultra Low Temperature Freezer	Thermo Fisher Scientific
Advanced Fluorescence Imager	Intas
Autoclave	H&P Laboratory Technology
Advia 120 hematology analyzer	Siemens Healthcare
Bio-Plex System	Bio-Rad
Cages	Tecniplast
Centrifuge 4-16K	Sigma
Centrifuge 5417R	Eppendorf
Cobas c501 module	Roche Diagnostics
Dounce tissue grinder	Sartorius
Flow cytometer fluorescence-associated cell sorting (FACS) Canto II	BD Bioscience
Flex Cycler	Analytik Jena
Fridge and freezer (4°C, -20°C)	Liebherr
Gel electrophoresis system	Bio-Rad
Heating plate Hi1220	Leica
Herolab UV transilluminator	Herolab
Leica microscope DM6000 B (with camera DFC420 and Fluorescence camera DFC340 FX)	Leica
IKA ROCKER 2D BASIC	Thermo Fisher Scientific
Illumina NovaSeq 6000 Sequencing System	Illumina
Magnetic stirrer	RCT classic IKA
Metabolic cages	Tecniplast
Microplate Reader Infinite 200 PRO	Tecan
Mini blot transfer chamber	Bio-Rad
NanoDrop-1000 spectrophotometer	Thermo Fisher Scientific
NIC-kidney device	Mannheim Pharma & Diagnostics
Phase contrast microscope Axiovert 40CFL	Zeiss
pH-Meter	Calimatic
Pipettes	Eppendorf
Pipetus pipetting aid	Hirschmann Laborgeräte
PowerPac HV	Bio-Rad
Roller mixer	Bibby Scientific Limited
Rotary microtome RM 2135	Leica
Seahorse XFe96 Analyzer	Agilent Technologie
Shaker vortex	VWR International
Spectrophotometer Infinite200 PRO	Tecan
Tabletop centrifuge	VWR International
ThermoMixer Comfort	Eppendorf
Tissue Ruptor	Qiagen
Ultra-pure water plant MilliQ	Merck Millipore
UV spectrometer Ultrospec 2100 Pro	Healthcare Bio-Sciences
UV transilluminator Luormat	Vilber
Vortex	IKA Vortex 1
Water bath	P-D Industriegesellschaft mbH
Xcell Sure Lock Mini Cell Elektrophorese System	Invitrogen
Zeiss Axiovert 200M inverted fluorescence microscope	Zeiss

2.2 Consumables

Table 4. Consumables

Consumable	Company
5 ml syringe	BD Bioscience
6-well plate	Greiner Bio-One
12-well plate	Greiner Bio-One
40 µm cell filter	Corning
70 µl cell filter	Corning
96 well V-bottom plate	Life Technologies
96 well white/clear bottom plate	Thermo Fisher Scientific
100 µl cell filter	Greiner Bio-One
Eppendorf tubes (1.5 ml and 2 ml)	Eppendorf
Falcon tubes (15 ml and 50 ml)	Eppendorf
FACS tubes	BD Bioscience
Roti nitrocellulose membrane	Carl Roth
Nobistrip	Hitado
NuPAGE 4-12% Bis Tris gel	Invitrogen
Parafilm „M“	Bemis
Pasteur pipettes	Carl Roth
Pipette tips epT.I.P.S	Eppendorf
PVDF membrane	Carl Roth
scapel	Feather
Seahorse XF96 cell culture microplates	Agilent Technologies
Seahorse XFe96 sensor cartridges	Agilent Technologies
Serological pipettes	TPP
Whatman paper	GE

2.3 PCR primers

Table 5. Polymerase chain reaction (PCR) primer sequences

Allele	Primer name	Primer sequence
<i>β-actin</i>	Forward (fwd)	AGAGAGGTATCCTGACCCTGAAGT
	Reverse (rev)	CACGCAGCTCATTGTAGAAGGTGT
<i>Aqp2</i>	fwd	ATGTGGGAACCTCCGGTCCATA
	rev	ACGGCAATCTGGAGCACAG
<i>Atp6v1b1</i>	fwd	TGCTCTACCTGGAGTTCCTGCAGAAGTTTGAGAAG
	rev	TCATGCTCTGCGGAATGCGCTTCAGCATCTCTTTC
<i>B2m</i>	fwd	AGCAAAGAGGCCTAATTGAAGTC
	rev	GAAGTAGCCACAGGGTTGGG
<i>mt1</i>	fwd	TGAACGGCTAAACGAGGGTC
	rev	AGCTCCATAGGGTCTTCTCGT
<i>mt2</i>	fwd	CAGTCCCCTCCCTAGGACTT
	rev	ACCCTGGTCCGTTTGATGTT
<i>mt3</i>	fwd	TAATCGCACATGGCCTCACA
	rev	GAAGTCCTCGGGCCATGATT
<i>Tuba1a</i>	fwd	CCGCGAAGCAGCAACCAT
	rev	CCAGGTCTACGAACACTGCC
<i>Ybx3</i>	fwd	CAGACTCAGAAAATGAAGGGCA
	rev	AGATGGGCAAGATTCTCAAGTC

2.4 Antibodies

Table 6. Primary and secondary antibodies used for Western blot

Antibody	Species	Company	Catalog nr.	Dilution
α SMA	Rabbit	Abcam	ab5694	1:1000
β -actin	Mouse	Sigma	A1978	1:1000
AE1	Rabbit	Merck Millipore	AB3500P	1:500
AMPK α	Rabbit	Cell Signaling Technology	2532	1:1000
Aqp1	Rabbit	Alpha diagnostic international	AQP11	1:1000
Aqp2	Rabbit	Abcam	ab199975	1:500
ATF4	Rabbit	Cell Signaling Technology	11815	1:500
Atp6v1b1	Rabbit	Invitrogen	PA5-56878	1:500
CA2	Rabbit	Abcam	ab191343	1:1000
DbpA C-terminal	Rabbit	Eurogentec	ED19016	1:1000
GAPDH	Goat	GenScript Biotech	A00191-40	1:1000
GPX4	Mouse	Santa Cruz Biotechnology	sc-166120	1:500
HIF1 α	Rabbit	Cell Signaling Technology	14179	1:1000
HO-1	Rabbit	Abcam	ab13243	1:1000
KIM1	Rabbit	Abcam	ab47635	1:1000
NGAL	Goat	R&D Systems	AF1757	1:500
Parkin	Rabbit	Cell Signaling Technology	2132	1:1000
PCNA	Mouse	Santa Cruz Biotechnology	sc-56	1:1000
Phospho-AMPK α (T ¹⁷²)	Rabbit	Cell Signaling Technology	2535	1:1000
PINK1	Mouse	Santa Cruz Biotechnology	sc-517353	1:1000
SOD2	Mouse	Santa Cruz Biotechnology	sc-137254	1:500
Tenascin-C	Rabbit	Abcam	ab108930	1:1000
Total OXPHOS Rodent WB Antibody Cocktail	Mouse	Abcam	ab110413	1:250
VDAC1	Rabbit	Abcam	ab15895	1:1000
Vinculin	Mouse	Santa Cruz Biotechnology	sc-59803	1:1000
XBP1s	Mouse	BioLegend	658802	1:1000
YB-1	Rabbit	Eurogentec	EP085177	1:1000
Goat anti-mouse IgG HRP	Goat	Southern Biotech	1031-05	1:5000
Goat anti-rabbit IgG HRP	Goat	Southern Biotech	4050-05	1:5000
Donkey anti-goat IgG HRP	Donkey	Jackson ImmunoResearch	705-035-147	1:5000

Table 7. Primary and secondary antibodies used for immunohistochemistry

Antibody	Species	Company	Catalog nr.	Dilution
4HNE	Rabbit	Abcam	ab46545	1:500
Atp6v1b1	Rabbit	Invitrogen	PA5-56878	1:50
Aqp2	Mouse	Santa Cruz Biotechnology	sc-515770	1:50
Calbindin D-28K	Chicken	Novus Biologicals	NBP2-50028	1:100
DbpA	Rabbit	Eurogentec	ED15001	1:500
NGAL	Rabbit	Boster Immunoleader	PB9609	1:500
SGLT2	Mouse	Santa Cruz Biotechnology	sc-393350	1:50
Goat anti-rabbit IgG HRP	Goat	DAKO/AgilentTechnologies	P0448	1:200
Goat anti-mouse IgG TRITC	Goat	Jackson Immno Research	115-026-003	1:100

Goat anti-rabbit IgG Alexa Fluor 488	Goat	Thermo Fisher Scientific	A11070	1:100
Goat anti-chicken IgY Alexa Fluor 647	Goat	Thermo Fisher Scientific	A-21449	1:100

Table 8. Antibodies used for flow cytometry

Antibody	Fluorochrome	Company	Catalog nr.	Dilution
CD3	APC	eBioscience	17-0031	1:100
CD11c	APC	Biozol	117309	1:200
CD11b	APC-Cy7	BioLegend	101226	1:200
CD45	BV510	BioLegend	103138	1:500
CD64	PE	BioLegend	139304	1:100
Ly6C	BV421	BioLegend	128032	1:200
Ly6G	PE-Cy7	BioLegend	127618	1:1000
MHC-II	FITC	BioLegend	107606	1:200

2.5 Kits

Table 9. Kits

Kits	Company	Catalog nr.
ATP determination kit	Thermo Fisher Scientific	A22066
DC Protein Assay Kit II	Bio-Rad	5000112
Dynabeads mRNA DIRECT Micro Purification Kit	Thermo Fisher Scientific	61021
ECL Prime Western Blotting Detection Reagent (Amersham)	GE Healthcare	12316992
FlexiGene DNA kit	Qiagen	51206
FOXP3 Fix/Perm buffer set	BioLegend	421403
Maxima H Minus First Strand cDNA Synthesis Kit	Thermo Fisher Scientific	K1652
Mitochondria/cytosol fractionation kit	Abcam	ab65320
NEBNext Ultra II Directional RNA Library Prep Kit	New England BioLabs	E7765
NovaSeq 6000 S1 Reagent Kit	Illumina	20028319
PCR Mastermix Kit	Qiagen	201445
Pierce ECL Western Blotting Substrate Kit	Thermo Fisher Scientific	32106
Quick Start Bradford Protein Assay Kit	Bio-Rad	5000201
Seahorse XF Cell Mito Stress Test kit	Agilent Technologies	103015-100
Seahorse XF Glycolysis Stress Test kit	Agilent Technologies	103020-100
XF Palmitate Oxidation Stress Test Kit	Agilent Technologies	103693-100
Transcriptor High Fidelity cDNA Synthesis Kit	Sigma-Aldrich	5081955001
Tetramethylrhodamine, ethyl ester (TMRE) - mitochondrial membrane potential assay kit	Abcam	ab113852

2.6 Chemicals and Reagents

Table 10. Chemicals and reagents

Chemicals and reagents	Company	Catalog nr.
0.05% Trypsin-EDTA	Gibco	14190169
2-(N-(7-Nitrobenz-2-oxa-1,3-diazol-4-yl)Amino)-2-Desoxyglucose (2-NBDG)	Thermo Fisher Scientific	N13195
3,3',5 Triiodothyronine (T3)	Sigma-Aldrich	BCBP6441

4x LDS sample buffer	Invitrogen	NP0007
4% paraformaldehyde (PFA)	Otto Fischar	27279
6x DNA-loading	Thermo Fisher Scientific	R0611
20x NuPAGE transfer buffer	Invitrogen	NP00061
30% Hydrogen peroxide	Carl Roth	CP26.5
100 bp DNA ladder	Thermo Fisher Scientific	SM0241
β -Mercaptoethanol	Carl Roth	4227.3
Acetic acid	Carl Roth	6755.2
Acryl-/bisacrylamide 30%	Serva	10688.01
Agarose	Carl Roth	3910.3
Alexa Fluor 488 phalloidin	Thermo Fisher Scientific	A12379
Ammonium chloride (NH ₄ Cl)	Riedel-de Haen	31107
Ammonium persulfate (APS)	Carl Roth	9592.2
Antibody diluent	DCS Innovative Diagnostik-Systeme	AL120R500
Aqua dest. nuclease free	Thermo Fisher Scientific	R0581
BODIPY FL C16	Invitrogen	D-3821
BODIPY FL complex	Invitrogen	L3483
Boric acid	Carl Roth	P010.1
Bovine serum albumin (BSA)	Carl Roth	8076.3
Bromphenol blue	Merck	1.081.220.005
C1-BODIPY 500/510 C12	Invitrogen	D-3823
Chloroform	Sigma-Aldrich	3313.2
Collagenase D	Roche Diagnostics	1088866
Complete Mini Protease Inhibitor Cocktail	Sigma-Aldrich	11836153001
Direct PCR Lysis Reagent Ear	Viagen Biotech	402-E
Direct Red 80	Sigma	365548
DMEM	Thermo Fisher Scientific	21063-029
DNase	Sigma-Aldrich	D-5025
DNA Stain G	Serva	39803.01
DreamTaq Green PCR Master Mix	Thermo Fisher Scientific	K1081
Dulbecco's phosphate-buffered saline (DPBS)	Thermo Fisher Scientific	14190-094
Dulbecco's phosphate-buffered saline (DPBS) (+CaCl ₂ +MgCl ₂)	Thermo Fisher Scientific	14040-091
Ethanol (EtOH)	Otto Fischar	27698
Ethylendiamintetraacetat (EDTA)	Bio-Rad	161-0729
Filtrated bovine serum (FBS)	PAN-Biotech	P40-39500
FcR Blocking Reagent, mouse	Miltenyi Biotec	130-092-575
Glycerol	Carl Roth	3783.2
Glycine	Carl Roth	3790.3
GoTaq Flexi DNA Polymerase	Promega	M8291
Hematoxylin solution, Gill No. 3	Sigma-Aldrich	GHS316
Hemalum solution acid acc. to Mayer	Carl Roth	T865.1
Hydrochloric acid (37%)	Carl Roth	4625.2
Hydrocortisone (HC)	Sigma-Aldrich	H6909
Insulin, transferrin, selenious acid (ITS) premix universal culture supplement	Thermo Fisher Scientific	41400045
Isoflurane	Baxter International	HAGG9623
Isopropanol (2-Propanol)	Carl Roth	CP41.3
Liquid diaminobenzidine (DAB) Substrate Chromogen System	Dako	K3468

Macrophage colony-stimulating factor (M-CSF)	R&D Systems	216-MC
Methanol	Carl Roth	CP43.3
Milk powder	Carl Roth	T145.3
MitoTracker Red CMXRos	Thermo Fisher Scientific	M7512
MitoTracker Green	Thermo Fisher Scientific	M7514
MitoSOX Red Mitochondrial Superoxide Indicator	Thermo Fisher Scientific	M36008
MOPS	Sigma-Aldrich	M1254
NBD-cholesterol	Invitrogen	N1148
Nonidet P40 (NP-40)	Thermo Fisher Scientific	J60766.AP
Roticlear (xylene substitutes)	Carl Roth	A538.5
ROTI Mount	Carl Roth	HP68.1
RPMI 1640 medium	Thermo Fisher Scientific	21875091
PagerRuler Plus Pre-Stained Protein Ladder	Thermo Fisher Scientific	26619
Penicillin-Streptomycin (Pen/Strep)	Gibco	15144-122
Periodic acid solution	Sigma-Aldrich	395132
PhosStop	Sigma-Aldrich	4906845001
Picric acid (1.2%)	Hollborn & Söhne	P09-1000
Prostaglandin E1	Sigma-Aldrich	P7527
Proteinase K	Roche Diagnostics	03115879001
ProLong Gold Antifade mountant with DAPI	Thermo Fisher Scientific	P36930
Recombinant murine epidermal growth factor (EGF)	PeptoTech	3154-09
Schiff's reagent	Sigma-Aldrich	3952016
Seahorse XF Calibrant Solution	Agilent Technologies	100840-000
Seahorse XF DMEM medium, pH 7,4	Agilent Technologies	103680-100
Seahorse XF 1.0 M glucose solution	Agilent Technologies	100840-000
Seahorse XF 100 mM pyruvate solution	Agilent Technologies	103578-100
Seahorse XF 200 mM glutamine solution	Agilent Technologies	103579-100
Sodium chlorid (NaCl)	Carl Roth	3957.2
Sodium dodecyl sulfate (SDS)	Carl Roth	CN30.3
Sodium hydrogen carbonate (NaHCO ₃)	AppliChem	A3590,1000
SYBR Green qPCR MasterMix	Thermo Fisher Scientific	A46012
SYTOX Green	Thermo Fisher Scientific	S7020
Tetramethylethylendiamin (TEMED)	Carl Roth	2367.3
Transcription Factor Buffer Set (Fixation/ permeabilization buffer, diluent buffer, perm/ wash buffer)	BD Bioscience	562574
TriFast reagent	Peqlab	30-2010P
Tris	Carl Roth	4855.3
Tris-HCl	AppliChem	A1087,1000
Triton X-100	Carl Roth	3051.2
Trizol	Thermo Fisher Scientific	15596026
Tween 20	AppliChem	A4974,0250

2.7 Buffers and solutions

Table 11. Buffers and solutions

Buffer/solution	Composition
0.01 N HCl	829 µl HCl (37%), add to 1000 ml dH ₂ O
1x NuPAGE transfer buffer	20x NuPAGE transfer buffer 50 ml, methanol 200 ml, add to 1000 ml dH ₂ O

1x TBE buffer	100 ml 10x TBE buffer, add to 1000 ml dH ₂ O
5x sample buffer	1,18 g Tris-HCl, 15 ml Glycerol, 6 ml SDS, 12 ml β-Mercaptoethanol, 1 Spatula tip Bromphenol Blue, add to 50 ml dH ₂ O
10x TBE buffer	107,8 g Tris, 55 g boric acid, 7,4 g EDTA, add to 800 ml dH ₂ O, adjust pH 8.3, add to 1000 ml dH ₂ O
10x TBS stock solution	9 g Tris, 68.5 g Tris-HCl, 87.8 g NaCl, add to 1000 ml dH ₂ O
20x NuPAGE MOPS SDS running buffer	MOPS 104.6 g, Tris 60.6 g, SDS 10 g, EDTA 3 g, add to 500 ml dH ₂ O, adjust pH 7.7
APS (10%)	10 g APS, add to 100 ml dH ₂ O
Blocking buffer	100 µl FcR Blocking Reagent, add to 10 ml perm/wash buffer
Blocking solution (5%)	5 g milk powder/BSA, add to 100 ml TBST
BSA stock solution	BSA 10 mg, add to 1 ml dH ₂ O
Citrate stock solution	29.42 g Tri-sodium citrate dihydrate, add to 1000 ml dH ₂ O
Citric acid stock solution	6.13 g citric acid, add to 200 ml dH ₂ O
Citrate buffer	75 ml citrate stock solution, 25 ml citric acid stock solution, add to 1000 ml dH ₂ O
Digestion buffer	10 mg BSA, 200 µl Collagenase D, 100 µl DNase, add to 10 ml RPMI-medium
DNA Ladder	100 bp DNA Ladder (100 µl, 0.5 µg/µl, 50 µg), 100 µl 6x DNA Loading, 400 µl sterile distilled water
Erythrocyte lysis buffer	0.8401 g NaHCO ₃ , 8.29 g NH ₄ Cl, 200 µl EDTA, add to 1000 ml dH ₂ O
FACS buffer	50 ml 20x PBS, 50 ml FBS, 5 g BSA, 1 ml 10% sodium azid, add to 1000 ml dH ₂ O
Lysis buffer	100 µl Direct PCR Lysis Reagent Ear, 1.25 µl Proteinase K for each sample
Methacarn	600 ml methanol, 300 ml chloroform, 100 ml acetic acid
Resolving buffer	Tris 90.86 g, add to 500 ml dH ₂ O, adjust pH 8.8
RIPA lysis buffer	Tris 3.03 g, NaCl 4.38 g, ad to 75 ml dH ₂ O, adjust pH 7.4, NP-40 50 ml, Sodium desoxycholate 12.5 ml, EDTA 1 ml, ad to 500 ml dH ₂ O, Complete Mini, PhosStop
Running buffer (10x)	144 g Glycine, 30 g Tris, 10 g SDS, add to 1000 ml dH ₂ O, adjust pH 8.6
Proteinase K	90 mg Lyophilisate, 4.5 ml sterile distilled water
SDS (10%)	10 g SDS, add to 100 ml dH ₂ O
Sirius-Red solution	0,25 g Direct Red 80, add to 250 ml Picric acid
Stacking buffer	Tris 30.29 g, add to 500 ml dH ₂ O, adjust pH 6.8
TBS	50 ml 1 M Tris (pH 8.0), 60 ml 5 M NaCl, add to 2000 ml dH ₂ O
TBST	50 ml 1 M Tris (pH 8.0), 60 ml 5 M NaCl, 1 ml Tween 20, add to 2000 ml dH ₂ O
Transfer buffer	6 g Tris, 28.8 g Glycine, 400 ml Methanol (20 %), add to 2000 ml dH ₂ O, adjust pH 8.2
Tubular cell culture medium	450 ml DMEM, 50 ml FBS, 5 ml Pen/Strep, 5 ml ITS premix, 500 µl HC, 850 µl T3, 10 µl Prostaglandin E1, 12.5 µl EGF

2.8 Software

Table 12. Software

Name	Version	Company
Chemostar	0.4.14.0	Intas Science Imaging Instruments
Endnote	X7	Clarivate Analytics
FACS Diva Software	6.1.3	BD Bioscience
FlowJo	7.6.4	FlowJo

GraphPad Prism 8	8.3.0	GraphPad Software
ImageJ	1.52a	National Institutes of Health
LabImage 1D	4.1	Kapelan Bio-Imaging GmbH
MPDlab	1.0	Mannheim Pharma & Diagnostics GmbH
Servier Medical Art	3.0	Servier
Wave	2.6.1.53	Agilent Technologies

3 Methods

3.1 Animals

Animal studies were performed with genetically modified mice on a C57BL/6N background. *Ybx3^{-/-}* mice were provided by Timothy J. Ley (Washington University School of Medicine, St. Louis, USA). Equal numbers of males and females were analyzed for phenotyping. Animals were maintained according to the FELASA guidelines (Federation of European Laboratory Animal Science Association) in a 12 h/12 h light dark cycle at 22°C in the animal facility of the Otto-von-Guericke University Magdeburg under specific pathogen-free (SPF) conditions using individual ventilated cages with free access to food and water. All procedures were performed in accordance with the German National Guidelines for the use of Experimental Animals (Animal Protection Act) and approved by the state of Saxony-Anhalt (AZ UniMD 42502-2-1634 UniMD).^{164,165}

3.2 Genotyping

Ear biopsies were lysed with 100 µl DirectPCR Lysis Reagent Ear containing 25 µg of proteinase K. PCR primer pairs are listed in **Table 5**. Following conditions were used for PCR: 95°C for 5 min, 35 cycles at 95°C for 30 sec, 58°C for 30 sec, 72°C for 1 min and 72°C for 10 min. The products were separated on 1% agarose-DNA stain G gels. The expected sizes were 419 bp for *Ybx3^{+/+}* mice and 627 bp for the *Ybx3^{-/-}* genotype. Heterozygous animals show both PCR products.^{165,166}

3.3 Renal ischemia/reperfusion injury (IRI) model

IRI was performed with male 9 to 14 weeks old mice. All mice were anesthetized and placed on a 37°C operating platform. Through an abdominal incision, the renal arteries and veins were occluded bilaterally with surgical clamps for 25 min. The clamps were removed and the kidneys were examined to ensure renal perfusion. The abdomen was closed with continuous polypropylene sutures. All animals received a subcutaneous analgesic at the end of the procedure and were placed on a heating plate adjusted to 37°C until they awake from anesthesia to prevent cooling down with internal body temperature controlled by thermometer (BIO-TK8851, BIOSEB). Mice were placed in a temperature-controlled environment during the recovery phase and returned to their cages with free access to food and water. Littermates that did not undergo this procedure served as control animals. Animals were sacrificed 24 h (d1) or 28 days (d28) following renal IRI to obtain blood and tissue samples. Both kidneys were harvested for preparation of RNA, protein lysates, immunohistochemistry and flow cytometry.

3.4 Organ perfusion

Animals were placed under deep, irreversible anesthesia by Rompun and Ketamine at the end of the experiments. The thorax of the mouse was opened, a cannula was inserted into the left ventricle and the animal was exsanguinated and thus killed. After opening the right ventricle, the animal was perfused with 50 ml DPBS via the same cannula.

3.5 Blood and plasma analyses

Blood samplings by heart puncture were subjected to a complete blood cell count (ADVIA 120, Bayer Diagnostics Munich). Renal function was assessed by measuring plasma creatinine using an enzymatic creatinine assay kit (Abcam) and blood urea nitrogen (BUN) with a kinetic urease assay (Roche Diagnostics, Cobas c501 module) according to the manufacturer's instructions.¹⁶⁷

3.6 Urine measurements

Urine samples from mice were collected individually in metabolic cages. Mice were placed in cages for 24 h with access to pelleted and water *ad libitum*. The metabolic parameters albumin and pH were determined using NobiStrip U10 test strips according to the manufacturer's instructions. Urine osmolality was measured according to the manufacturer's instructions (Roche Diagnostics, Cobas c501 module). Protein content was determined using the Quick Start Bradford protein assay.¹⁶⁵

3.7 Transcutaneous measurement of glomerular filtration rate (GFR)

GFR (normalization to body weights (b.w.) of mice) was measured in 3-months old mice by the transcutaneous clearance of fluorescein isothiocyanate (FITC)-sinistrin using a NIC-kidney device. Animals were anesthetized and the miniaturized fluorescence detector was attached to a depilated area on the back of the mice using a double-sided adhesive patch and an adhesive tape. The measurements were started with activation of the device before FITC-sinistrin (70 mg/kg b.w.) was injected into the tail vein, to detect the background signal. Data acquisition lasted 2 h from the time of injection. At the end of the recording period, the mice were anesthetized and the device removed. The data were analyzed using NIC-kidney device partner software. The half-life ($t_{1/2}$) of the FITC-sinistrin was used to calculate the GFR using the formula $GFR (\mu\text{l}/\text{min per } 100 \text{ g b.w.}) = 14616.8 \mu\text{l}/100 \text{ g b.w. per half-life of FITC-sinistrin (min)}$.^{168,169}

3.8 Tissue lysate preparation and Western blot analysis

Tissues were mechanically homogenized in RIPA buffer containing complete protease inhibitor cocktail at 4°C for 30 min. Protein content was determined using the DC Protein Assay Kit II. Denatured protein samples were separated using 10% SDS-PAGE and blotting on nitrocellulose membranes. Membranes were blocked with 5% dry milk in TBST and incubated with primary antibodies diluted in TBST overnight at 4°C, followed by incubation with HRP-conjugated secondary antibody for 1 h at room temperature (RT). After washing, Super Signal chemiluminescence substrate Pierce ECL was added and emitted light measured using an Intas imaging system. The primary and secondary antibodies used for Western blot are listed in **Table 6**. The NuPAGE system from Invitrogen was used to detect DbpA according to the manufacturer's instructions. For denaturation, tissue or cell lysates were incubated for 30 min at RT in NuPAGE loading buffer.^{165,167}

3.9 Immunohistochemistry

Formalin-fixed, paraffin-embedded 2-4 µm tissue sections were used for immunohistochemistry (avidin-biotin complex method). Sections were deparaffinized in xylene, dehydrated and boiled for 20 min in 10 mM sodium citrate buffer (pH 6) for antigen unmasking. Endogenous peroxidase was inactivated by incubation in 3% hydrogen peroxide. After washing, the sections were incubated overnight at 4°C with primary antibodies diluted in antibody diluent. After washing, the sections were incubated with peroxidase-labeled secondary antibodies for 45 min at RT. Sections were developed with diaminobenzidine substrate and counterstained with hematoxylin solution to visualize nuclei. Subsequent dehydration was achieved by an ascending alcohol series. Embedding was performed with ROTI Mount according to the manufacturer's instructions. For immunofluorescence staining, secondary antibodies conjugated with fluorescent dyes were incubated for 45 min at RT. Coverslips were mounted using ProLong Gold Antifade mountant with DAPI. Tissue sections were imaged with a Leica DM6000B microscope using Leica application suite advanced fluorescence software and ImageJ for image acquisition. The primary and secondary antibodies used for immunohistochemistry are listed in **Table 7**.^{11,164}

For mitochondrial reactive oxygen species (mROS) measurement renal tissues from mice were immediately frozen. 5 µm cryo-sections were incubated with 5 µM MitoSOX Red (Thermo Fisher Scientific) and Hoechst at 37°C for 30 min. Section were washed twice with DPBS and images were acquired by fluorescence microscope.¹⁷⁰

3.10 Periodic acid-Schiff (PAS) staining and Picro Sirius Red staining

Formalin-fixed, paraffin-embedded 2 μm tissue sections were deparaffinized and rehydrated. Sections were stained in periodic acid solution, washed several times and incubated in Schiff's reagent. Tubular injury was scored on a scale of 0-4: 0=none; 1=0-25%; 2=25-50%; 3=50-75%; 4=more than 75% affected tubules. Tubulointerstitial injury was defined as inflammatory cell infiltrates, tubular dilation and/or atrophy or interstitial fibrosis. The morphological study was done in blinded fashion. The total score is the calculated average of all tubular scores. Two investigators assessed the tubular score.¹⁶⁴

For Picro Sirius Red staining the sections were incubated with 0.1% Sirius Red in saturated picric acid and were destained with 0.01 N hydrochloric acid. Counterstaining, dehydration, embedding and imaging were performed as described above.¹⁶⁴

3.11 Transmission electron microscopy

Fixed kidneys were post-fixed with osmium tetroxide and embedded in epoxy resin. Ultra-thin sections (70 nm) were stained with uranyl acetate.

3.12 Flow cytometry

Single cell suspensions of kidney tissue samples were labeled with antibodies directed against surface receptors/proteins. Fixation and cell membrane permeabilization were performed using the FOXP3 Fix/Perm buffer set. Non-specific binding was minimized with 5% mouse serum. Flow cytometry was performed with a FACS Canto II. Data acquisition and analysis were performed using FlowJo software. Spectral spillover was corrected by creating a compensation matrix generated with the help of single antibody stainings and fluorescence minus one (FMO) control samples. Antibodies used for Flow cytometry are listed in **Table 8**.^{164,166}

3.13 Isolation of total RNA and quantitative PCR

Total RNA was extracted from kidney tissue samples using TriFast™ reagent according to the manufacturer's instructions. RNA was reverse transcribed using the Transcriptor High Fidelity cDNA kit. PCR was performed using the PCR Mastermix kit. The standard temperature profile included initial denaturation for 2 min at 95°C, followed by 35 cycles of denaturation at 95°C for 15 seconds, annealing at 56°C to 63°C for 30 seconds or 1 min (primer dependent), and extension at 72°C for 1 min. Products were separated on 2% agarose gels. The expected product sizes are 137 bp for *aquaporin 2 (Aqp2)* and 158 bp for *ATPase H⁺ transporting V1 subunit B1 (Atp6v1b1)*. Relative gene expression values were normalized to β -actin (105 bp). Primers are listed in **Table 5**.¹⁶⁶

3.14 Transcriptome analysis using RNA-seq

RNA was quantified using a NanoDrop-1000 spectrophotometer. The quality and integrity of total RNA was monitored using an Agilent Technologies 2100 Bioanalyzer. The RNA sequencing library was prepared from 500 ng of total RNA using the Dynabeads mRNA DIRECT Micro Purification Kit for mRNA purification followed and thr NEBNext Ultra II Directional RNA Library Prep Kit according to the manufacture's protocol. Libraries were sequenced on Illumina NovaSeq 6000 using NovaSeq 6000 S1 Reagent Kit (100 cycles, paired-end run) with an average of 3×10^7 reads per RNA sample. Each FASTQ file receives a quality report generated by the FASTQC tool. Before alignment to the reference genome, each sequence in the raw FASTQ files was trimmed for base call quality and sequencing adapter contamination using the Trim Galore! wrapper tool. Reads shorter than 20 bp were removed from the FASTQ file. Trimmed reads were aligned to the reference genome using the open-source short read aligner STAR (<https://code.google.com/p/rna-star/>) with the settings according to log file. Feature counts were determined using the R package "Rsubread". Only genes that had a value greater than 5 at least twice in all samples were considered for further analysis (data cleaning). Gene annotation was performed using the R package "bioMaRt". Before starting the statistical analysis steps, expression data were log2 transform and normalized according to TMM normalization using "edgeR" package. Differential gene expression was calculated using the R package "edgeR". RNA-seq data have been deposited in the Gene Expression Omnibus database accession number GSE264448.^{164,167,171}

3.15 Bioinformatic analysis

Each list of differentially expressed genes derived from the respective comparisons was subjected to functional and biochemical pathway analysis using g:Profiler, a web server for functional enrichment analysis and conversions of gene lists. Enrichment blots were generated in Python using the Matplotlib library and the Spyder programming environment.¹⁶⁴

3.16 Isolation of primary TECs from mice

Kidneys were isolated, mechanically crushed and incubated in digestion buffer containing 1 mg/ml collagenase for 30 min at 37°C. Tissue lysates were resuspended in DBPS and passed through cell filters. Tubular cells were resuspended in DMEM supplemented with 10% bovine calf serum, 50 U/ml penicillin, 50 mg/ml streptomycin, and a hormone mixture (1.25 ng/ml prostaglandin E1, 34 pg/ml triiodothyronine, 50 nM hydrocortisone, and 25 ng/ml epidermal growth factor, insulin-transferrin-selenium) and transferred into a cell culture flask. 50% of the medium was changed every second day for 2 weeks.¹⁶⁷

3.17 Isolation of primary bone marrow-derived macrophages (BMDMs) from mice

Mice were killed by cervical dislocation. Subsequently, the pelvic bones, femur and tibia were dissected using sterile techniques. Texwipes were used to mechanically clean the tissue from the bones. The cleaned bones were crushed several times using a pestle and washed with DPBS. Bone marrow cells were collected after filtration through a 70- μ m cell strainer and centrifuged at 1400 rpm at RT for 5 min. The supernatant was decanted and the pellet resuspended in ammonium chloride-potassium buffer to lyse the erythrocytes. After washing, the cells were cultured in DMEM medium supplemented with 10% fetal bovine serum and 50 U/ml penicillin, 50 mg/ml streptomycin, and 10 ng/ml M-CSF overnight in a cell culture plate. The next day, nonadherent cells were cultured for 6 days in the cell culture medium with 10 ng/ml M-CSF. Half of the medium was replaced daily.^{164,167}

3.18 *In vitro* hypoxia/reoxygenation (HR) and ferroptosis model

The oxygen-glucose deprivation (OGD) and reoxygenation model for primary renal TECs was chosen for *in vitro* analysis. Therefore, cells were maintained in DPBS (+CaCl₂ +MgCl₂) in a hypoxic atmosphere containing 1% O₂, 94% N₂ and 5% CO₂ for 6 h. For reoxygenation, cells were again maintained in complete medium and 21% O₂. Control cells were continually treated with 21% O₂. For the induction of ferroptosis, 1.13 μ M RSL3 (Sellek Chemicals) was added to OGD treated cells. 10 μ M N-acetyl-L-cysteine (NAC, Sigma Aldrich) was used as antioxidant.

3.19 Immunofluorescence staining of cells on glass slides

Cultured TECs were seeded onto glass slides. For mitochondrial staining, 200 nM MitoTracker Red CMXRos was used according to the manufacturer's instructions. Cells were fixed with 4% PFA and permeabilized. Primary antibodies against DbpA and fluorescence-labeled secondary antibodies were incubated subsequently (**Table 7**). Alexa Fluor 488 phalloidin was used to visualize the actin/cytoskeleton. Glass slides were mounted with ProLong Gold Antifade mountant with DAPI. Leica DM6000B microscope was used with Leica application suite advanced fluorescence software.

3.20 Metabolism assays

The Agilent Seahorse XF mito stress test, XF glycolysis stress test, advanced XF palmitate oxidation stress test and XFe96 Analyzer were used according to the manufacturer's instructions. Cells were counted and the same number of cells were pipetted for each genotype per well in the Seahorse experiments. In addition, cells were examined microscopically for adherence to the culture plates immediately before Seahorse quantifications. Cell nuclei were stained by Hoechst dye and fluorescence intensities (FI) per well were determined.

Glucose uptake was measured by the 2-NBDG assay, according to the manufacturer's instructions. MitoSOX Red mitochondrial superoxide indicator was used according to the manufacturer's specifications to detect mitochondrial superoxide levels. Adherent cells were stained, and MitoSOX fluorescence intensity was measured using a fluorescence plate reader (Ex/Em= 510/580 nm). TMRE-mitochondrial membrane potential assay kit was used according to the manufacturer's instructions. Adherent cells were stained and TMRE fluorescence intensity was measured using a fluorescence plate reader (Ex/Em= 549/575 nm). For determination of mitochondrial mass, primary cells were stained with 200 nM MitoTracker Red CMXRos according to the manufacturer's instructions. Fluorescence intensity was measured using a fluorescence plate reader (Ex/Em= 579/599 nm). To determine mitochondrial copy number, total DNA was isolated from primary cells using the FlexiGene DNA kit. Primers against three different regions of mitochondrial DNA (*mt1*, *mt2*, *mt3*), and three regions of genomic DNA (*B2m*, *Tuba1a*, *β -actin*) were used (**Table 5**). Quantitative real time PCR was performed using SYBR Green qPCR MasterMix. The mtDNA copy numbers were calculated relative to genomic DNA as previously described.¹⁷² ATP concentrations are directly quantified by ATP determination kit. Uptake of short- or medium-chain fatty acids was measured by incubation with C1-BODIPY 500/510. For long-chain fatty acid uptake, cells were incubated with BODIPY FL C16. LDL uptake was quantified by incubation with low density lipoprotein from human plasma BODIPY FL. Uptake of cholesterol was determined by incubation with NBD-Cholesterol.

3.21 Mitochondria fractionation and transfer

Mitochondria/cytosol fractionation was performed using the mitochondria/cytosol fractionation kit according to the manufacturer's instructions. Mitochondria were transferred as described previously¹⁷³. In brief, isolated mitochondrial pellets were resuspended in DPBS (+CaCl₂ +MgCl₂) and kept on ice. Recipient cells were transferred to a microcentrifuge tube containing cell culture medium and were kept on ice for transfer. The mitochondrial suspension was slowly added to each tube containing recipient cells. For TECs, 100 μ g of isolated mitochondrial fraction was added to 4x10⁵ primary recipient cells. For BMDMs, 200 μ g of isolated mitochondria was used for transfer. Tubes were centrifuged at 1500 g for 5 min at 4°C. Cells were rinsed twice with DPBS (+CaCl₂ +MgCl₂). Cells were transferred to a Seahorse XF96 cell culture microplate (TECs: 10,000 cells/well and BMDMs: 20,000 cells/well) and rested overnight in cell culture medium. Mito stress test was used according to the manufacturer's instructions to determine mitochondrial respiration. To confirm successful mitochondrial transfers, donor cells were stained with 200 nM MitoTracker Red CMXRos and recipient cells were stained with 200 nM MitoTracker Green prior mitochondrial isolation and transfer. Medium was replaced by DBPS (+CaCl₂ +MgCl₂) and cells were stained with Hoechst 33342.

Zeiss Axiovert 200M inverted fluorescence microscope was used to visualize mitochondrial transfer of live cells.

3.22 Cell death assay using time-lapse microscopy

Cells were seeded into cell culture dishes and rested overnight. The medium was replaced by DBPS (+CaCl₂ +MgCl₂) containing 50 nm SYTOX Green nucleic acid stain (Invitrogen) and 1.13 μM RSL3 (Sellek Chemicals). Repetitive images were acquired for all fields of view over 24 h for TECs. First, cells were kept under normoxic conditions (21% O₂) for 30 min. Thereafter, the O₂ content was reduced to a hypoxic atmosphere containing 1% O₂. For the analysis of cell death, SYTOX-positive nuclei were counted per image.

3.23 Knockdown of DbpA by lentiviral transduction

DbpA knockdown was performed as previously described.⁶² DbpA small hairpin RNA (shRNA, Sigma-Aldrich, SHCLNG, shRNA_1: NM011733, shRNA_2: NM003651) and scrambled shRNA vectors were used. Human embryonic kidney cells (HEK Lenti X) were cotransfected with 3 μg DbpA constructs plasmid, 3 μg psPAX2, and 1 μg pVSV-G after growing to 70% confluence. The transfection was performed with metafectene and opti-MEM in antibiotic-free medium. After 1 day, medium was exchanged with normal culture medium, which contained the produced virus and cultured for another 24 h. Virus containing supernatant was harvested and filtered. 4 μg/ml polybrene was added and a human-derived renal proximal tubular cell line (HKC-8) and a mouse proximal tubule-derived cell line (BUMPT) as target cells were infected. Cells were centrifuged for 2 h at 33°C and 2000 rpm and the medium was exchanged to fresh medium. Target cells were used 3 days after the transduction for additional analysis.⁶²

3.24 Microarray data

Gene expression dataset GSE30718 was downloaded from GEO (<http://www.ncbi.nlm.nih.gov/geo>)¹⁷⁴ and contained microarray data sets from 28 AKI biopsies and 11 protocol biopsies.¹⁷⁵

3.25 Statistical Analysis

All results were confirmed as triplicates in at least two independent experiments. Data are presented as mean values. Statistical analysis was performed using GraphPad™ prism 8. For survival experiments log-rank tests were applied. One-way ANOVA followed by post hoc Tukey's multiple comparisons test was used for data sets with more than two groups. Student's t-test was used to compare two experimental groups. Data were considered significant when *P*-values reached < 0.05.¹⁶⁶

4 Results

4.1 Phenotyping of $Ybx3^{+/+}$, $Ybx3^{+/-}$ and $Ybx3^{-/-}$ mice

4.1.1 Phenotyping and long-term survival of mice with genetic $Ybx3$ deletion

The genetically modified $Ybx3^{-/-}$ animals have been phenotyped before.⁹ No defect in embryonic development or animal survival rates until an age of 12 months were observed. However, male knockout mice are less fertile with reduced testis weight due to seminiferous tubule degradation and enhanced spermatocyte apoptosis. Male mice testosterone levels were not different between the wild type and knockout animals.⁹

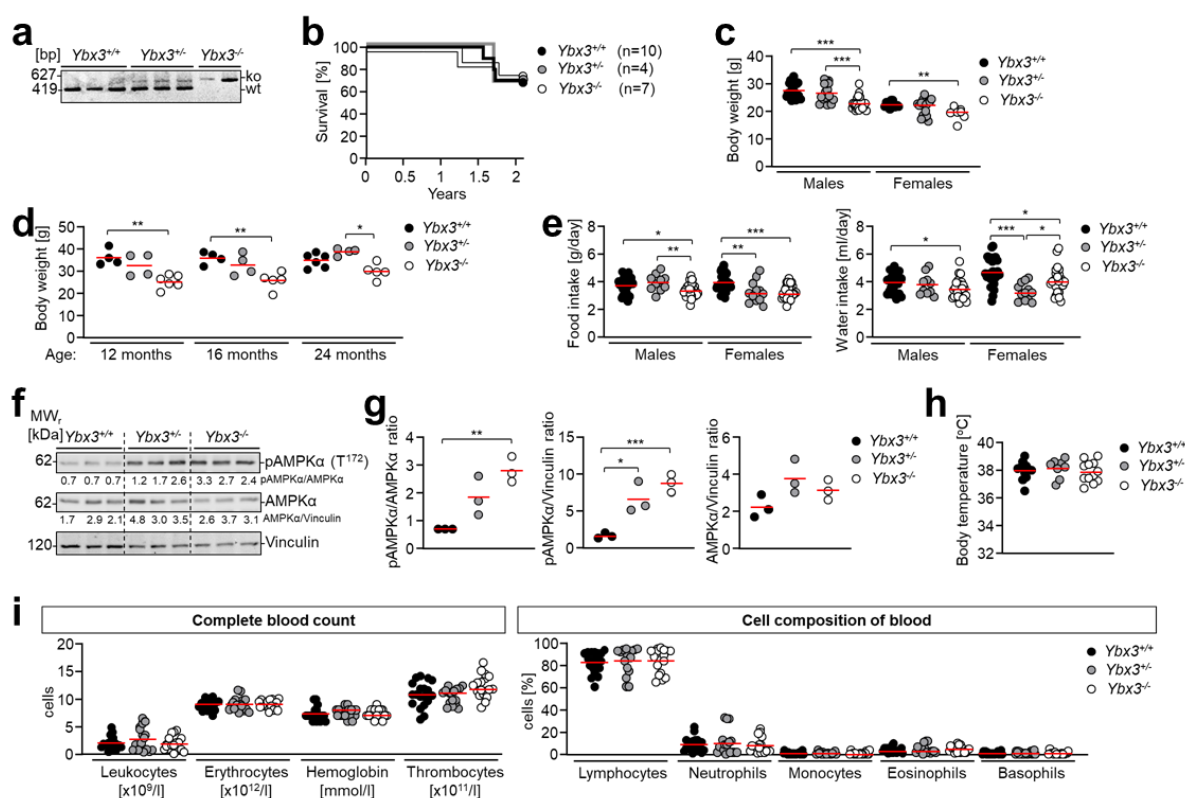


Figure 7. Phenotyping and long-term survival of mice with genetic $Ybx3$ deletion.

(a) Genotyping revealed deletion of $Ybx3$ in $Ybx3^{+/-}$ or $Ybx3^{-/-}$ animals. (b) Survival analysis over 2 years demonstrated no differences in the mortality rates between wild type (n=10), $Ybx3^{+/-}$ (n=4) and $Ybx3^{-/-}$ (n=7) mice. (c) In male and female mice aged 3 months (n=9-20) body weights were significantly lower in $Ybx3^{-/-}$ animals compared to wild type animals. (d) 12, 16, and 24-months-old $Ybx3^{-/-}$ male mice (n=4-6) showed consistently lower body weights compared to wild type and $Ybx3^{+/-}$ animals. (e) In male and female mice aged 3 months (n=9-30) food and water intake were significantly lower in $Ybx3^{-/-}$ animals. (f) Given the lowered body weight and reduced food/water intake, Western blot analyses for AMPK α as a key enzyme in energy metabolism were performed with kidney lysates from mice aged 10-12 weeks. (g) The pAMPK α (T¹⁷²)/AMPK α and pAMPK α (T¹⁷²)/vinculin ratios were significantly higher in $Ybx3^{+/-}$ and $Ybx3^{-/-}$ compared to wild type animals. (h) Body temperatures determined by rectal thermometers were not different in the strains. (i) Complete blood count (leukocytes, erythrocytes, hemoglobin and thrombocytes) was not altered in 3-months-old mice when $Ybx3$ was deleted. In addition, cell composition of blood (lymphocytes, neutrophils, monocytes, eosinophils, and basophiles) was similar in animals. Data represent mean values. All results were confirmed as triplicates in at least 2 independent experiments. One-way analysis of variance followed by Tukey *post hoc* test was used for comparisons of 3 groups. Student's *t* test was used when 2 experimental groups were compared with * $P < 0.05$, ** $P < 0.01$, *** $P < 0.001$.

First, a phenotyping of kidneys in $Ybx3^{+/+}$, $Ybx3^{-/-}$ and $Ybx3^{+/-}$ animals (**Figure 7a**) up to 2 years of age was performed. Mortality rates were similar for $Ybx3^{+/+}$, $Ybx3^{-/-}$ and $Ybx3^{+/-}$ mice (**Figure 7b**). Compared to wild type animals, a significantly lower body weight became apparent in $Ybx3^{-/-}$ male and female mice, which however remained within the normal range of 20-40 g (**Figure 7c**). A lower body weight of $Ybx3^{-/-}$ mice became apparent over time up to 24 months (**Figure 7d**). Reduced food and water intake indicated a relative fasting state (**Figure 7e**). The nutrient and energy sensor AMPK α was abundantly detected as a phosphorylated protein. Increased phosphorylation of AMPK α (pAMPK α) was observed in kidney lysates from mice with heterozygous or homozygous $Ybx3$ knockout (**Figures 7f-g**). Reduced body weights did not affect rectal core body temperature, an indicator of energy consumption (**Figure 7h**). Complete blood cell count and cell composition of blood were similar in wild type, $Ybx3^{+/+}$ and $Ybx3^{-/-}$ animals (**Figure 7i**).

Overall, our data demonstrated an unrestricted life expectancy in $Ybx3^{-/-}$ mice. The lower body weights of the $Ybx3^{-/-}$ animals and the detection of abundant pAMPK α enzyme suggested unknown functions of DbpA related to energy homeostasis.

4.1.2 DbpA is expressed in tubular structures of healthy kidneys

DbpA is described to be predominantly expressed during embryogenesis¹² and restricted later on, except in smooth muscle cells and testis.⁹

Immunohistochemistry in kidneys of wild type animals revealed DbpA positivity in smooth muscle cells, podocytes, and tubular cells (**Figure 8a**), which corroborated with the Healthy Mouse Dataset¹⁷⁶ (**Figure 8b**). Immunofluorescence staining of DbpA and sodium-glucose cotransporter-2 (SGLT2) or Aqp2 confirmed tubular localization of DbpA in the kidney cortex and medulla of healthy wild type mice (**Figure 8c**). Western blot analyses of kidney lysates from 3 and 24 months-old mice demonstrated less DbpA_a and DbpA_b expression in $Ybx3^{+/-}$ animals, and almost no DbpA isoforms were detected in $Ybx3^{-/-}$ animals (**Figures 8d-e**). In addition, DbpA_a and DbpA_b were detected in healthy liver tissues of young and old mice (**Figures 8f-g**).

Taken together, in addition to previous literature, we were able to show, that DbpA was not only expressed except in smooth muscle cells and testis but DbpA is also present in podocytes and TECs in healthy kidney of adult mice.

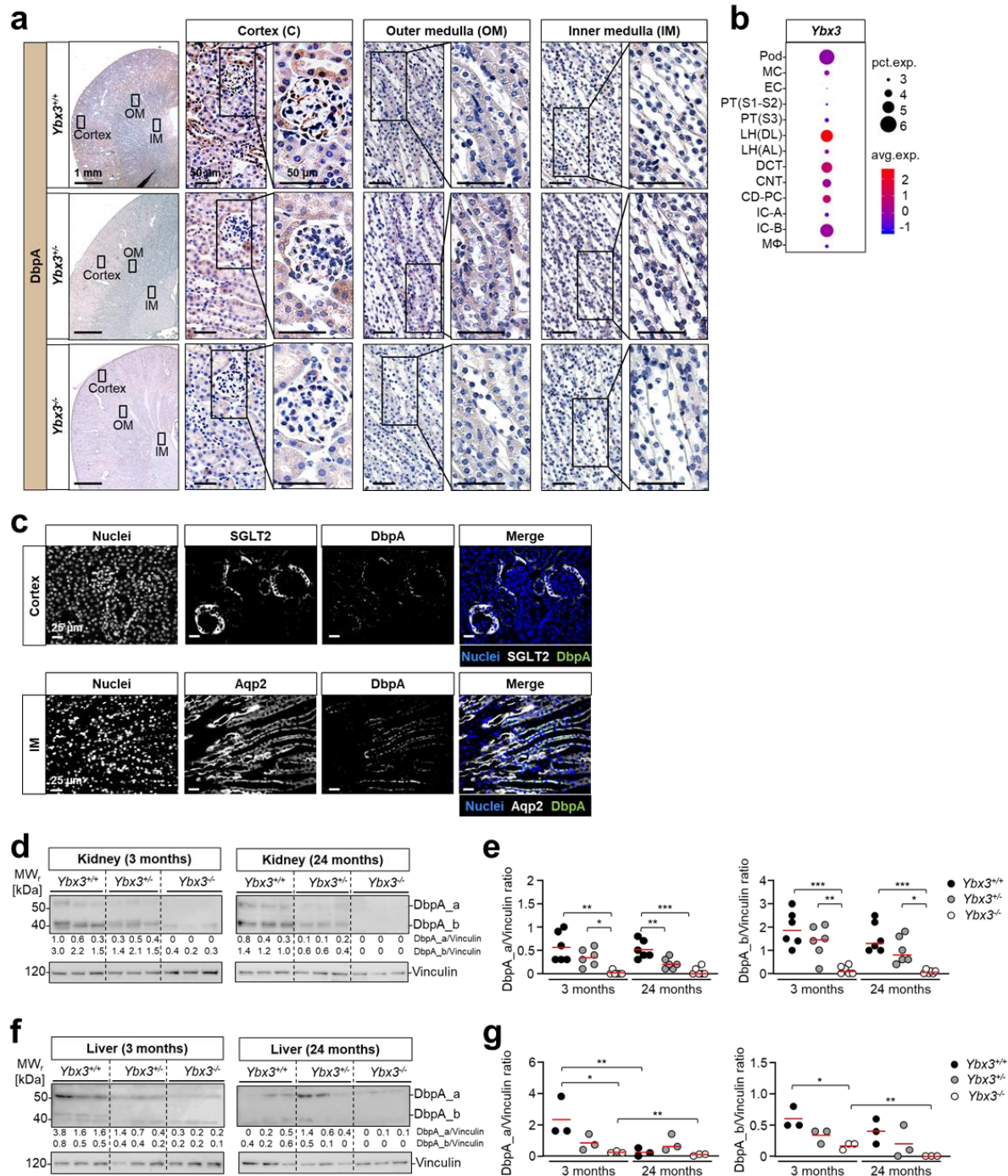


Figure 8. DbpA is expressed in healthy kidneys and liver.

(a) Immunohistochemistry of kidney tissue from 3 months old wild type mice with the anti-C-terminal antibody demonstrated DbpA immunopositive staining in smooth muscle cells from small vessels, individual distal tubular cells, glomerular podocytes and mesangial cells. *Ybx3^{+/-}* and *Ybx3^{-/-}* animals exhibited lower or absent DbpA expression in the respective cells. Scale bars, 1 mm or 50 µm. (b) Single cell sequencing data sets (Healthy Mouse Dataset 32, KIT software, <http://humphreyslab.com/SingleCell/>, accessed on 22.04.2022) revealed abundant *Ybx3* transcripts in podocytes and distal tubular cells matched with immunohistochemistry findings. Diameters of circles represent the number of positive cells and the color changes according to *Ybx3* transcript numbers. (c) Immunofluorescence staining of kidney sections revealed co-localization of DbpA with the proximal tubule marker SGLT2 and distal tubule marker Aqp2. Scale bars, 25 µm. (d) By means of a polyclonal anti-C-terminal antibody, two DbpA isoforms (DbpA_a, DbpA_b) were detected in kidney tissue lysates. (e) DbpA_a was detected at low levels in *Ybx3^{+/+}* and *Ybx3^{+/-}* animals. DbpA_b expression was predominant in kidney lysates of young and old *Ybx3^{+/+}* and *Ybx3^{+/-}* animals, whereas in *Ybx3^{-/-}* animals both isoforms were absent. (f) Western blotting revealed two DbpA isoforms (DbpA_a, DbpA_b) in liver tissue lysates. (g) The expression levels were lower at 24 months compared to 3 months. *Ybx3^{+/-}* animals revealed no clear reduction in the expression of DbpA at 24 months in the liver, whereas in *Ybx3^{-/-}* animals both isoforms were almost absent. Higher expression levels of isoform DbpA_a were detected. -Figure legend continued on the next page-

-continued- Abbreviations: podocyte (Pod), mesangial cell (MC), endothelial cell (EC), proximal tubule (PT), loop of Henle descending loop (LH(DL)), loop of Henle ascending loop (LH(AL)), distal convoluted tubule (DCT), connecting tubule (CNT), collecting duct-principal cell (CD-PC), intercalated cell type A (IC-A), intercalated cell type B (IC-B), macrophage (MΦ). Data represent mean values. All results were confirmed as triplicates in at least 2 independent experiments. One-way analysis of variance followed by Tukey *post hoc* test was used for comparisons of 3 groups. Student's *t* test was used when 2 experimental groups were compared with **P* < 0.05, ***P* < 0.01, ****P* < 0.001.

4.1.3 DbpA is dispensable for kidney development, function and tissue homeostasis under healthy conditions

Given the report by Lima et al. describing high level *Ybx3* expression in cycling tubular cells during kidney ontogeny¹², we hypothesized that a severe tubular cell defect exists in *Ybx3* deficient animals. Contrary to these expectations, PAS staining confirmed normal glomerular and tubular structures in the cortex (C), and similar tubular structures in the outer (OM) and inner medulla (IM), when *Ybx3* was genetically deleted (**Figure 9a**). Furthermore, kidney function assessments of plasma creatinine, BUN and GFR (**Figure 9b**) were similar in wild type, *Ybx3*^{+/-} and *Ybx3*^{-/-} animals. Urine analyses (osmolality, pH, urine output, albuminuria and proteinuria) were equally for all genotypes under healthy conditions (**Figure 9c**).

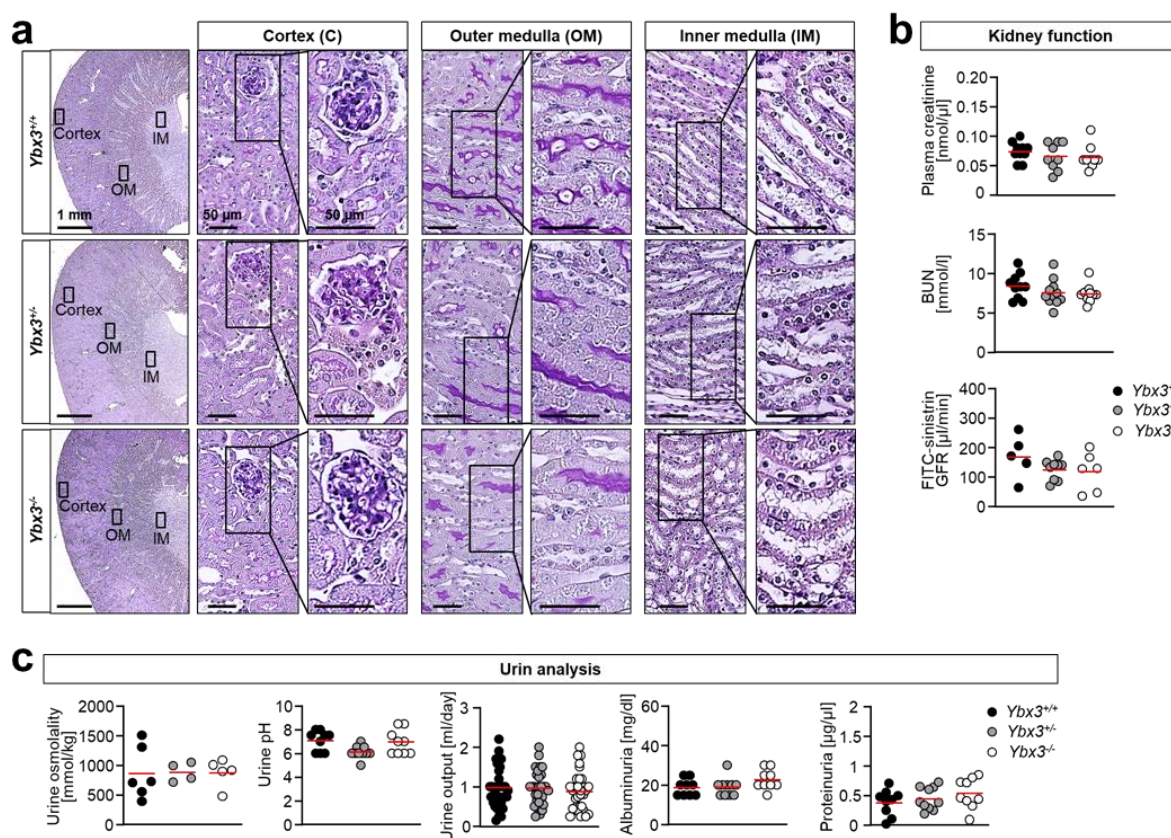


Figure 9. Kidney function is preserved despite genetic deletion of DbpA.

(a) In wild type and *Ybx3*^{-/-} animals the kidney architecture was not different, that was the appearance of nephron segments and substructures corresponding to the cortex, OM and IM. Scale bars, 1 mm or 50 μm. (b) Kidney function assessed by plasma creatinine, BUN and GFR revealed values within normal range. (c) Urine analysis demonstrated similar urine osmolality, pH values and urine output in the different strains and absence of relevant albuminuria and proteinuria. Data represent mean values. All results were confirmed as triplicates in at least 2 independent experiments. One-way analysis of variance followed by Tukey *post hoc* test was used for comparisons of 3 groups. Student's *t* test was used when 2 experimental groups were compared.

Since DbpA is expressed during early development, we expect that DbpA has an impact on the TECs composition in the kidney.¹⁷⁷

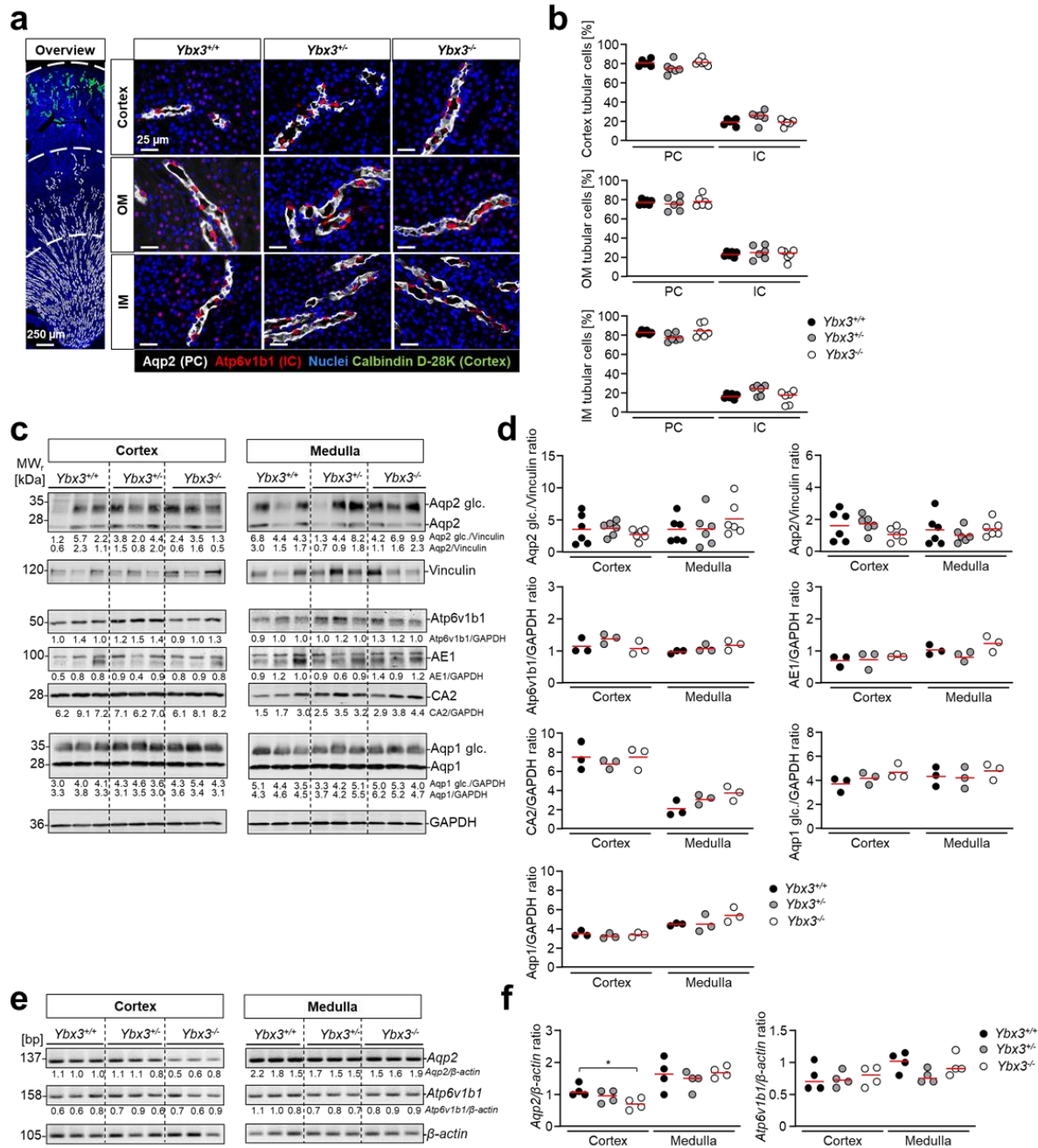


Figure 10. Tubular cell composition with ion and water transporter expression in wild type and genetically modified animals lacking DbpA.

(a) Immunofluorescence staining for Aqp2 as marker protein for principal cells (PC) and Atp6v1b1 as marker protein for intercalating cells (IC) with (b) quantification of relative cell numbers [%] within the cortex, OM and IM revealed no differences in the examined wild type, *Ybx3*^{+/-} and *Ybx3*^{-/-} animals. Scale bars, 250 μ m or 25 μ m (n=6). (c) Western blotting was performed with kidney tissue lysates that correspond to the cortex as well as medulla to quantify key transporter proteins. Aqp2 and glycosylated Aqp2 as marker proteins for PC and Atp6v1b1, AE1 and CA2 for IC marker proteins were tested. Furthermore, Aqp1 and glycosylated Aqp1 functioned as marker proteins for proximal tubule. (d) Distal and proximal cell phenotypes seemed to be unaltered by changes of the *Ybx3* genotype. The expressions of PC and IC marker proteins as well as Aqp1 were similar in all strains. (e and f) Semiquantitative PCR with cortex but not medulla tissue yielded lowered copy numbers for *Aqp2* transcripts in *Ybx3*^{-/-} compared to *Ybx3*^{+/-} and *Ybx3*^{+/+} animals. *Atp6v1b1* transcript numbers were similar in all genotypes. Data represent mean values. All results were confirmed as triplicates in at least 2 independent experiments. One-way analysis of variance followed by Tukey *post hoc* test was used for comparisons of 3 groups. Student's *t* test was used when 2 experimental groups were compared with **P* < 0.05.

Immunohistochemistry for key proteins of water reabsorption (PC, principal cells) and pH regulation (IC, intercalated cells) revealed no differences in the average PC and IC numbers along the nephrons in the cortex, OM and IM of *Ybx3^{+/-}* and *Ybx3^{-/-}* mice (**Figures 10a-b**). These data were confirmed by Western blot analyses of PC (Aqp2, glycosylated Aqp2) and IC marker proteins (Atp6v1b1, carbonic anhydrase 2 (CA2), anion exchanger 1 (AE1)), as well as proximal tubular proteins (Aqp1, glycosylated Aqp1) of kidney cortex and medulla tissue lysates (**Figures 10c-d**). Merely transcript numbers of *Aqp2* were decreased in the kidney cortex of *Ybx3^{-/-}* mice compared to *Ybx3^{+/+}* and *Ybx3^{+/-}* animals (**Figures 10e-f**).

In summary, DbpA is dispensable for kidney development, function and tissue homeostasis under healthy conditions. DbpA deletion does not affect TEC composition in the kidney. However, subtle differences exist in *Aqp2* expression.

4.2 Tubular expression of DbpA inversely correlates with metabolic processes

Kidneys are in demand of a large amount of energy in form of ATP, which is provided through mitochondrial respiration.

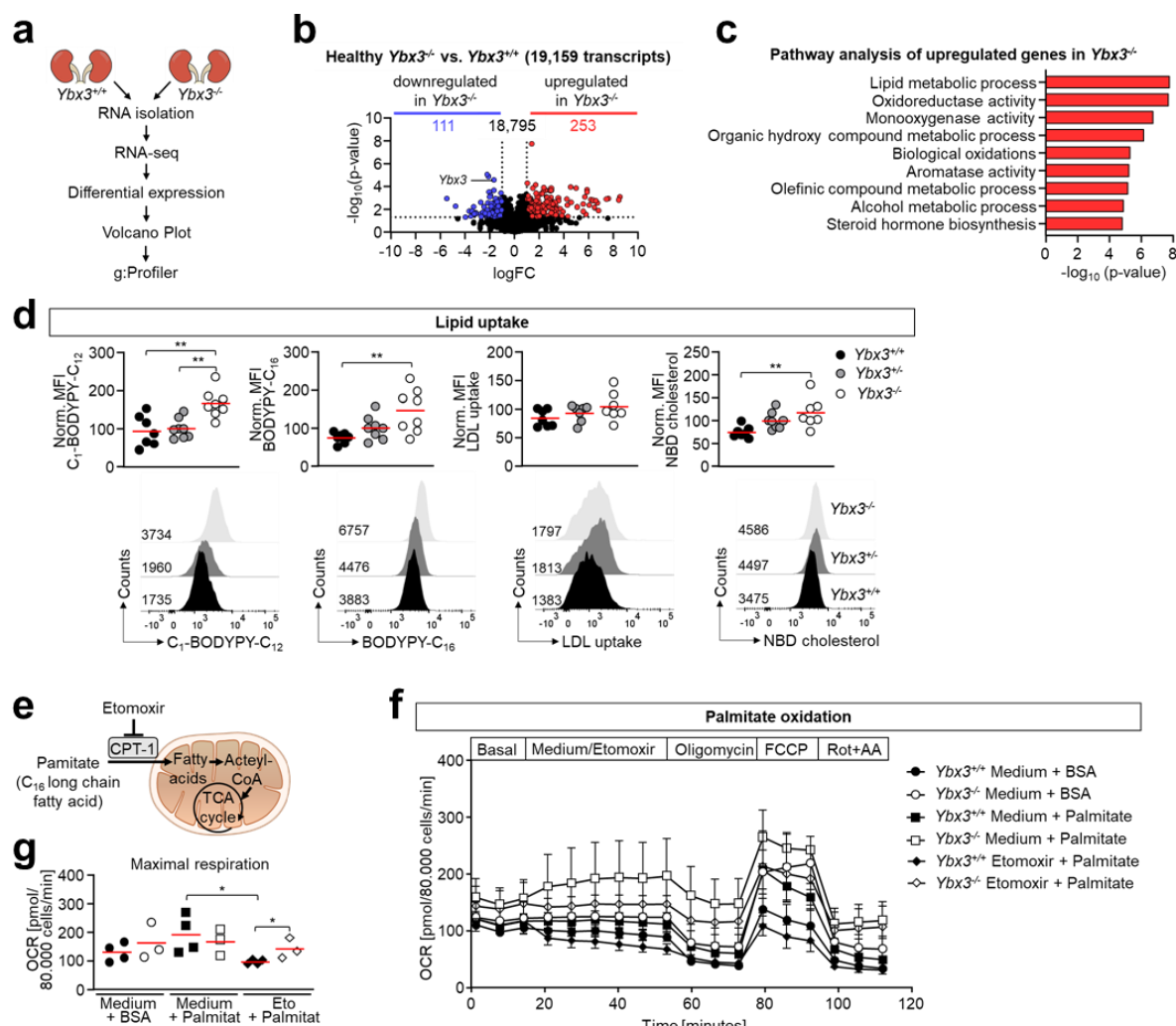


Figure 11. Tubular expression of DbpA inversely correlates with lipid metabolic processes.

(a) Total RNA from kidneys from healthy wild type and *Ybx3^{-/-}* mice aged 9-15 weeks ($n=3$) were isolated and RNA-seq was performed. -Figure legend continued on the next page-

-continued- (b) Whole RNA-seq data (19,159 transcripts) were summarized in a Volcano plot of differentially expressed genes of healthy kidneys from *Ybx3*^{+/+} versus *Ybx3*^{-/-} mice. The most significantly upregulated genes in *Ybx3*^{-/-} mice are shown in red, whereas blue represent the significantly downregulated genes compared to wild type kidneys. Black dots are genes that were differentially expressed below the cutoff values of log-fold change (logFC) and $-\log_{10}$ of the p-value. Significantly regulated transcripts were those with a logFC $\leq \pm 1$ and $-\log_{10}$ (p-value) > 1.3 (dotted lines). (c) Pathway analysis of upregulated genes in *Ybx3*^{-/-} kidneys revealed a strong connection to metabolic pathways and processes. (d) Lipid uptake was analyzed by flow cytometry. *Ybx3*^{-/-} TECs revealed significantly higher lipid uptake than wild type cells. Histograms show representative lipid uptake of *Ybx3*^{+/+}, *Ybx3*^{-/-} and *Ybx3*^{-/-} TECs (n=7-8). (e) Palmitate oxidation stress test was used to analyze long chain fatty acids (LCFAs) oxidation in cells. Etomoxir inhibits the metabolism of LCFAs through the inhibition of carnitine palmitoyl transferase 1a (CPT1a). (f-g) Basal and maximal OCR was increased in *Ybx3*^{-/-} TECs compared to wild type in the control groups (medium + BSA). Furthermore, basal and maximal OCR significantly increased upon palmitic acid supply, suggesting efficient palmitate metabolism. This increase in OCR was inhibited by the CPT1a inhibitor etomoxir, affirming its specificity. Additionally, TECs isolated from *Ybx3* knockout mice exhibited higher OCR associated with fatty acid oxidation (FAO) compared to those from wild type mice. Wild type TECs were more susceptible to etomoxir (n=3-4). OCR data were normalized to cell numbers. Data represent mean values. All results were confirmed as triplicates in at least 2 independent experiments. One-way analysis of variance followed by Tukey *post hoc* test was used for comparisons of 3 groups. Student's *t* test was used when 2 experimental groups were compared with **P* < 0.05, ***P* < 0.01.

In our quest to identify differential regulated pathways in *Ybx3*^{-/-} animals, kidneys from healthy mice were harvested to generate Agilent Micro Array libraries (**Figure 11a**). 364 differentially expressed genes were identified (**Figure 11b**). Gene set enrichment analysis revealed that the most significantly upregulated genes in the kidneys from *Ybx3*^{-/-} mice related to metabolic processes, especially lipid metabolic processes (**Figure 11c**). The uptake of short- and long-chain fatty acids (**Figure 11d**) as well as the OCR associated with fatty acid oxidation (FAO) were increased when *Ybx3* was genetically deleted (**Figures 11e-g**).

Functional metabolic analyses of *Ybx3*^{-/-} TECs revealed increased mitochondrial respiration in terms of OCR (**Figures 12a-c**), intracellular ATP content (**Figure 12d**), glycolysis (**Figures 12e-g**) and glucose uptake (**Figure 12h**). This indicates a higher metabolic activity and increased energy supply in *Ybx3* deficient TECs. However, uptake of the amino acid analog BPA was not significantly different in the tubular cells with knockout (**Figure 12i**). Transcriptome analyses of amino acid transporters revealed differential abundance of single transporters (**Figure 12j**).

In summary, these data revealed that genetic deletion of *Ybx3* in TECs increased the metabolic activity by upregulating genes related to metabolic processes.

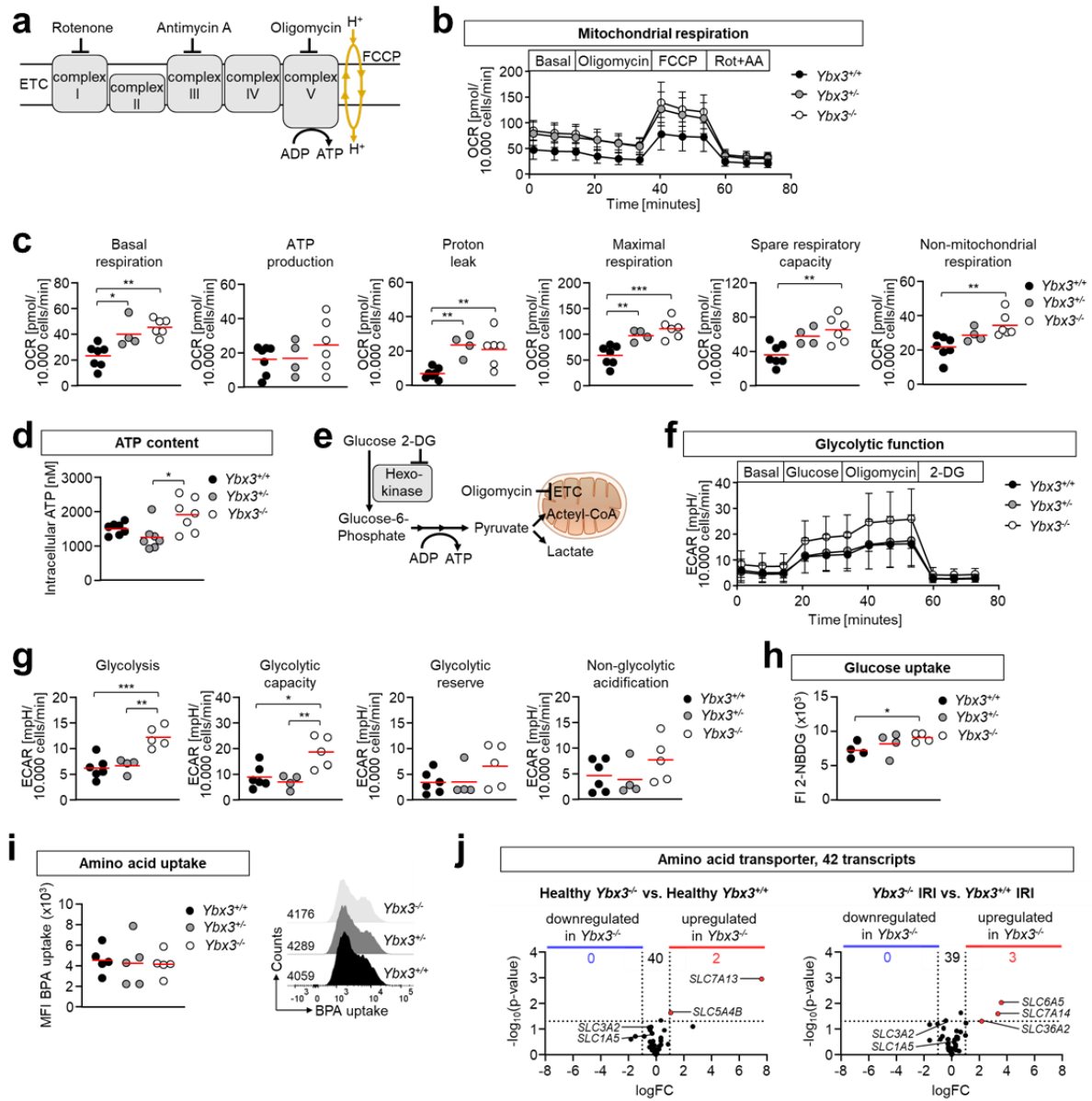


Figure 12. Tubular expression of DbpA inversely correlates with the mitochondrial oxygen consumption rate and glycolysis.

(a) Mito stress test was used to determine mitochondrial respiration. Oligomycin was injected first following basal measurement and inhibited the ATP synthase (complex V). Carbonyl cyanide-4 (trifluoromethoxy) phenylhydrazone (FCCP) is an uncoupling agent that collapses the proton gradient. Electron flow through the ETC is uninhibited, and oxygen consumption by complex IV reaches the maximum. Rotenone (complex I inhibitor) and antimycin A (complex III inhibitor) shut down the mitochondrial respiration. (b) OCR of TECs from *Ybx3*^{+/+}, *Ybx3*^{+/-} and *Ybx3*^{-/-} mice were quantified. OCR were measured under basal level and following addition of 1 μM oligomycin, 1 μM FCCP and 0.5 μM rotenone + antimycin A (Rot+AA). OCR data were normalized to cell numbers. Genetic deletion of *Ybx3* led to elevated basal and stimulated OCR (n=7-4). (c) Individual parameters for basal respiration, ATP production, proton leakage, maximal respiration rate, spare respiratory capacity and non-mitochondrial oxygen consumption were calculated based on the mitochondrial respiration profiles. All parameters were increased in *Ybx3*^{+/-} or *Ybx3*^{-/-} cells compared to *Ybx3*^{+/+} cells, except for ATP production. Data were normalized to cell numbers. (d) Intracellular ATP concentrations were directly quantified by ATP determination kit and revealed significantly higher ATP levels in *Ybx3*^{-/-} compared to *Ybx3*^{+/-} TECs (n=7). (e) Agilent Seahorse XF glycolysis stress test was used to analyze glycolysis. Glucose fuels glycolysis, whereas oligomycin inhibits ATP synthase in the mitochondria resulting in a state of glycolysis-dependency. 2-deoxy-glucose (2-DG) is a competitive inhibitor of glucose and shuts down glycolysis. (f) Enhanced glycolytic activity of *Ybx3*^{-/-} cells was detected by extracellular acidification rates (ECAR) of TECs from *Ybx3*^{+/+}, *Ybx3*^{+/-} and *Ybx3*^{-/-} mice (Seahorse XF glycolysis stress test). Under basal conditions and following addition of 10 mM glucose, 1 μM oligomycin and 50 mM 2-DG the ECAR levels were measured. Basal ECAR levels were similar in TECs from *Ybx3*^{+/+}, *Ybx3*^{+/-} and *Ybx3*^{-/-} mice, whereas the addition of glucose led to increased glycolysis in cells with *Ybx3*^{-/-} genotype (n=4-6). Data were normalized to cell numbers analyzed per well. -Figure legend continued on the next page-

-continued- (g) Individual parameters for glycolysis, glycolytic capacity, glycolytic reserve and non-glycolytic acidification were calculated based on the glycolysis stress test profile. Glycolysis and glycolytic capacity were increased in $Ybx3^{-/-}$ compared to $Ybx3^{+/+}$ and wild type cells. (h) These data were confirmed by the detection of 2-NBDG, a fluorescently-labeled deoxy-glucose analog, as a measurement of glucose uptake by cultured TECs ($n=4$, kidneys from three mice were pooled in each experiment). (i) The uptake of the fluorescence-labeled amino acid analog boronophenylalanine (BPA) was detected. It was quantified in primary TECs and did not reveal differences between the genotypes. Histogram shows representative BPA uptake of $Ybx3^{+/+}$, $Ybx3^{+/-}$ and $Ybx3^{-/-}$ TECs ($n=5$) (j) Transcripts related to amino acid transporters were retrieved from RNA-seq data. Here, *solute carrier family 7 member 13 (SLC7A13)* and *solute carrier family 5 (neutral amino acid transporters, system A), member 4b (SLC5A4B)* transcripts were more abundant in kidneys from $Ybx3^{-/-}$ animals, whereas the majority did not show differences between the genotypes. Following IRI *SLC6A5*, *SLC7A14* and *SLC36A2* transcripts were upregulated in kidneys from $Ybx3^{-/-}$ animals in comparison to wild type animals. Blue color indicates down-, red color indicates up-regulation whereas black color indicates not-regulated transcripts. Data represent mean values. All results were confirmed as triplicates in at least 2 independent experiments. One-way analysis of variance followed by Tukey *post hoc* test was used for comparisons of 3 groups. Student's *t* test was used when 2 experimental groups were compared with * $P < 0.05$, ** $P < 0.01$, *** $P < 0.001$.

4.2.1 Mitochondrial transfer equalizes respiratory capacity of TECs

As a vital hub of cellular metabolism and tissue viability, the mitochondrion often undergoes changes in its morphology or localization within the cell in response to various stresses and energy demands.¹⁷⁸ In addition to intracellular changes, mitochondria can also be transferred between cells. This intercellular mitochondrial transfer not only helps to restore stressed cells and damaged tissues due to mitochondrial dysfunction, but also takes place under physiological conditions.^{178,179}

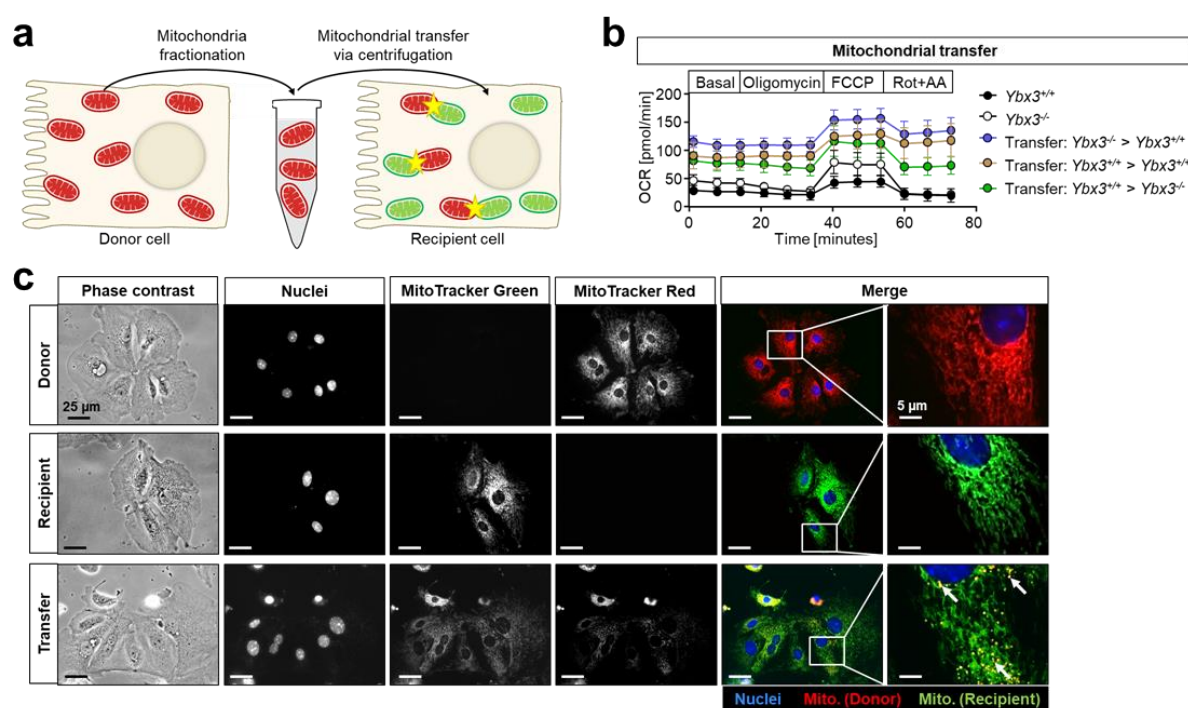


Figure 13. Mitochondrial transfer equalizes respiratory capacity of wild type TECs.

(a) Mitochondria of donor TECs were stained with MitoTracker Red and mitochondria of recipient cells were stained with MitoTracker Green before the transfer of mitochondria. Mitochondria were isolated from TECs derived from $Ybx3^{+/+}$ or $Ybx3^{-/-}$ mice using mitochondria fractionation. Isolated mitochondria were transferred into $Ybx3^{+/+}$ or $Ybx3^{-/-}$ TECs. (b) OCR were quantified by means of a mito stress test. Mitochondrial transfers were able to increase basal and stimulated OCR of TECs. Normalization to cell numbers per well was performed. (c) Successful mitochondrial transfers were confirmed by live cell imaging. Yellow dots indicated a successful transfer of donor mitochondria into recipient cells. Scale bars, 25 μ m or 5 μ m. Data represent mean values. All results were confirmed as triplicates in at least 2 independent experiments.

To test whether a transfer of mitochondria can increase the mitochondrial activity of wild type TECs, we next transferred mitochondria isolated from *Ybx3^{-/-}* TECs into *Ybx3^{+/+}* TECs and vice versa via several centrifugation steps (**Figure 13a**). The highest metabolic activity in terms of the mitochondrial respiration, measured as OCR, was detected, when mitochondria isolated from *Ybx3^{-/-}* TECs were transferred into *Ybx3^{+/+}* TECs (**Figure 13b**, blue curve). Successful transfer of mitochondria into the recipient cells was confirmed by live cell imaging and overlay of fluorescent signals (**Figure 13c**).

In summary, transfer of isolated mitochondria from *Ybx3^{-/-}* TECs can equalize respiratory capacity of *Ybx3^{+/+}* TECs.

4.2.2 An increase in mitochondrial activity can be induced via a lentiviral knockdown of DbpA

In order to be able to classify the function of DbpA in connection with cell metabolism more precisely, an inducible knockdown via lentiviral infection was performed to specifically reduce the expression of DbpA protein in wild type TECs.

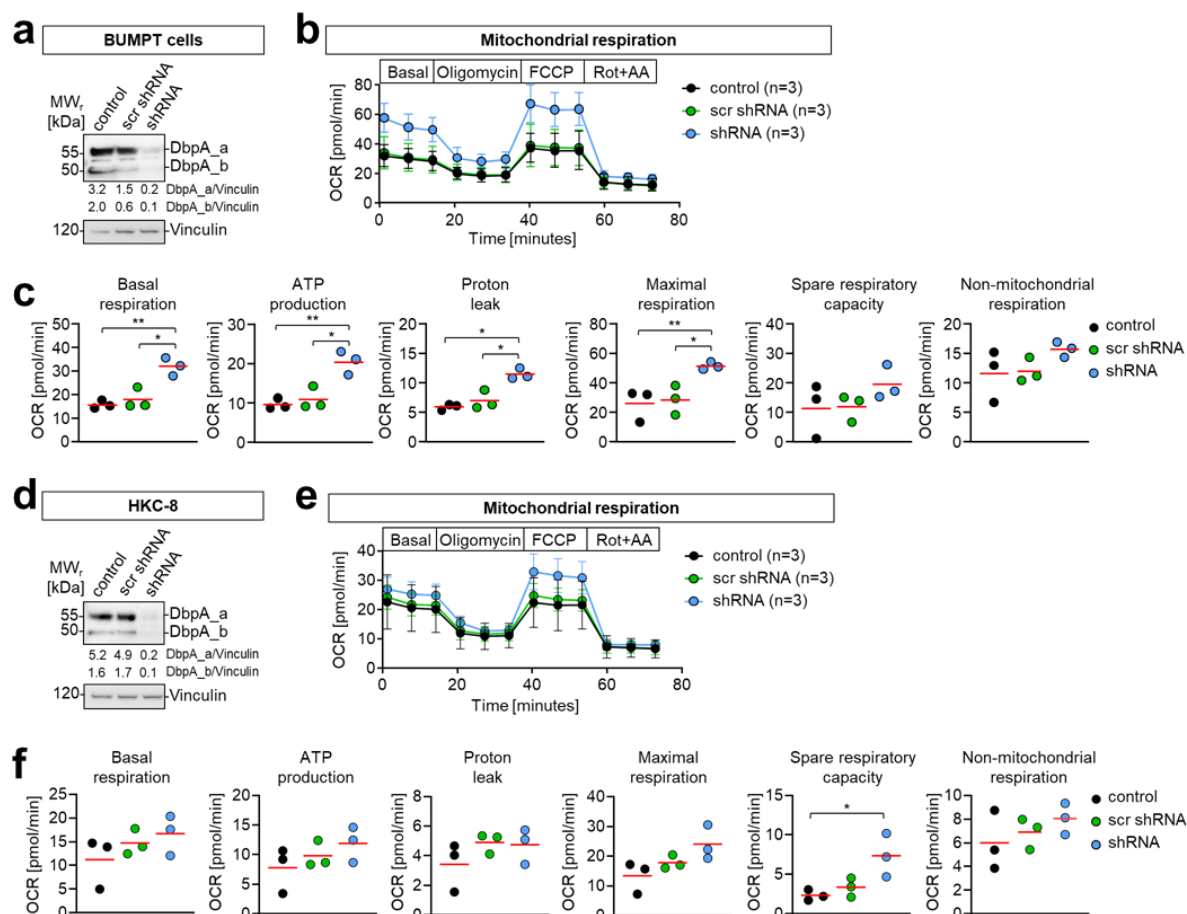


Figure 14. Lentiviral DbpA knockdown leads to increased mitochondrial respiration.

(a) Western blot analysis confirmed successful DbpA knockdown of transcripts by shRNA in an immortalized mouse proximal tubular cell line (BUMPT). (b and c) The mitochondrial respiration was increased following DbpA knockdown as measured by mito stress test (n=3). OCR data were normalized to cell numbers per well. (d) Western blot analysis confirmed successful DbpA knockdown in an immortalized human proximal tubular cell line (HKC-8). -Figure legend continued on the next page-

-continued- (e and f) The mitochondrial respiration, measured as OCR, was increased following DbpA knockdown in HKC-8 cells (n=3). Data represent mean values. All results were confirmed as triplicates in at least 2 independent experiments. One-way analysis of variance followed by Tukey *post hoc* test was used for comparisons of 3 groups. Student's *t* test was used when 2 experimental groups were compared with **P* < 0.05, ***P* < 0.01.

Western blotting of cell lysates indicated a clear knockdown of the isoforms DbpA_a and DbpA_b in BUMPT cells (**Figure 14a**). By means of a lentiviral knockdown of DbpA, an enhanced mitochondrial respiration were revealed (**Figures 14b-c**), indicating an inducible effect on mitochondrial function following DbpA deletion. Similar effects were obtained in a HKC-8 cell line (**Figure 14d-f**).

Thus, we were able to show that DbpA plays a decisive role in the functionality of mitochondrial respiration. Interestingly, an increase in mitochondrial activity can be directly induced by a specific deletion of DbpA in TEC *in vitro*.

4.2.3 DbpA co-localizes with mitochondrial marker proteins

Based on the differences in the metabolic activities of TECs, we next analyzed mitochondrial mass by MitoTracker fluorescence intensities and mtDNA copy numbers of isolated TECs. The aim was to investigate, whether the increased metabolic activity correlates with an increased number of mitochondria in TECs isolated from *Ybx3^{-/-}* animals. Mitochondrial mass and numbers were similar (**Figures 15a-b**), however the mitochondrial membrane potential was significantly increased in TECs isolated from *Ybx3^{-/-}* mice compared to wild type animals (**Figure 15c**). Furthermore, electron microscopic analysis of healthy kidney tissues of mice with different genotypes revealed intact outer and inner mitochondrial membranes (**Figure 15d**). Western blot analysis of proteins related to the ETC revealed increased expression of ATP5A (ETC complex V) and UQCRC2 (ETC complex III) in TECs of *Ybx3^{-/-}* mice, MTCO1 (ETC complex IV) and SDHB (ETC complex II) were less expressed in *Ybx3^{-/-}* cells (**Figures 15e-f**). In addition to the already described cytoplasmic, nuclear and cell-membrane localization²⁵, we identified DbpA co-localization with mitochondrial marker proteins in TECs derived from *Ybx3^{+/+}* and *Ybx3^{+/-}* mice. Western blot analyses detected DbpA in the cytoplasm/nuclear fraction as well as in the mitochondrial fractions (**Figure 15g**). These data were verified by immunofluorescence staining of TECs, where a co-localization of DbpA with mitochondria fluorescence dye (MitoTracker) was clearly visible in cells derived from *Ybx3^{+/+}* and *Ybx3^{+/-}* mice, but not in *Ybx3^{-/-}* cells (**Figure 15h**).

Taken together, our results clearly demonstrated, that genetic DbpA deletion has no effect on the total mitochondrial mass within TECs. However, DbpA was detected as a mitochondrial protein in TECs and in its absence the mitochondrial membrane potential increases.

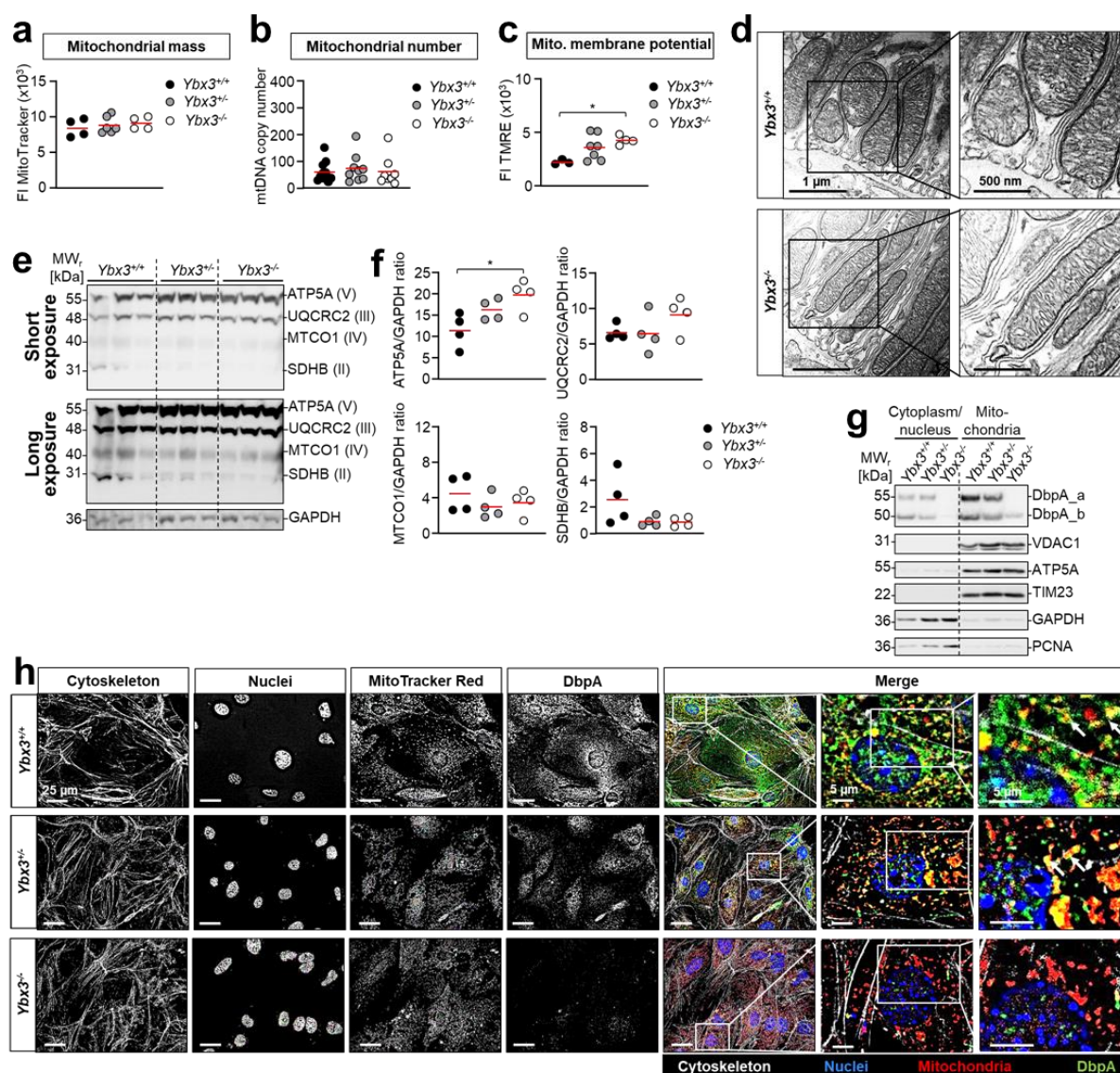


Figure 15. DbpA co-localizes with mitochondrial marker proteins.

(a) Mitochondrial mass was quantified by MitoTracker fluorescence intensity of adherent cells (n=4-6). Each individual measurement corresponds to samples with three animals pooled. (b) Mitochondrial numbers were calculated by mitochondrial DNA (mtDNA) copy numbers that were normalized to nuclear DNA content (n=8-12). Mitochondrial mass and copy numbers were equal in all strains. (c) Mitochondrial membrane potentials quantified by TMRE assay (n=3-7, kidneys from three mice were pooled in each experiment) were higher in TECs derived from Ybx3^{-/-} mice. (d) Integrity of mitochondrial outer and inner membrane was confirmed by transmission electron microscopy of kidney sections. Scale bars, 1 μ m or 500 nm. (e) Representative Western blots from Ybx3^{+/+}, Ybx3^{+/-} or Ybx3^{-/-} TECs revealed differential expressions of proteins related to the ETC. (f) Quantification of the Western blots demonstrated enhanced expression of ATP synthase lipid-binding protein (ATP5A, ETC complex V) and ubiquinol-cytochrome c reductase core protein 2 (UQCRC2, ETC complex III) in Ybx3^{+/-} and Ybx3^{-/-} cells. In contrast the expression of mitochondrially encoded cytochrome c oxidase 1 (MTCO1, ETC complex IV) and succinate dehydrogenase complex iron sulfur subunit B (SDHB, ETC complex II) were lower. (g) Following subcellular fractionation into cytoplasmic and mitochondrial proteins and Western blotting for DbpA (anti-C-terminal antibody) as well as voltage-dependent anion-selective channel 1 (VDAC1), ATP5A, translocase of inner mitochondrial membrane 23 (TIM23), glyceraldehyde 3-phosphate dehydrogenase (GAPDH) and PCNA was performed. Purity of fractionation was ascertained by GAPDH (cytosol), PCNA (nucleus) and VDAC1, ATP5A, TIM23 (mitochondria) co-determinations. Prominent bands for DbpA at 50 and 55 kDa were detected in the mitochondrial fractions. The lysates with Ybx3^{-/-} cells yielded a complete absence of DbpA in cytoplasmic/nuclear extracts whereas a weak band corresponding to DbpA_b was detected in the mitochondrial fraction. (h) TECs derived from Ybx3^{+/+}, Ybx3^{+/-} and Ybx3^{-/-} mice were tested for subcellular DbpA localization (green) following co-staining for DAPI (blue; nuclei), Alexa Fluor 488 Phalloidin (white; cytoskeleton) and MitoTracker Red CMXRos (red; mitochondria). TECs from Ybx3^{+/+} mice showed DbpA positive staining in the cytoplasm and nucleus. There was less DbpA positive staining in the cytoplasm and nucleus in Ybx3^{+/-} TECs, whereas there was almost no DbpA detectable in TECs isolated from Ybx3^{-/-} mice. The overlay of mitochondrial marker protein with the DbpA fluorochrome was visualized by yellow color and demonstrated a co-localization of DbpA with mitochondria. Scale bars, 25 μ m or 5 μ m. -Figure legend continued on the next page-

-continued- Data represent mean values. Data represent mean values. All results were confirmed as triplicates in at least 2 independent experiments. One-way analysis of variance followed by Tukey *post hoc* test was used for comparisons of 3 groups. Student's *t* test was used when 2 experimental groups were compared with **P* < 0.05.

4.2.4 DbpA fulfills tubular cell-specific metabolic functions

So far, it has been shown that DbpA has a decisive influence on the metabolic activity in TECs. In order to check whether these were cell-specific phenomena, primary BMDMs obtained from *Ybx3^{+/+}*, *Ybx3^{+/-}* and *Ybx3^{-/-}* mice were included into the analyses of metabolic processes.

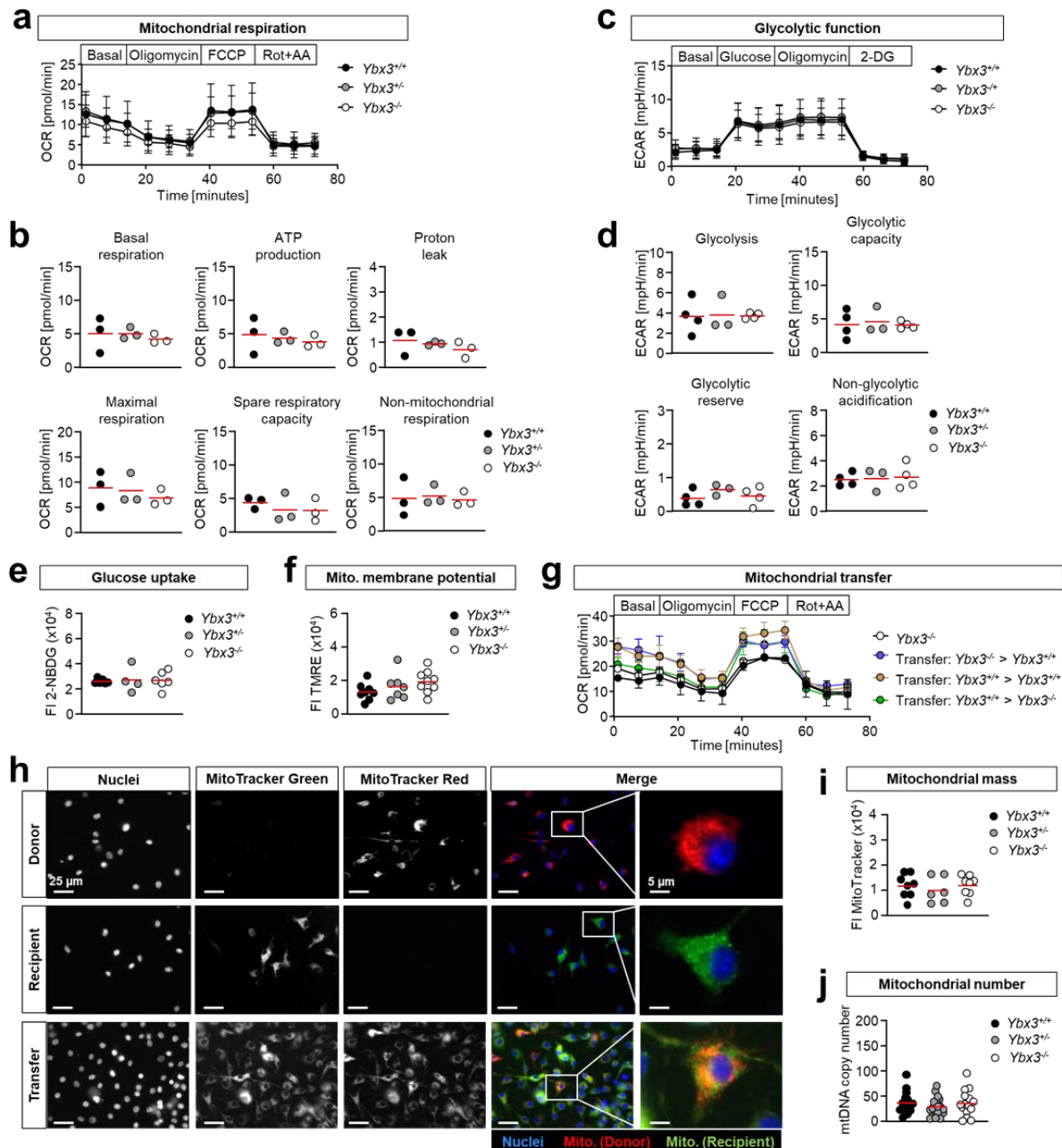


Figure 16. Mitochondrial analyses of primary BMDMs.

(a) OCR of BMDMs obtained from *Ybx3^{+/+}*, *Ybx3^{+/-}* and *Ybx3^{-/-}* mice were quantified by Seahorse XF mito stress test. OCR were measured under basal level and following addition of 1 μ M oligomycin, 1 μ M FCCP and 0.5 μ M Rot+AA. Genetic deletion of *Ybx3* did not affect OCRs (*n*=3). Data were normalized to cell numbers per well. (b) All individual parameters (basal respiration, ATP production, proton leakage, maximal respiration rate, spare respiratory capacity and non-mitochondrial oxygen consumption) were similar in *Ybx3^{+/+}*, *Ybx3^{+/-}* or *Ybx3^{-/-}* BMDMs. -Figure legend continued on the next page-

-continued- (c) The ECAR of BMDMs obtained from $Ybx3^{+/+}$, $Ybx3^{+/-}$ and $Ybx3^{-/-}$ mice were quantified by Seahorse XF glycolysis stress test. ECAR were measured under basal level and following addition of 10 mM glucose, 1 μ M oligomycin and 50 mM 2-DG. ECAR levels were similar in all three genotypes (n=3-4). Normalization to cell numbers per well was performed. (d) Individual parameters for glycolysis, glycolytic capacity, glycolytic reserve and non-glycolytic acidification were not altered when $Ybx3$ was genetically deleted. (e) Furthermore, BMDMs obtained from mice with $Ybx3^{+/+}$, $Ybx3^{+/-}$ and $Ybx3^{-/-}$ genotype revealed no significant differences in 2-NBDG levels as a measurement of glucose uptake (n=4-6). (f) Mitochondrial membrane potentials quantified by TMRE assay (n=7-9) revealed no significant differences. (g) Transferring mitochondria isolated from $Ybx3^{+/+}$ and $Ybx3^{-/-}$ BMDMs into $Ybx3^{+/+}$ and/or $Ybx3^{-/-}$ BMDMs increased the metabolic activity of the cells quantified by mito stress test. In all groups 20.000 cells per well were seeded and included in the measurement. (h) Successful mitochondrial transfers were confirmed by live cell imaging and the overlay of fluorescent signals. Mitochondria of donor BMDMs were stained with MitoTracker Red and mitochondria of recipient cells were stained with MitoTracker Green before the transfer. Overlay of the images indicated a successful transfer of donor mitochondria into recipient cells via centrifugation. Scale bars, 25 μ m or 5 μ m. (i) Mitochondrial mass quantified by MitoTracker fluorescence intensity (n=6-11) and (j) mitochondrial numbers calculated by mtDNA copy numbers (n=15-18) were similar. Data represent mean values. All results were confirmed as triplicates in at least 2 independent experiments. One-way analysis of variance followed by Tukey *post hoc* test was used for comparisons of 3 groups. Student's *t* test was used when 2 experimental groups were compared.

In contrast to the above described characteristics of TECs, analyses of the metabolic function in BMDMs in terms of OCR (**Figures 16a-b**), glycolysis (**Figures 16c-d**), glucose uptake (**Figure 16e**) and mitochondrial membrane potential (**Figure 16f**) were similar between the genotypes. In line with the data on mitochondrial transfer of TECs, an increased metabolic activity of wild type BMDMs after the transfer of mitochondria isolated from $Ybx3^{-/-}$ BMDMs were obtained (**Figures 16g-h**). Moreover, mitochondrial mass (**Figure 16i**) and mtDNA copy number (**Figure 16j**) were similar obtained from $Ybx3^{+/+}$, $Ybx3^{+/-}$ and $Ybx3^{-/-}$ mice.

These data suggest a tubular cell-specific function of DbpA in context with metabolic processes and mitochondrial membrane integrity.

4.3 DbpA mediates tubular cell damage in AKI and the absence of the protein is linked with cell protection

4.3.1 Following IRI upregulated DbpA expression confers acute tubular cell damage

TECs form a boundary in the tubular barrier system with immediate contact to urine. Because of their prominent role in the maintenance of fluid and acid-base homeostasis, they have a high energy requirement and are especially sensitive to ischemia. Due to the increased metabolic activity of $Ybx3^{-/-}$ TECs, we hypothesize that these cells play a key role during tubular cell injury *in vivo*.

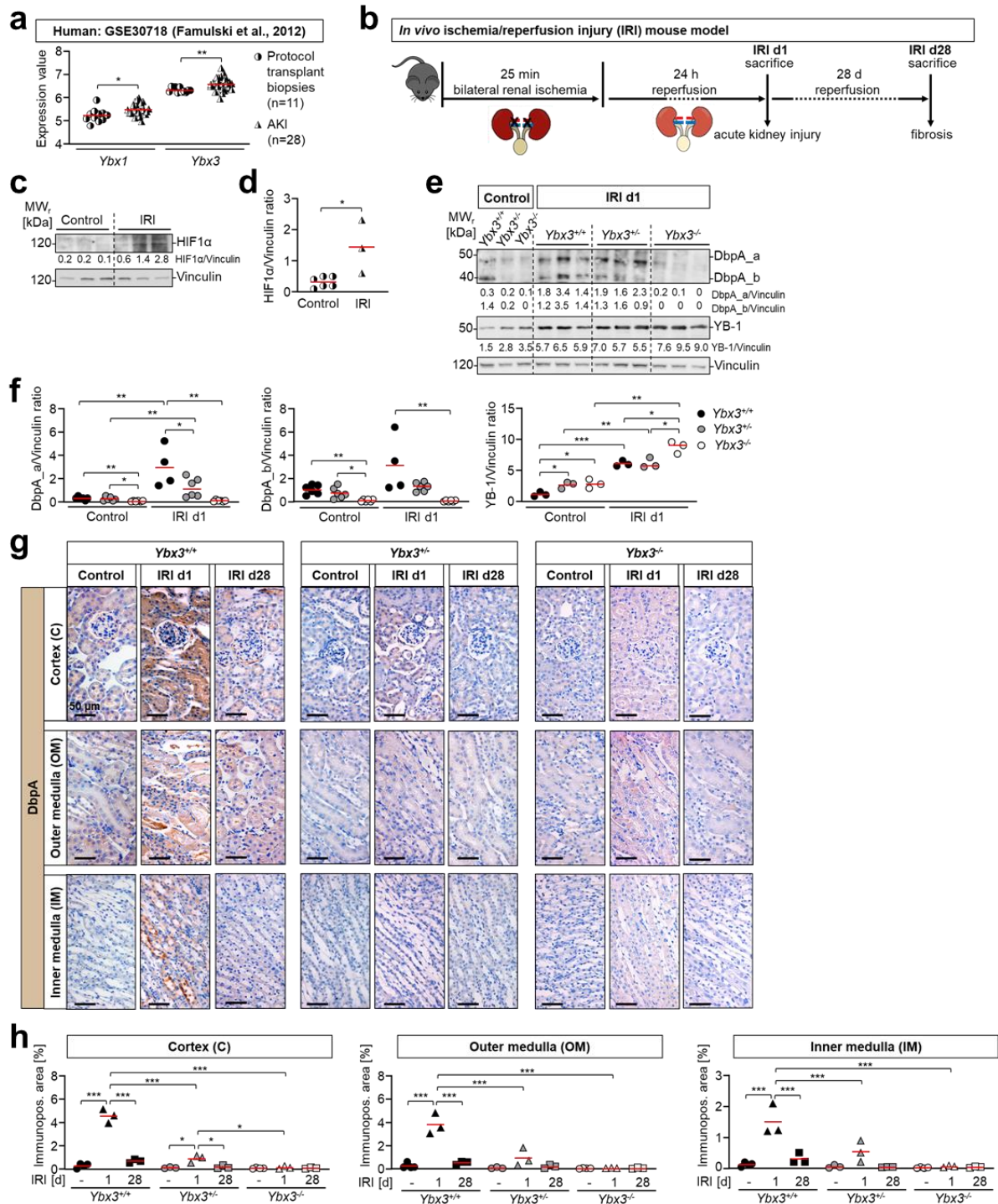


Figure 17. Ybx3 expression is upregulated following acute IRI.

(a) The gene expression dataset GSE30718 was used for microarray data analysis of human samples from AKI biopsies (n=28) and protocol transplant biopsies (n=11). AKI led to an increase of *Ybx1* and *Ybx3* expression. (b) *In vivo* model of experimental IRI was performed in mice with different genotypes. Blood vessels of both kidneys were occluded for 25 min using non-traumatic clamps. Afterwards, clamps were removed and reperfusion lasted for one or 28 day/s. Mice were sacrificed and blood and kidney was obtained. (c and d) Western blot analysis of hypoxia-inducible factor-1 alpha (HIF1 α) revealed hypoxic stress in kidney tissue by ischemia. (e and f) Western blot analyses of kidney lysates by means of a polyclonal anti-C-terminal antibody against DbpA indicated low level expression of DbpA in healthy kidney tissue, which was strongly upregulated following IRI. Similar results were obtained for cold shock protein YB-1. In kidney tissue lysate obtained from *Ybx3*^{-/-} animals the expression of YB-1 was increased compared to wild type. (g and h) Immunohistochemistry of kidney tissues from mice aged 8-12 weeks (using antibody directed against the C-terminus) demonstrated immunopositive cells for DbpA in tubular and glomerular structures. On d1 following IRI, a substantial DbpA upregulation in tubular cells was seen in wild type animals, which was less prominent in *Ybx3*^{+/-} and absent in *Ybx3*^{-/-} animals. Expression levels returned to basal levels within d28. Scale bars, 50 μ m. -Figure legend continued on the next page-

-continued- Data represent mean values. All results were confirmed as triplicates in at least 2 independent experiments. One-way analysis of variance followed by Tukey *post hoc* test was used for comparisons of 3 groups. Student's *t* test was used when 2 experimental groups were compared with * $P < 0.05$, ** $P < 0.01$, *** $P < 0.001$.

Ybx3 transcripts were present in kidney tissue from protocol transplant biopsies in humans and significant upregulation was observed in those with AKI.¹⁷⁵ Notably, another prominent cold shock protein YB-1 (*Ybx1*) was also upregulated as reported recently⁵² (**Figure 17a**). The *in vivo* IRI mouse model with a short- (d1) and long-term (d28) observation phase was used (**Figure 17b**), to analyze the tubular cell-specific functions of DbpA following AKI. Successful induction of hypoxic stress was confirmed by Western blotting of HIF1 α expression in kidney tissue lysates (**Figures 17c-d**). At the protein level, 25 min of renal ischemia followed by 24 h of reperfusion (IRI d1) resulted in a clear upregulation of the CSPs DbpA_a, DbpA_b and YB-1 in murine kidney lysates (**Figures 17e-f**). Increased DbpA expression was evident in all kidney compartments following IRI d1 which was transient and no longer detected on d28 post IRI (**Figures 17g-h**).

Survival analysis over 28 d following IRI revealed 100% survival of *Ybx3*^{-/-} mice, 90% of *Ybx3*^{+/-} whereas only 70% of *Ybx3*^{+/+} mice survived ($P < 0.05$ *Ybx3*^{-/-} versus *Ybx3*^{+/+}; **Figure 18a**). The overall appearance of kidneys from *Ybx3*^{+/+} and *Ybx3*^{+/-} animals following IRI was a deep red color, whereas kidneys from *Ybx3*^{-/-} animals were a pale brownish color, similar to healthy controls (**Figure 18b**). Correspondingly, kidney function (assessed by plasma creatinine) was significantly better in *Ybx3*^{-/-} animals compared to wild type following IRI (**Figure 18c**). Wild type animals showed marked tubular cell injury following IRI, which was less prominent in *Ybx3*^{+/-} and *Ybx3*^{-/-} mice (**Figures 18d-e**). Tubular cell damage marker neutrophil gelatinase-associated lipocalin (NGAL) was strongly upregulated following IRI in *Ybx3*^{+/+} kidney sections (**Figures 18f-g**) and TECs lysates (**Figures 18h-i**), but to a lesser extent in *Ybx3* knockout animals.

Overall, DbpA mediates tubular cell damage in AKI and the absence of the protein is linked with cell protection.

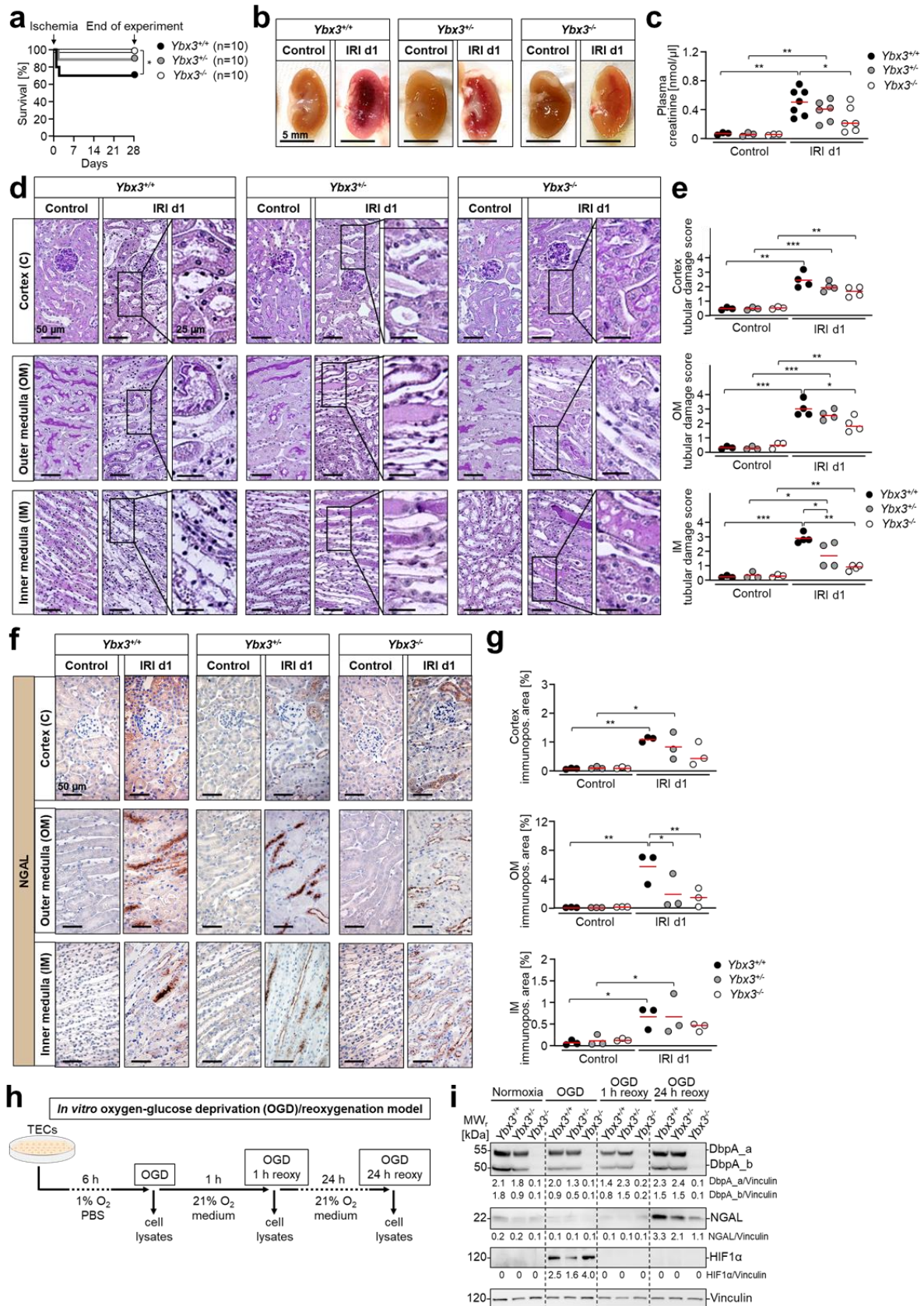


Figure 18. DbpA expression confers acute tubular cell damage.

(a) Survival analysis over 28 d was performed following ischemia and subsequent reperfusion of the kidneys. Significantly higher mortality rates in wild type than in $Ybx3^{-/-}$ animals became apparent (n=10, log-rank test was used for statistics). (b) Representative macroscopic images of longitudinal kidney sections obtained following ischemia and on d1 of reperfusion. In wild type animals the kidney tissue appeared congested and filled with blood following IRI although PBS perfusion was performed prior harvesting of the kidneys. Scale bars, 5 mm. -Figure legend continued on the next page-

-continued- (c) Plasma creatinine levels indicated severe AKI following IRI in wild type animals, whereas creatinine values were significantly lower in *Ybx3^{-/-}* animals. (d) PAS staining of kidney sections revealed increased tubular cell damage following IRI in wild type animals in the cortex, OM and IM. Enlargement of images for IRI obtained from the cortex visualized nuclear condensation of the majority of tubular cells, that was less abundant in *Ybx3^{+/-}* animals and not present in *Ybx3^{-/-}* animals. Scale bars, 50 μm or 25 μm (quantified in e). (f) Kidney damage protein NGAL was detected by immunohistochemistry of kidney tissue. Scale bars, 50 μm . (g) NGAL quantification following IRI of immunopositive area revealed significant more abundance in the OM of *Ybx3^{+/-}* compared to *Ybx3^{-/-}* mice. (h) These data were confirmed by an *in vitro* assay, where primary TECs were maintained in PBS (+CaCl₂ +MgCl₂) in a hypoxic atmosphere containing 1% O₂ for 6 h. For reoxygenation, cells were maintained in complete medium and 21% O₂ for 1 h or 24 h. (i) Western blot analysis revealed increased NGAL expression 24 h following OGD in wild type compared to *Ybx3^{-/-}* TECs. Data represent mean values. All results were confirmed as triplicates in at least 2 independent experiments. One-way analysis of variance followed by Tukey *post hoc* test was used for comparisons of 3 groups. Student's *t* test was used when 2 experimental groups were compared with **P* < 0.05, ***P* < 0.01, ****P* < 0.001.

4.3.2 *Ybx3^{-/-}* animals do not develop an inflammatory response following induced hypoxic stress

Inflammation and tubular cell damage in the kidney are closely interconnected processes. Acute inflammation is the body's response to an injury or harmful stimulus. It is a protective, localized, short-term and well-controlled process aimed at eliminating the cause of cell injury, clearing out damaged cells or tissues, and initiating tissue repair.¹⁸⁰

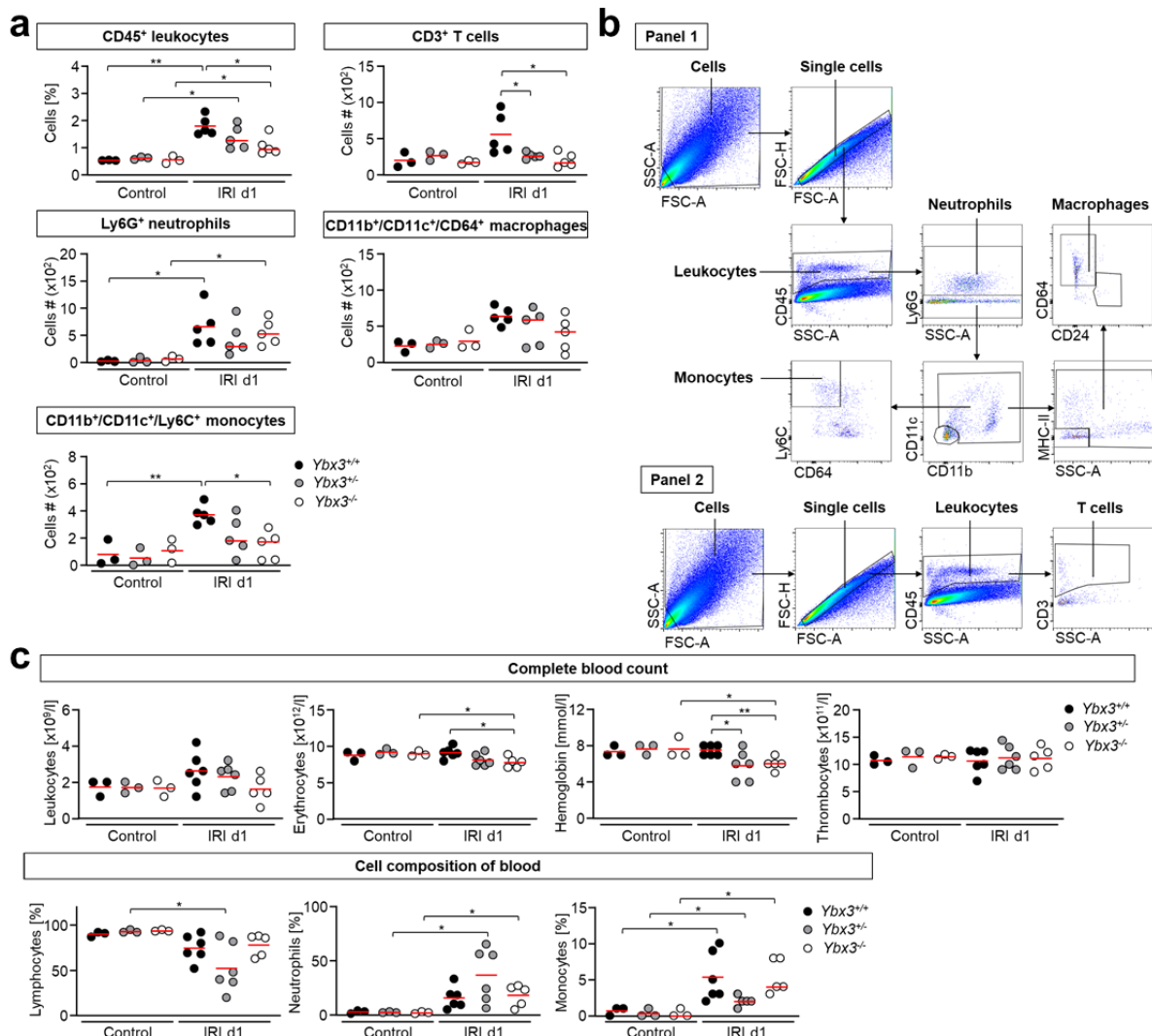


Figure 19. *Ybx3^{-/-}* animals do not develop an inflammatory response following induced hypoxic stress.

-Figure legend continued on the next page-

-continued- (a) Infiltrating immune cells quantified by flow cytometry following kidney tissue disintegration revealed a similar influx of CD45⁺ leukocytes in the kidneys of all genotypes following IRI. Subanalysis of CD3⁺ T cells, Ly6G⁺ neutrophils, CD11b⁺/CD11c⁺/CD64⁺ macrophages and CD11b⁺/CD11c⁺/Ly6C⁺ monocytes revealed less immune cell infiltration in kidneys of *Ybx3*^{-/-} animals following IRI. (b) Gating strategy for flow cytometry analysis of infiltrating immune cells. Renal lymphocytes were defined by doublet exclusion of live cells (using the forward and side scatter properties) followed by gating for CD45⁺ leukocytes. The different subsets were gated out of the CD45⁺ population using the markers CD45⁺/Ly6G⁺ for neutrophils, CD45⁺/CD11b⁺/CD11c⁺/CD64⁺ for macrophages, CD11b⁺/CD11c⁺/Ly6C⁺ for monocytes and CD45⁺/CD3⁺ for T cells. (c) Cell composition of blood (lymphocytes, neutrophils, monocytes) was similar in animals with different genotypes following IRI (n=3-6). Cell numbers of leukocytes and thrombocytes were not altered in *Ybx3*^{+/+}, *Ybx3*^{+/-} or *Ybx3*^{-/-} mice following IRI. However, erythrocyte numbers and hemoglobin were reduced in *Ybx3*^{-/-} animals following IRI compared to wild type. Neutrophil and monocyte levels were upregulated in all genotypes following IRI (n=3-6). Data represent mean values. All results were confirmed as triplicates in at least 2 independent experiments. One-way analysis of variance followed by Tukey *post hoc* test was used for comparisons of 3 groups. Student's *t* test was used when 2 experimental groups were compared with **P* < 0.05, ***P* < 0.01.

In accordance with increased tubular cell damage on IRI d1 in *Ybx3*^{+/+} animals, immune cell infiltration into the kidney was induced by IRI. However in kidneys of *Ybx3*^{-/-} mice, infiltrating T cell, neutrophil, macrophage and monocyte cell numbers remained low following IRI (**Figure 19a**). Gating strategy is shown in **Figure 19b**. Circulating leukocytes, erythrocytes and hemoglobin levels were decreased in *Ybx3*^{-/-} animals following IRI, whereas thrombocyte, lymphocyte, neutrophils and monocyte levels in the blood revealed no significant differences in the genotypes following IRI (**Figure 19c**).

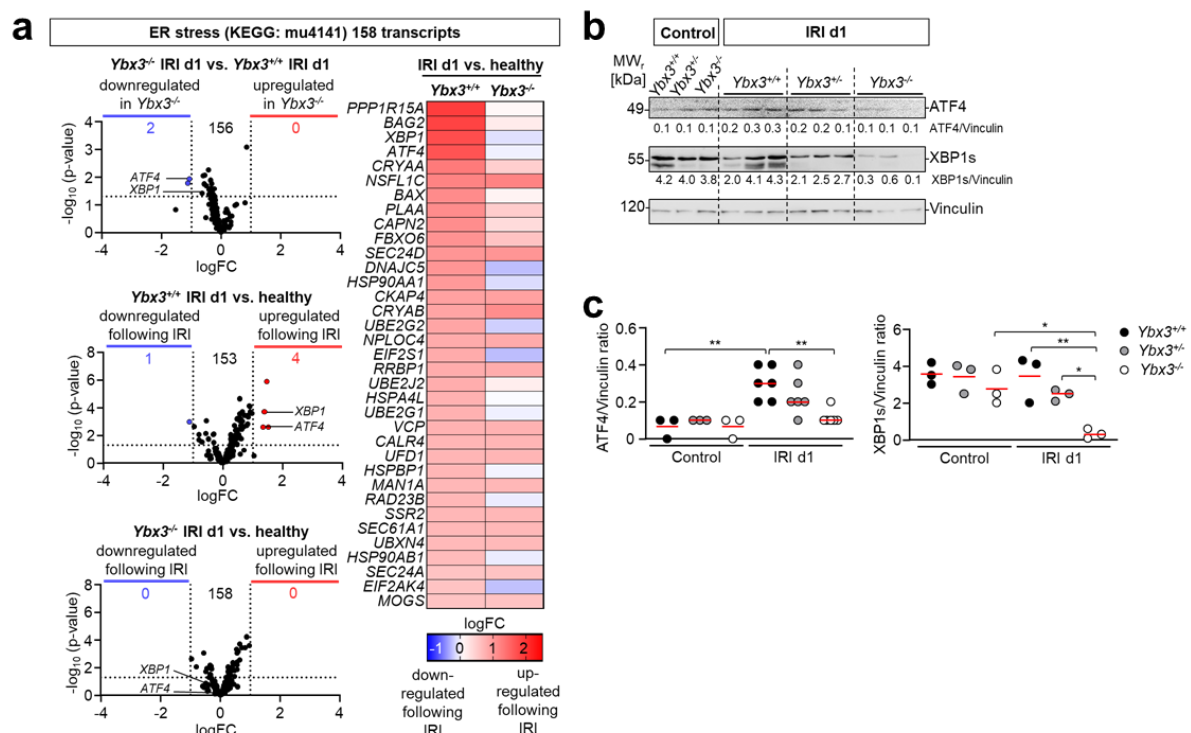


Figure 20. Kidneys with genetic *Ybx3* deletion demonstrated decreased ER stress following ischemia.

(a) Transcript analysis related to ER stress (KEGG: mu4141) revealed enhanced upregulation of ER stress in wild type animals following IRI. Blue represent downregulation following IRI, red upregulation and black not differentially expressed genes. Top 35 differential expressed transcripts of wild type animals are shown in the heat map compared to *Ybx3*^{-/-}. Transcript analysis indicating downregulation of *ATF4* and *XBP1* in kidneys obtained from *Ybx3*^{-/-} mice compared to wild type. 156 transcripts were not regulated (black). (b and c) The expression of ER stress marker proteins *ATF4* and *XBP1s* were increased in wild type animals following IRI. Whereas activation of ER stress did not occur in *Ybx3*^{-/-} animals following IRI. Data represent mean values. All results were confirmed as triplicates in at least 2 independent experiments. One-way analysis of variance followed by Tukey *post hoc* test was used for comparisons of 3 groups. Student's *t* test was used when 2 experimental groups were compared with **P* < 0.05, ***P* < 0.01.

ER stress was detected in *Ybx3^{+/+}*, but not in *Ybx3^{-/-}* animals, as indicated by increased ER stress transcript levels (**Figure 20a**). These data were confirmed by Western blot analyses of the ER stress marker proteins activating transcription factor 4 (ATF4) and X-box binding protein 1 (XBP1s) (**Figures 20b-c**).

In summary, both immune cell infiltration and ER stress are increased as a result of IRI induction in wild type mice. However, *Ybx3^{-/-}* animals showed significantly reduced signs of inflammation.

4.3.3 Long-term analysis following IRI revealed an attenuated fibrotic response in kidneys of *Ybx3^{-/-}* animals

Prolonged ER stress is associated with the progression of kidney fibrosis; i.e. the accumulation of extracellular matrix.^{181,182} Long-term analysis at d28 following IRI revealed an attenuated fibrotic response in kidneys obtained from *Ybx3^{-/-}* animals. Matrisome-related transcripts at d1 following IRI (**Figure 21a**) and the fibrosis marker proteins alpha-smooth muscle actin (α SMA) and Tenascin-C (**Figures 21b-c**) were not upregulated in *Ybx3^{-/-}* animals at d28 following IRI.

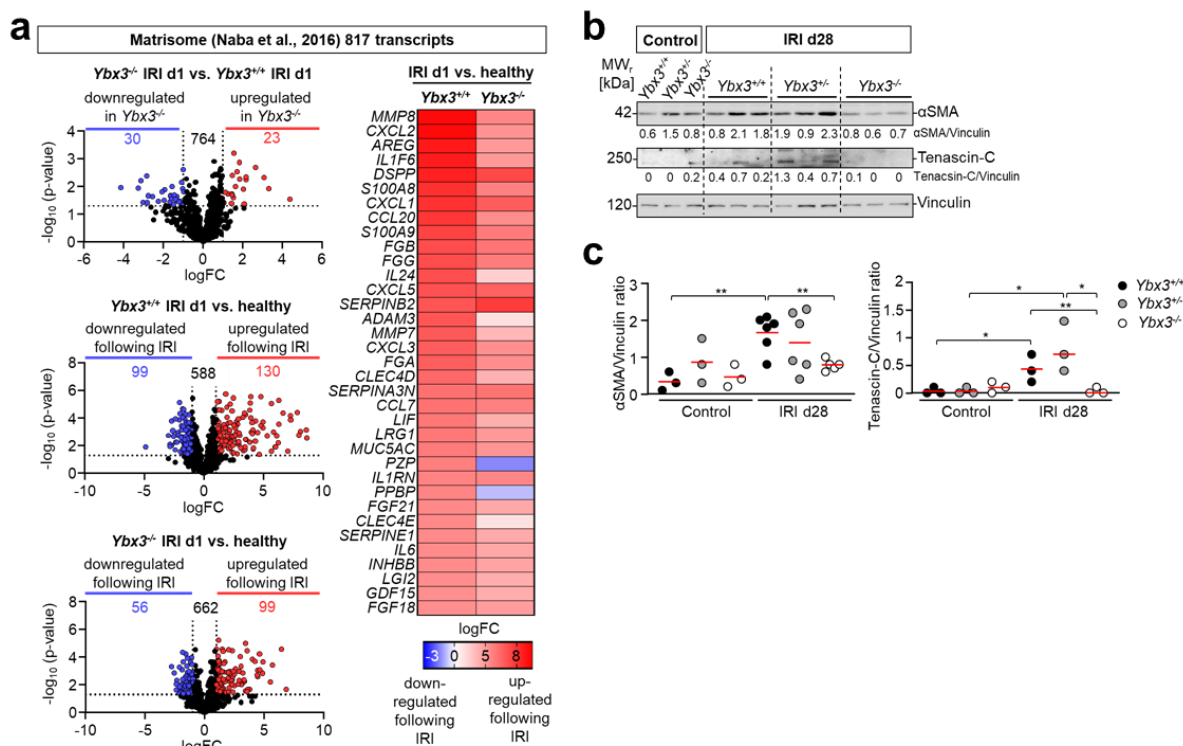


Figure 21. *Ybx3^{-/-}* animals showed a decreased activation of matrisome-related proteins.

(a) RNA-seq data demonstrated an increased number of downregulated genes (blue) related to matrisome (according to Naba et al., 2016) in the kidney of *Ybx3^{-/-}* mice compared to wild type at IRI 1d. Red represents upregulated transcripts. Black dots are genes that were differentially expressed below the cutoff values of logFC and p-value. Top 35 differential expressed transcripts of wild type animals were shown in the heat map. (b and c) Kidney lysates from animals 28d following IRI quantified the expression of α SMA and Tenascin-C as markers for matrisome-related proteins. α SMA and Tenascin-C were significantly less abundant in *Ybx3^{-/-}* animals 28d following ischemia. Data represent mean values. All results were confirmed as triplicates in at least 2 independent experiments. One-way analysis of variance followed by Tukey *post hoc* test was used for comparisons of 3 groups. Student's *t* test was used when 2 experimental groups were compared with * $P < 0.05$, ** $P < 0.01$.

In addition, collagens-related transcripts at IRI d1 (**Figure 22a**) and proteins as indicated by Picro sirius red staining (collagens type I and III) (**Figures 22b-c**) were upregulated following IRI in wild type and *Ybx3^{+/-}*, but not detected in kidneys obtained from *Ybx3^{-/-}* animals.

In summary, the absence of DbpA protects kidneys from fibrosis following IRI.

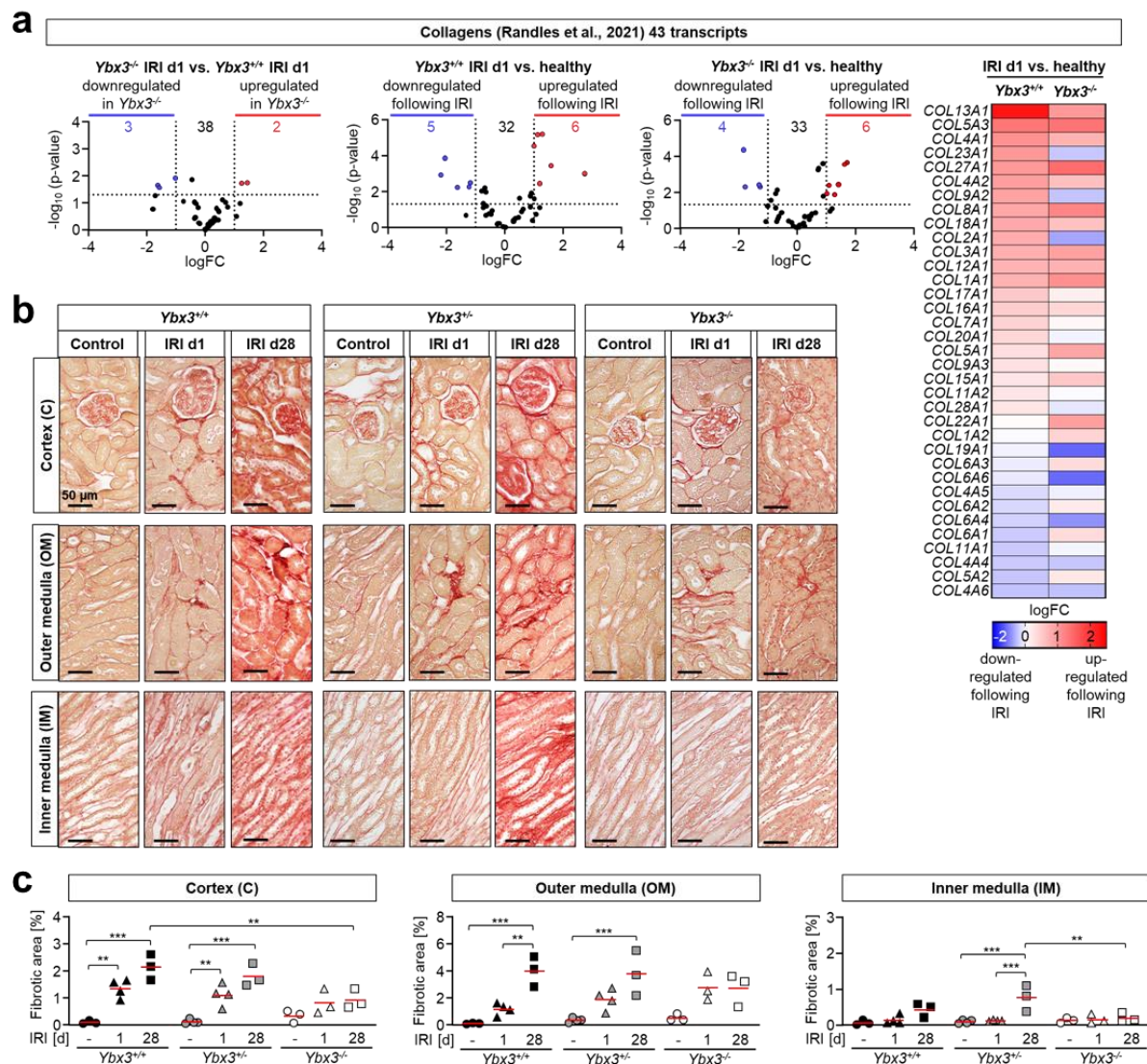


Figure 22. Following IRI fibrotic response was attenuated in kidneys of *Ybx3^{-/-}* animals.

(a) RNA-seq data demonstrated a higher number of downregulated genes (blue) related to collagens (according to Randles et al., 2021) in the kidney of *Ybx3^{-/-}* mice compared to wild type. Red represents upregulated transcripts. Black dots are genes that were differentially expressed below the cutoff values of logFC and p-value. Top 35 differential expressed transcripts of wild type animals were shown in the heat map. (b) Picro sirius red staining of kidney sections at IRI 1d and IRI 28d visualized fibrosis as reddish color. A prominent tubulointerstitial and glomerular collagen deposition 28d following IRI was seen for the cortex, OM and IM in the animals with *Ybx3^{+/-}* and *Ybx3^{-/-}* genotype. In contrast, *Ybx3^{-/-}* animals exhibited minor tubulointerstitial and glomerular fibrosis and collagen deposition, (c) which was quantified by staining-positive tissue areas. Scale bars, 50 μ m. Data represent mean values. All results were confirmed as triplicates in at least 2 independent experiments. One-way analysis of variance followed by Tukey *post hoc* test was used for comparisons of 3 groups. Student's *t* test was used when 2 experimental groups were compared with ** $P < 0.01$, *** $P < 0.001$.

4.3.4 Deletion of DbpA leads to minor ferroptotic cell death following IRI

Tubular cell damage and cell death are closely linked in the context of AKI. The renal tubules are essential structures in the kidneys responsible for reabsorbing water and essential substances from the urine, maintaining electrolyte balance, and regulating acid-base equilibrium. When these tubular cells are subjected to cell stress or injury, it can lead to damage and cell death.¹⁸³

Based on the already detected tubular damage, the next step was to investigate tubular cell death following induced IRI. Unexpectedly, no significant apoptosis-related transcript regulation was detected in wild type animals compared to *Ybx3*^{-/-} animals (**Figure 23a**). However, transcript analysis showed upregulation of ferroptosis-related genes following IRI in kidneys of wild type animals, which was less evident in the kidneys of *Ybx3*^{-/-} animals (**Figure 23b**).

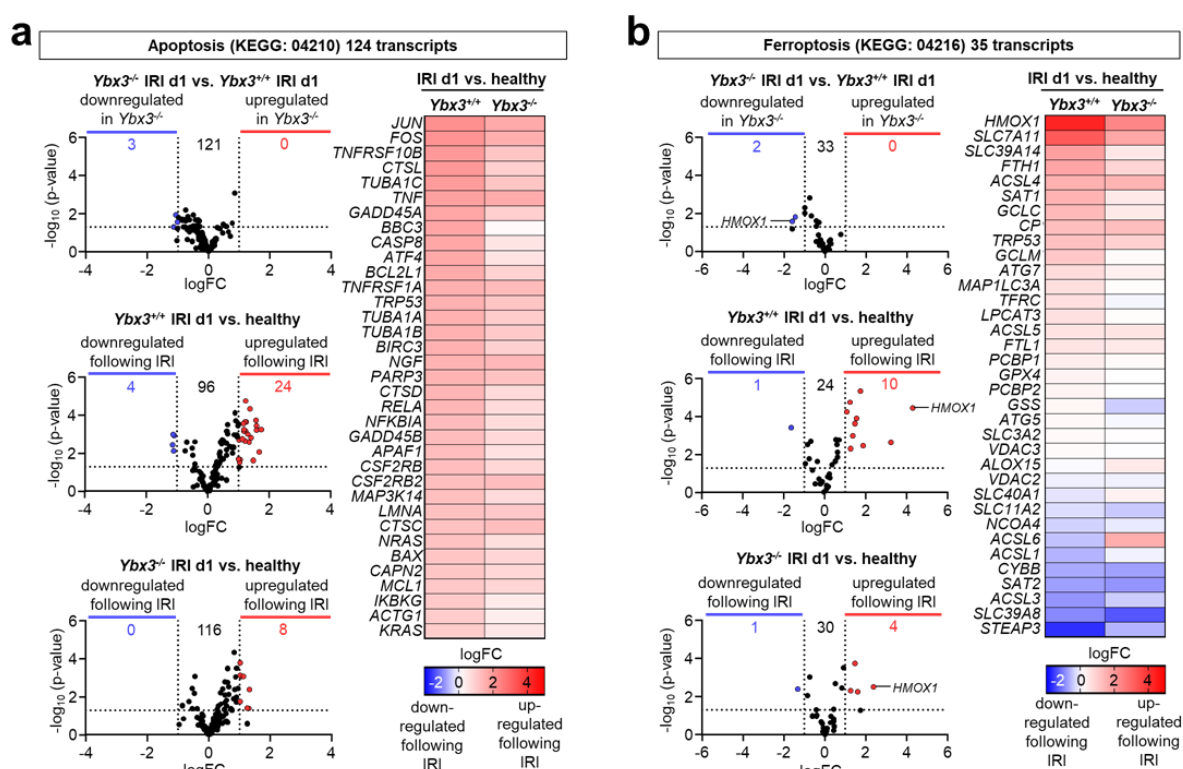


Figure 23. Deletion of DbpA leads to minor ferroptotic cell death following IRI.

(a) RNA-seq data revealed no significant differences in the regulation of apoptotic genes (KEGG: 04210) in kidneys following IRI d1 in wild type versus *Ybx3*^{-/-} mice. Blue dots represent downregulated genes. Red shows upregulation and black not differentially expressed genes. Top 35 differential expressed transcripts of wild type animals are shown in the heat map. (b) Analysis of ferroptosis-related transcripts (KEGG: 04216) revealed enhanced *heme oxygenase 1 (HMOX1)* expression following IRI d1 in wild type animals and less upregulation of ferroptosis-related genes in *Ybx3*^{-/-} animals. Blue represents downregulation, red upregulation and black indicates no significant change in gene expression.

4.3.5 Increased antioxidant activity provides the basis for the protective mechanism after induced hypoxia conditions

In line with the RNA-seq data, that served as a screening method, kidney sections of wild type and *Ybx3*^{+/-} animals revealed more positive staining of the lipid peroxidation marker 4-hydroxynonenal (4-HNE) especially at the corticomedullary junction, suggesting increased ferroptosis (**Figure 24a**). The most differentially expressed transcript heme oxygenase 1 gene (*HMOX1*) (**Figure 23b**) was similarly expressed on the protein level (HO-1) in all genotypes following IRI (**Figures 24b-c**). However, the expression of the antioxidant enzyme glutathione peroxidase 4 (GPX4) was significantly increased following IRI in kidney tissue lysates of *Ybx3*^{-/-} mice (**Figures 24b-c**). Increased GPX4 correlated with decreased levels of mROS in kidney tissue (**Figure 24d**). Furthermore, mitochondrial damage following IRI was detected by an increased expression of the mitophagy marker protein PINK1 in wild type animals. Lower levels of PINK1 were detected when *DbpA* was genetically deleted (**Figures 24b-c**). Following ischemia the phosphorylation of the nutrient and energy sensor AMPK α was markedly upregulated in kidney tissue lysates from *Ybx3* knockout animals, indicating a higher metabolic activity (**Figures 24b-c**).

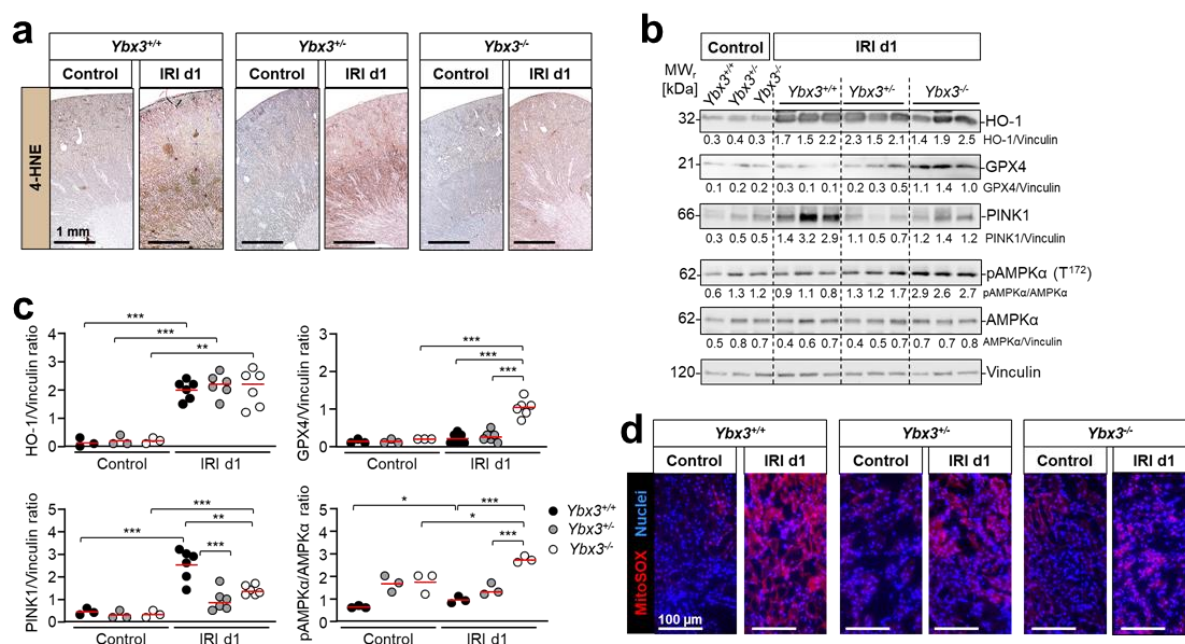


Figure 24. Increased antioxidant activity provides the basis for the protective mechanism *in vivo*.

(a) 4-HNE staining of kidney sections showed increased lipid peroxidation in wild type and *Ybx3*^{+/-} animals especially, in the outer medulla when compared to *Ybx3*^{-/-} animals following IRI. Scale bars, 1 mm. (b and c) The expression of HO-1, as a critical mediator of ferroptosis, was increased in kidney tissue lysates of all genotypes following IRI. However, the expression of the antioxidant enzyme GPX4 was significantly increased in kidney lysates of *Ybx3*^{-/-} animals. Mitophagy marker protein PINK1 was significantly increased in kidney lysates of wild type animals, but not in animals with *Ybx3* deletion. The phosphorylation of AMPK α (T¹⁷²) in kidney tissue lysates of *Ybx3*^{-/-} mice was significantly increased following IRI compared to wild type animals. (d) Corresponding to the increased expression of GPX4 the mROS levels analyzed by MitoSOX staining were decreased in kidney sections of *Ybx3*^{-/-} animals. Scale bars, 100 μ m. Data represent mean values. All results were confirmed as triplicates in at least 2 independent experiments. One-way analysis of variance followed by Tukey *post hoc* test was used for comparisons of 3 groups. Student's *t* test was used when 2 experimental groups were compared with **P* < 0.05, ***P* < 0.01, ****P* < 0.001.

In addition, *in vitro* analyses revealed a significantly increased expression of GPX4 at baseline in TECs obtained from *Ybx3^{-/-}* mice (Figures 25a-b). The *in vivo* results shown in Figures 23-24 were corroborated by an *in vitro* assay of ferroptosis (Figure 25c).

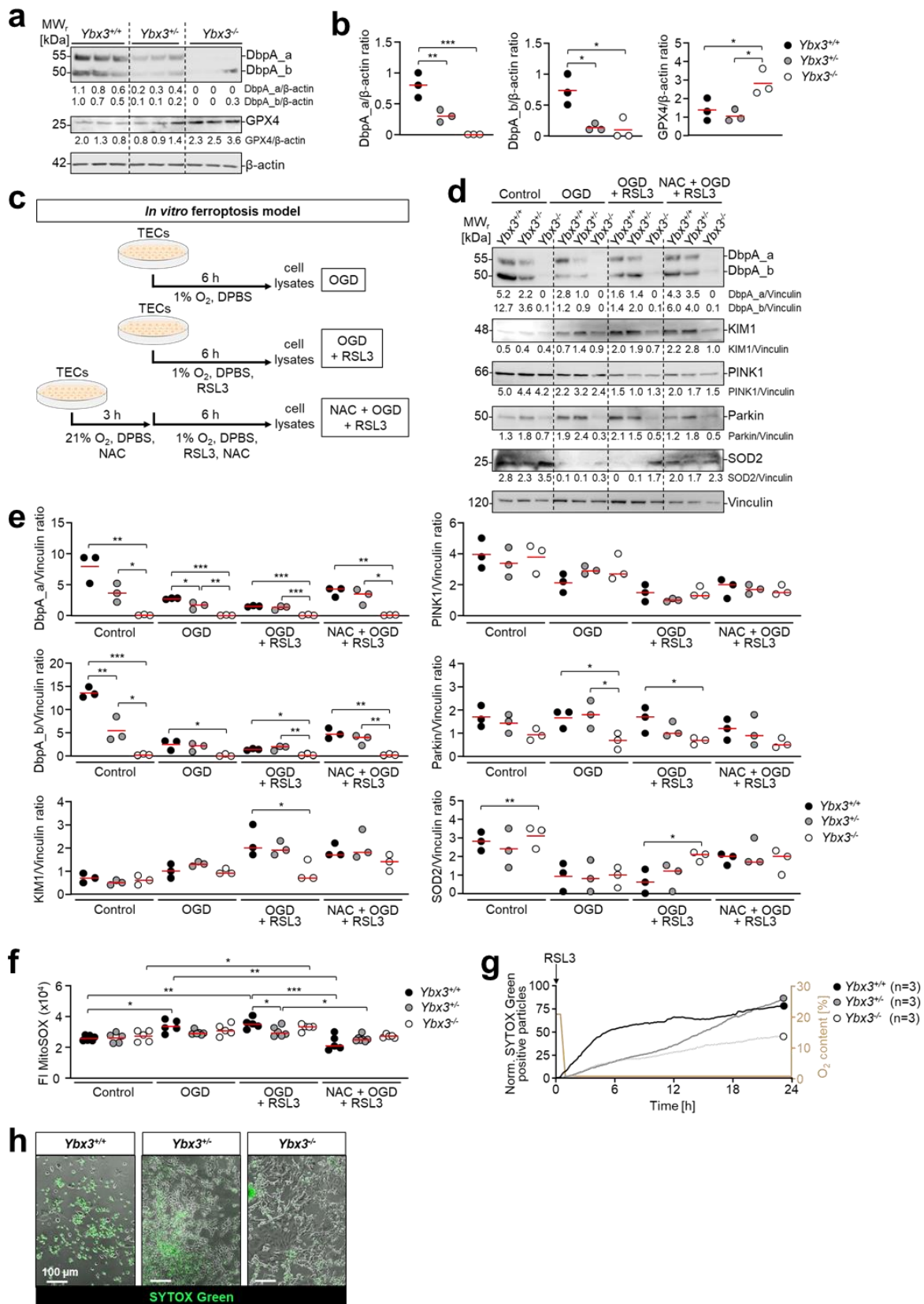


Figure 25. Increased antioxidant activity protects *Ybx3^{-/-}* TECs from ferroptotic cell death *in vitro*.
 -Figure legend continued on the next page-

-continued- (a) Western blot analyses of TECs obtained from $Ybx3^{+/+}$, $Ybx3^{+/-}$ and $Ybx3^{-/-}$ mice were performed to analyze the expression of antioxidant protein GPX4 at baseline. (b) Increased expression levels of GPX4 was detected in $Ybx3^{-/-}$ tubular cells compared to wild type. (c) Ferroptosis was induced *in vitro* by the addition of the GPX4 inhibitor RSL3 under hypoxia. NAC was used as an antioxidant agents. (d and e) Western blot analyses and quantification revealed increased expression of KIM1 and Parkin following OGD, with a lower expression in TECs obtained from $Ybx3^{-/-}$ animals, whereas the antioxidant enzyme superoxide dismutase 2 (SOD2) was significantly increased. (f) Basal mROS levels were similar in TECs under normoxic conditions and increased following OGD and ferroptosis induction by adding RSL3. NAC was able to reduce the levels of mROS (n=4-6). (g) Resistance against ferroptotic cell death of $Ybx3^{-/-}$ TECs was confirmed by live cell imaging of TECs following OGD and RSL3 addition. O₂ content in the hypoxic chamber was reduced from 21% to 1% after 30 min until the end of the experiment and SYTOX Green stained TECs were analyzed in PBS medium to quantify death cells. (n=3) (h) Representative images demonstrated less SYTOX Green positive staining in $Ybx3^{-/-}$ TECs 24 h after ferroptosis induction. Scale bars, 100 μ m. Data represent mean values. All results were confirmed as triplicates in at least 2 independent experiments. One-way analysis of variance followed by Tukey *post hoc* test was used for comparisons of 3 groups. Student's *t* test was used when 2 experimental groups were compared with **P* < 0.05, ***P* < 0.01, ****P* < 0.001.

By adding ferroptosis inducer RSL3 to primary TECs, tubular cell damage was incited, as indicated by increased KIM1 expression in wild type and heterozygous DbpA TECs. Similar results were obtained for Parkin, which is a downstream target of PINK1. However, PINK1 expression levels were similar between the different genotypes. Contrary to a decreased KIM1 and Parkin expression the antioxidant enzyme superoxide dismutase 2 (SOD2) was increased in TECs obtained from $Ybx3^{-/-}$ animals (**Figures 25d-e**). *In vitro* induction of ferroptosis following OGD and the addition of RSL3 resulted in an increased production of mROS in wild type TECs, which was less evident in $Ybx3^{-/-}$ TECs. The addition of the antioxidant substance NAC attenuated the production of mROS in all genotypes (**Figure 25f**). Induction of hypoxic stress via OGD and ferroptosis via RSL3 in TECs obtained from $Ybx3^{-/-}$ mice revealed less cell death compared to wild type cells in a SYTOX Green assay (**Figure 25g-h**).

In conclusion, $Ybx3^{-/-}$ TECs were metabolically more active at baseline and better adapted to hypoxic conditions due to their upregulated antioxidant functions, which probably prevents mROS generation. Since mROS are the main cause of ferroptosis, kidneys from $Ybx3^{-/-}$ animals are thus protected from transient hypoxia.

5 Discussion

5.1 Challenges and strategies in the comprehensive detection and characterization of DbpA

DbpA is difficult to detect with MS/MS. There are some obstacles that make the detection of DbpA in tissue lysate with Western blotting difficult. Our experiences showed, that a mild denaturation strategy and gradient gels must be used to detect the two isoforms of the protein. There are similar problems within the detection of DbpA by immunohistochemistry in tissue samples. Here, a stepwise unmasking of the tissue sample is indispensable. This creates the prerequisite to show that the protein DbpA is not only expressed in smooth muscle cells, but also in other cells of the kidney, such as podocytes and tubular epithelial cells. In addition, DbpA is transcriptionally than translationally regulated. Subcellular functions of DbpA as a tight junction associated protein at the cell membrane and in the nucleus are known. However, the main function of DbpA is largely unclear.

5.2 Unveiling the protective mechanisms of DbpA in IRI and tubular cell adaptation

In our study a simple model of transient kidney ischemia was applied to test the contribution of CSPs in the orchestration of pro- and anti-inflammatory steps with immune cell recruitment and tubular cell turnover. DbpA has been described as a binding partner of ZO-1 in tubular cells.²⁵ It may shuttle to the nucleus and act as transcription factor to orchestrate inflammatory processes and alter the cell phenotype.^{12,28,29,184} Due to the reported upregulation of DbpA expression during embryogenesis and kidney development^{9,12}, we expected alterations of TEC composition and kidney function in *Ybx3*^{-/-} animals. Close phenotyping of the animals revealed normal tubular cell composition and renal function over the whole life span.

The performed IRI with an ischemia time of 25 min represents a reversible AKI model with prominent tubular cell damage visualized after a reperfusion time of 24 h in wild type animals. In *Ybx3*^{-/-} animals a resistance to tubular cell damage following transient ischemia became apparent (**Figure 27**), which was not mediated through changes of circulating testosterone levels.⁹ Thus, testosterone-dependent differences in the IRI damage pattern may be excluded.¹⁸⁵ Body weight and food/water intake were significantly lower in adult *Ybx3*^{-/-} animals (**Figures 7c-e**). The phosphorylation of the nutrient and energy sensor AMPK α was markedly upregulated in kidney tissue lysates from healthy *Ybx3* knockout animals (**Figures 7f-g**) and following IRI (**Figures 24b-c**), suggesting that food restriction (without malnutrition) additionally improved metabolic health and increased resistance to stress in experimental animals. Rojas-Morales et al. showed that short-term time restricted feeding protects kidneys against IRI in rodents, that is tubular cell damage is reduced, oxidative stress attenuated with less mitochondrial damage and interstitial fibrosis.¹⁸⁶

How does DbpA mediate the deleterious effect during tubular stress? Firstly, our findings indicated that DbpA expression is not restricted to vascular smooth muscle cells and that the protein is expressed and highly regulated in TECs beyond embryonic development (**Figure 8a-e**). Secondly, our imaging and cell fractionation experiments evidenced a mitochondrial localization of DbpA (**Figures 15g-h**). Thirdly, the mitochondrial functional assays revealed elevated mitochondrial respiration and glycolysis rates in *Ybx3*^{-/-} TECs (**Figures 12b-h, 27**), whereas mitochondrial mass and mitochondrial numbers were unaltered (**Figures 15a-c**). TECs with a deletion of *Ybx3* are more effectively adapt to the inhibition of the mitochondrial FAO pathway (**Figures 11d-g**), possibly by transitioning from mitochondrial FAO to peroxisomal FAO.^{187,188} In contrast to the published work by Cooke et al.¹⁸⁹ and Awad et al.¹⁹⁰ obtained with immortalized HeLa cells or smooth muscle cells, our data do not indicate changes in the amino acid metabolism following DbpA deletion (**Figures 12i-j**). The expression of ATP5A, a component of complex V in the ETC was increased (**Figures 15e-f**), which may promote mitochondrial ATP synthesis and respiration. Elevated mitochondrial membrane potentials in *Ybx3*^{-/-} TECs stabilized the outer mitochondrial membrane, indicating a functional change that renders the cells more resistant to hypoxia (**Figures 15c**). Fourthly, autologous mitochondrial transfer improved mitochondrial respiration of recipient wild type TECs (**Figure 13**). As the above described characteristics with differential metabolic activities and stabilization of the outer mitochondrial membrane was detected in TECs (**Figures 11-15**), but not in BMDMs (**Figure 16**), DbpA fulfills tubular cell-specific functions.

5.3 Mitochondrial-ER interactions and cold shock proteins in renal stress resistance and fibrosis prevention

Given the inter-organelle communication of mitochondria and the ER through mitochondrial-ER-associated membranes (MAMs)¹⁹¹, we next tested the sensing of ER stress in *Ybx3*^{-/-} animals. ER stress was upregulated in wild type animals, but to a much lesser degree in *Ybx3*^{-/-} animals following IRI (**Figure 20**).

Furthermore, prolonged ER stress is associated with the progression of kidney fibrosis, e.g. in the UUO injury model.^{181,182} Therefore, we can assume that the crosstalk among ROS, inflammation, mitochondrial dysfunction and ER stress is one of the major players during renal disease. Indeed, long-term organ damage following tubular cell stress was absent and *Ybx3*^{-/-} animals did not develop kidney fibrosis, which was in contrast to profound matrix deposition in wild type animals following IRI (**Figures 21-22**) and following UUO.⁶⁶

5.4 Mitochondrial transfer as a new technique for the prevention and therapy of kidney disease

The most striking findings relate to the mitochondrial transfer experiments. Mitochondria from *Ybx3^{-/-}* cells improved respiration from recipient wild type TECs (**Figure 13**). Here it should be noted, that further steps to improve the mitochondrial transfer should be considered. Based on the small amount of cells obtained during the mitochondria isolation of primary cells from mice, we decided to use the mitochondria/cytosol fractionation kit. According to the manufacturer's instructions, only a small amount of cells are required to isolate a highly enriched mitochondrial fraction. However, electron microscopic analyses showed that the obtained mitochondrial fractions contained also non-mitochondrial components (**Figure 26**).

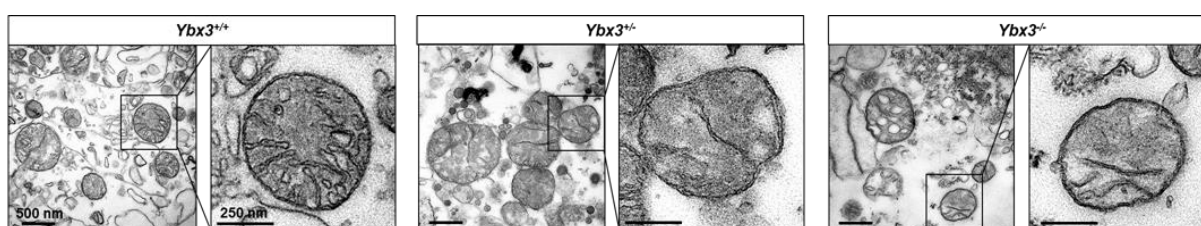


Figure 26. Visualization of mitochondria enrichment by electron microscopy.

Mitochondrial fractions obtained from TECs of *Ybx3^{+/+}*, *Ybx3^{+/-}* and *Ybx3^{-/-}* mice revealed non-mitochondrial components like nuclear or cell membrane fragments.

Beside chemical compounds that target the dysfunction of mitochondria (**Figure 6**), mitochondrial transplantation is a new experimental technique for the prevention and therapy of kidney disease. Therefore, mitochondrial transfer represents a starting point for protective strategies in IRI of the kidney and heart. Recently, such an approach improved cardiomyocyte function in pediatric patients requiring postcardiotomy extracorporeal membrane oxygenation (ECMO) for severe refractory cardiogenic shock after IRI.¹⁹² Furthermore, mitochondrial transfer from mesenchymal stem cells structurally and functionally repaired renal proximal TECs in diabetic nephropathy by regulating SOD2, B-cell lymphoma 2 (Bcl-2), Bcl-2-associated X protein (Bax) and PGC-1 α expression and suppressing ROS production, thereby inhibiting apoptosis.¹⁹³ In Yorkshire pigs, mitochondrial transfer by intra-arterial injection protected from bilateral IRI.¹⁹⁴ Mitochondrial transplantation therapy has shown to increase renal function and antioxidant enzyme levels in an AKI model in rats. Kubat et al. showed that, the transfer of isolated mitochondria from mesenchymal stem cell following doxorubicin-mediated nephrotoxicity into the renal cortex, decreases the cellular oxidative stress and promotes the regeneration of tubular cells after renal injury.¹⁹⁵

However, there is a need of clinical studies to evaluate these mitochondria-related therapies. With a better understanding of the mitochondrial genome, physiology and function, benefits will be realized in animal studies to improve the efficacy and safety of mitochondria-related therapies in human clinical trials.

5.5 Protective mechanisms against ferroptosis in *Ybx3* knockout TECs following IRI

Other groups report ferroptosis as a key cell death pathway in tubular cells following IRI.¹⁹⁶⁻²⁰⁰ Our *in vitro* and *in vivo* analyses support this, e.g. the transcriptome data (**Figure 23b**), SYTOX Green assay (**Figures 25g-h**) and confirmatory Western analyses (**Figures 24b-c**). Remarkably, several mechanisms of cell protection are operative in *Ybx3* knockout cells. First, the antioxidant system is upregulated, which renders the cells less susceptible towards intra- and extracellular ROS exposure (**Figures 24b-c, 25d-f**). Unexpectedly, mROS levels in the kidneys of *Ybx3* knockout animals following IRI were lower than in wild type animals although the mitochondrial activity is higher (**Figure 24c**). The latter phenomenon contradicts common views, however it may reflect a net effect of cell protection. It has been recently shown that GPX4 protects cells against oxidative stress and ferroptosis. Inactivation of GPX4 in mice contributed to IRI-induced AKI by sensitizing kidneys to tubular ferroptosis.¹⁹⁶ We therefore assume that increased levels of GPX4 in *Ybx3*^{-/-} TECs protect cells from ferroptosis, whereas apoptosis is not effected by *Ybx3* deletion (**Figure 23a**). Second, the ATP content of *Ybx3* knockout cells is higher (**Figure 12b**) and these cells have a higher fatty acid uptake rate (**Figure 11d**). Thus, the threshold for energy deficiency is skewed towards cell protection. Third, our overall findings indicate a pronounced change of the transcriptome with less abundance of ferroptosis-related transcripts in stressed *Ybx3* knockout animals (**Figure 23b**).

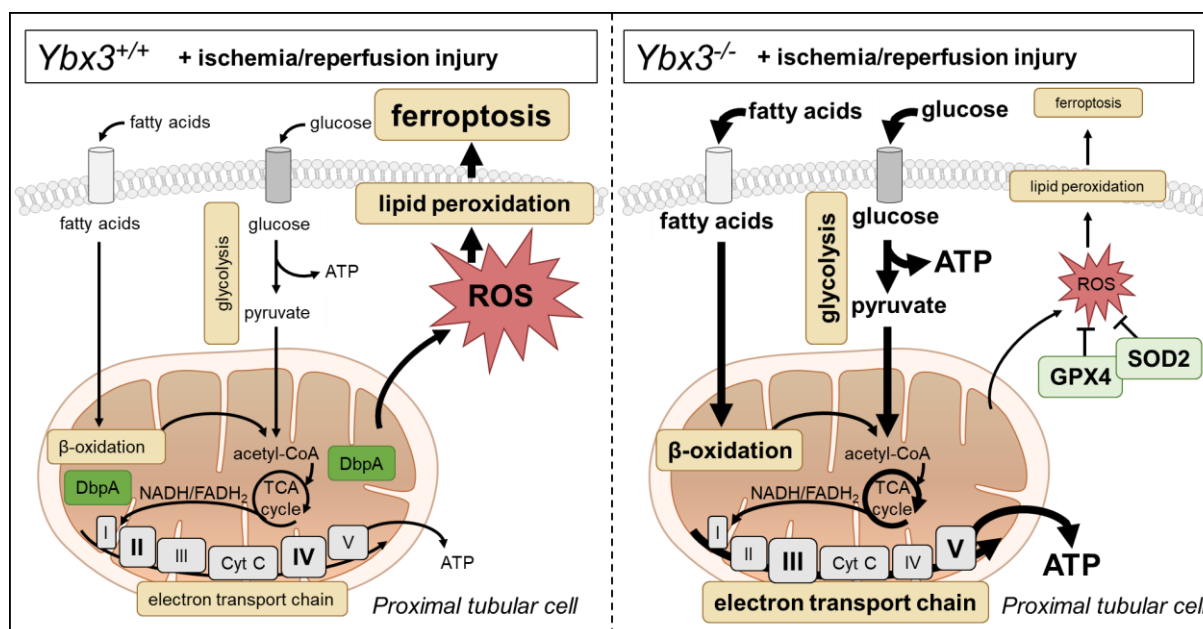


Figure 27. Protective mechanisms against ferroptosis in *Ybx3* knockout TECs.

The deletion of *DbpA* results in phenotypic changes of proximal tubular cells that become particularly apparent following hypoxia. Metabolism for fatty acids, β -oxidation, glycolysis and mitochondrial respiration via the ETC result in differences of ATP synthesis. In addition, antioxidant mechanisms are more activated in cells that lack *DbpA*. Ultimately ROS synthesis differs. Following experimental IRI ferroptosis takes place as distinguishing injury pattern in wild type but not *Ybx3* knockout animals.

Moreover, the expression of the mitophagy marker PINK1 was decreased in kidney tissue lysates obtained from *Ybx3^{-/-}* animals (**Figures 24b-c**), as well as its downstream target Parkin in TECs (**Figures 25d-e**). Thus, an altered mitochondria turnover is likely. We hypothesize that regular and effective mitophagy and mitochondrial renewal takes place in the *Ybx3^{-/-}* TECs cells, resulting in powerful mitochondria with increased metabolic activity and mitochondrial membrane potential.

5.6 AKI as a global public health concern

The diagnosis of AKI is mainly based on rising serum creatinine values, according to the KDIGO guidelines.^{84,201} The molecular mechanisms underlying injury patterns are closely linked with activated cell stress programs and cell damage, given the high oxygen consumption rate of tubular cells and their metabolic activity.⁶⁷ Episodes of acute tubular cell stress are common events, e.g. with acute blood loss during traumatic accidents or postpartum. Other causes include episodes of hypotension with bacterial infection and sepsis or in aging patients diagnosed with morbidities, such as heart failure or arterial hypotension.²⁰² Hypotension may ensue under circumstances of impaired fluid intake and negative water balance with sequela of AKI. Numbers on AKI sum up to 13.3 million patients with 1.7 million deaths per year globally, which is a major public health concern.⁷⁵ National health systems, such as the UK National Health Service, report on AKI-associated costs that sum up to a share exceeding the combined costs for lung, breast and skin cancer altogether.²⁰³ Thus, the overall clinical and socioeconomic relevance of AKI is immense. Given these circumstances, there is an urgent need to understand the critical steps in cell damage, especially for the most oxygen-dependent, vulnerable proximal tubular cells.¹¹¹ Ideally, one envisions a remedy that confines damage and limits the inflammatory response and organ fibrosis.

5.6.1 Animal models of AKI

Animal models have provided important insights into the underlying pathophysiology of AKI. However, until now, only a few therapeutic agents with protective effects in regard of AKI in these animal models, have been successfully translated to the clinic. Current *in vivo* models of AKI in young and healthy rodents point out pathophysiological mechanisms of injury and repair. However, they cannot mimic the complex comorbidities of a heterogeneous patient population including aging, diabetes mellitus, hypertension, vascular disease and pre-existing CKD.⁷⁷ Therefore, animal models that better represents the patient population are necessary. Rodent models of renal ischemia-reperfusion associated with aging, diabetes and CKD induced by three-quarter-nephrectomy have been developed.²⁰⁴⁻²⁰⁶

5.6.2 DbpA as a promising therapeutic targeting protein in the context of AKI

The expression of cold shock protein YB-1 serves as a reliable biomarker for various diseases, i.e. cancer.⁵⁴⁻⁵⁶ Therapeutic interventions targeting CSPs are feasible, given their diverse roles both inside and outside the cell. Since the CSD of the CSPs is highly conserved, it can be assumed that similar interventions of YB-1 are possible to reduce the activity of DbpA.

We propose that targeting DbpA is a promising therapeutic intervention in the context of AKI. A possible starting point for intracellular DbpA blockade is the application of microRNAs (miR). Pan et al. showed that overexpression of miR-191 suppresses the expression of DbpA and its downstream factor cyclin D1.¹⁶³ Hence, pre-emptive DbpA targeting in situations with expected IRI, such as kidney transplantation or cardiac surgery, may potentially preserve kidney function.

5.7 Limitations and future directions in studying DbpA's role in kidney IRI

There are several limitations in our study. The kidney phenotyping and extensive analyses on cell composition within the tubular compartments in conventional *Ybx3* knockout animals may not preclude systemic changes of cell and lipid metabolism. Our analyses indicate that a key enzyme for ATP homeostasis, the phosphorylation of AMPK, is more abundant in knockout animals and may have a major impact on cell homeostasis in and beyond the kidney. These may arise due to changes of amino acid metabolism or other regulatory pathways. To exclude a compromised tubular cell differentiation process within the kidney of knockout animals, we performed extensive quantification of principal and intercalating cells. The tubular structures are normal in composition, indicating no primary developmental deficit. Kidney function parameters such as urine output, osmolality, pH, albuminuria, proteinuria, plasma creatinine, BUN and FITC-sinistrin are unaffected in knockout animals. A cohort of *Ybx3* knockout animals was observed over 24 months, yielding no apparent phenotypic changes or altered life expectancies. Thus, the lower body weight does not translate into a clinical relevant phenotype of animals that are kept in a pathogen-free environment. It remains elusive what proportion of the cellular pool is found in the mitochondria and how DbpA is shuttled there. Respective consensus mitochondrial targeting motifs were not yet published, thus mapping of functional domains may be elusive. In this study we did not address overall alterations of cell metabolism in *Ybx3* knockouts given the profound upregulation of the phosphorylation of AMPK α and lean body mass.

In summary, we introduce cold shock protein DbpA as a key mediator of renal IRI. In animals and cells that lack DbpA protein, mitochondrial function and antioxidant activities are adjusted to levels that convey resistance towards acute cell damage.

References

1. Lindquist, J.A., and Mertens, P.R. (2018). Cold shock proteins: from cellular mechanisms to pathophysiology and disease. *Cell Commun Signal* 16, 63. 10.1186/s12964-018-0274-6.
2. Wolffe, A.P. (1994). Structural and functional properties of the evolutionarily ancient Y-box family of nucleic acid binding proteins. *BioEssays : news and reviews in molecular, cellular and developmental biology* 16, 245-251. 10.1002/bies.950160407.
3. Lindquist, J.A., Brandt, S., Bernhardt, A., Zhu, C., and Mertens, P.R. (2014). The role of cold shock domain proteins in inflammatory diseases. *J Mol Med (Berl)* 92, 207-216. 10.1007/s00109-014-1136-3.
4. Matsumoto, K., and Wolffe, A.P. (1998). Gene regulation by Y-box proteins: coupling control of transcription and translation. *Trends Cell Biol* 8, 318-323. 10.1016/s0962-8924(98)01300-2.
5. Jones, P.G., and Inouye, M. (1994). The cold-shock response--a hot topic. *Mol Microbiol* 11, 811-818. 10.1111/j.1365-2958.1994.tb00359.x.
6. Gottesman, S. (2018). Chilled in Translation: Adapting to Bacterial Climate Change. *Mol Cell* 70, 193-194. 10.1016/j.molcel.2018.04.003.
7. Graumann, P.L., and Marahiel, M.A. (1998). A superfamily of proteins that contain the cold-shock domain. *Trends Biochem Sci* 23, 286-290. 10.1016/s0968-0004(98)01255-9.
8. Lu, Z.H., Books, J.T., and Ley, T.J. (2005). YB-1 is important for late-stage embryonic development, optimal cellular stress responses, and the prevention of premature senescence. *Mol Cell Biol* 25, 4625-4637. 10.1128/mcb.25.11.4625-4637.2005.
9. Lu, Z.H., Books, J.T., and Ley, T.J. (2006). Cold shock domain family members YB-1 and MSY4 share essential functions during murine embryogenesis. *Mol Cell Biol* 26, 8410-8417. 10.1128/mcb.01196-06.
10. Fan, L., Jones, S.N., Padden, C., Shen, Q., and Newburger, P.E. (2006). Nuclease sensitive element binding protein 1 gene disruption results in early embryonic lethality. *J Cell Biochem* 99, 140-145. 10.1002/jcb.20911.

11. Bernhardt, A., Häberer, S., Xu, J., Damerau, H., Steffen, J., Reichardt, C., Wolters, K., Steffen, H., Isermann, B., Borucki, K., et al. (2021). High salt diet-induced proximal tubular phenotypic changes and sodium-glucose cotransporter-2 expression are coordinated by cold shock Y-box binding protein-1. *Faseb j* 35, e21912. 10.1096/fj.202100667RR.
12. Lima, W.R., Parreira, K.S., Devuyt, O., Caplanusi, A., N'Kuli, F., Marien, B., Van Der Smissen, P., Alves, P.M., Verroust, P., Christensen, E.I., et al. (2010). ZONAB promotes proliferation and represses differentiation of proximal tubule epithelial cells. *J Am Soc Nephrol* 21, 478-488. 10.1681/asn.2009070698.
13. Berghella, L., De Angelis, L., De Buysscher, T., Mortazavi, A., Biressi, S., Forcales, S.V., Sirabella, D., Cossu, G., and Wold, B.J. (2008). A highly conserved molecular switch binds MSY-3 to regulate myogenin repression in postnatal muscle. *Genes Dev* 22, 2125-2138. 10.1101/gad.468508.
14. Kudo, S., Mattei, M.G., and Fukuda, M. (1995). Characterization of the gene for dbpA, a family member of the nucleic-acid-binding proteins containing a cold-shock domain. *Eur J Biochem* 231, 72-82. 10.1111/j.1432-1033.1995.tb20672.x.
15. Eliseeva, I.A., Kim, E.R., Guryanov, S.G., Ovchinnikov, L.P., and Lyabin, D.N. (2011). Y-box-binding protein 1 (YB-1) and its functions. *Biochemistry (Mosc)* 76, 1402-1433. 10.1134/s0006297911130049.
16. Scott, N.E., Rogers, L.D., Prudova, A., Brown, N.F., Fortelny, N., Overall, C.M., and Foster, L.J. (2017). Interactome disassembly during apoptosis occurs independent of caspase cleavage. *13*, 906. 10.15252/msb.20167067.
17. Wolffe, A.P., Tafuri, S., Ranjan, M., and Familari, M. (1992). The Y-box factors: a family of nucleic acid binding proteins conserved from *Escherichia coli* to man. *New Biol* 4, 290-298.
18. Sakura, H., Maekawa, T., Imamoto, F., Yasuda, K., and Ishii, S. (1988). Two human genes isolated by a novel method encode DNA-binding proteins containing a common region of homology. *Gene* 73, 499-507. 10.1016/0378-1119(88)90514-8.
19. Landsman, D. (1992). RNP-1, an RNA-binding motif is conserved in the DNA-binding cold shock domain. *Nucleic Acids Res* 20, 2861-2864. 10.1093/nar/20.11.2861.
20. Tafuri, S.R., and Wolffe, A.P. (1992). DNA binding, multimerization, and transcription stimulation by the *Xenopus* Y box proteins in vitro. *New Biol* 4, 349-359.

21. Ladomery, M., and Sommerville, J. (1994). Binding of Y-box proteins to RNA: involvement of different protein domains. *Nucleic Acids Res* 22, 5582-5589. 10.1093/nar/22.25.5582.
22. Bouvet, P., Matsumoto, K., and Wolffe, A.P. (1995). Sequence-specific RNA recognition by the *Xenopus* Y-box proteins. An essential role for the cold shock domain. *J Biol Chem* 270, 28297-28303. 10.1074/jbc.270.47.28297.
23. Hasegawa, S.L., Doetsch, P.W., Hamilton, K.K., Martin, A.M., Okenquist, S.A., Lenz, J., and Boss, J.M. (1991). DNA binding properties of YB-1 and dbpA: binding to double-stranded, single-stranded, and abasic site containing DNAs. *Nucleic Acids Res* 19, 4915-4920. 10.1093/nar/19.18.4915.
24. Seufert, L., and Benzing, T. (2022). RNA-binding proteins and their role in kidney disease. *18*, 153-170. 10.1038/s41581-021-00497-1.
25. Balda, M.S., and Matter, K. (2000). The tight junction protein ZO-1 and an interacting transcription factor regulate ErbB-2 expression. *Embo j* 19, 2024-2033. 10.1093/emboj/19.9.2024.
26. Spadaro, D., Tapia, R., Jond, L., Sudol, M., Fanning, A.S., and Citi, S. (2014). ZO proteins redundantly regulate the transcription factor DbpA/ZONAB. *J Biol Chem* 289, 22500-22511. 10.1074/jbc.M114.556449.
27. Spadaro, D., Le, S., Laroche, T., Mean, I., Jond, L., Yan, J., and Citi, S. (2017). Tension-Dependent Stretching Activates ZO-1 to Control the Junctional Localization of Its Interactors. *Curr Biol* 27, 3783-3795.e3788. 10.1016/j.cub.2017.11.014.
28. Matter, K., and Balda, M.S. (2007). Epithelial tight junctions, gene expression and nucleo-junctional interplay. *J Cell Sci* 120, 1505-1511. 10.1242/jcs.005975.
29. Balda, M.S., and Matter, K. (2009). Tight junctions and the regulation of gene expression. *Biochim Biophys Acta* 1788, 761-767. 10.1016/j.bbamem.2008.11.024.
30. Sourisseau, T., Georgiadis, A., Tsapara, A., Ali, R.R., Pestell, R., Matter, K., and Balda, M.S. (2006). Regulation of PCNA and cyclin D1 expression and epithelial morphogenesis by the ZO-1-regulated transcription factor ZONAB/DbpA. *Mol Cell Biol* 26, 2387-2398. 10.1128/mcb.26.6.2387-2398.2006.
31. Frankel, P., Aronheim, A., Kavanagh, E., Balda, M.S., Matter, K., Bunney, T.D., and Marshall, C.J. (2005). RalA interacts with ZONAB in a cell density-dependent manner and regulates its transcriptional activity. *Embo j* 24, 54-62. 10.1038/sj.emboj.7600497.

32. Nie, M., Aijaz, S., Leefa Chong San, I.V., Balda, M.S., and Matter, K. (2009). The Y-box factor ZONAB/DbpA associates with GEF-H1/Lfc and mediates Rho-stimulated transcription. *EMBO Rep* 10, 1125-1131. 10.1038/embor.2009.182.
33. Buchert, M., Darido, C., Lagerqvist, E., Sedello, A., Cazevieuille, C., Buchholz, F., Bourgaux, J.F., Pannequin, J., Joubert, D., and Hollande, F. (2009). The symplekin/ZONAB complex inhibits intestinal cell differentiation by the repression of AML1/Runx1. *Gastroenterology* 137, 156-164, 164.e151-153. 10.1053/j.gastro.2009.03.037.
34. Kavanagh, E., Buchert, M., Tsapara, A., Choquet, A., Balda, M.S., Hollande, F., and Matter, K. (2006). Functional interaction between the ZO-1-interacting transcription factor ZONAB/DbpA and the RNA processing factor symplekin. *J Cell Sci* 119, 5098-5105. 10.1242/jcs.03297.
35. Moorthamer, M., Zumstein-Mecker, S., and Chaudhuri, B. (1999). DNA binding protein dbpA binds Cdk5 and inhibits its activity. *FEBS Lett* 446, 343-350. 10.1016/s0014-5793(99)00248-3.
36. Sears, D., Luong, P., Yuan, M., Nteliopoulos, G., Man, Y.K., Melo, J.V., and Basu, S. (2010). Functional phosphoproteomic analysis reveals cold-shock domain protein A to be a Bcr-Abl effector-regulating proliferation and transformation in chronic myeloid leukemia. *Cell Death Dis* 1, e93. 10.1038/cddis.2010.72.
37. Coles, L.S., Lambrusco, L., Burrows, J., Hunter, J., Diamond, P., Bert, A.G., Vadas, M.A., and Goodall, G.J. (2005). Phosphorylation of cold shock domain/Y-box proteins by ERK2 and GSK3beta and repression of the human VEGF promoter. *FEBS Lett* 579, 5372-5378. 10.1016/j.febslet.2005.08.075.
38. Brandt, S., Raffetseder, U., Djudjaj, S., Schreiter, A., Kadereit, B., Michele, M., Pabst, M., Zhu, C., and Mertens, P.R. (2012). Cold shock Y-box protein-1 participates in signaling circuits with auto-regulatory activities. *Eur J Cell Biol* 91, 464-471. 10.1016/j.ejcb.2011.07.002.
39. Yin, Q., Zheng, M., Luo, Q., Jiang, D., Zhang, H., and Chen, C. (2022). YB-1 as an Oncoprotein: Functions, Regulation, Post-Translational Modifications, and Targeted Therapy. *Cells* 11. 10.3390/cells11071217.

40. Dahl, E., En-Nia, A., Wiesmann, F., Krings, R., Djudjaj, S., Breuer, E., Fuchs, T., Wild, P.J., Hartmann, A., Dunn, S.E., and Mertens, P.R. (2009). Nuclear detection of Y-box protein-1 (YB-1) closely associates with progesterone receptor negativity and is a strong adverse survival factor in human breast cancer. *BMC cancer* 9, 410. 10.1186/1471-2407-9-410.
41. Bargou, R.C., Jürchott, K., Wagener, C., Bergmann, S., Metzner, S., Bommert, K., Mapara, M.Y., Winzer, K.J., Dietel, M., Dörken, B., and Royer, H.D. (1997). Nuclear localization and increased levels of transcription factor YB-1 in primary human breast cancers are associated with intrinsic MDR1 gene expression. *Nature medicine* 3, 447-450. 10.1038/nm0497-447.
42. Giménez-Bonafé, P., Fedoruk, M.N., Whitmore, T.G., Akbari, M., Ralph, J.L., Ettinger, S., Gleave, M.E., and Nelson, C.C. (2004). YB-1 is upregulated during prostate cancer tumor progression and increases P-glycoprotein activity. *The Prostate* 59, 337-349. 10.1002/pros.20023.
43. Chatterjee, M., Rancso, C., Stühmer, T., Eckstein, N., Andrulis, M., Gerecke, C., Lorentz, H., Royer, H.D., and Bargou, R.C. (2008). The Y-box binding protein YB-1 is associated with progressive disease and mediates survival and drug resistance in multiple myeloma. *Blood* 111, 3714-3722. 10.1182/blood-2007-05-089151.
44. Jayavelu, A.K., Schnöder, T.M., Perner, F., Herzog, C., and Meiler, A. (2020). Splicing factor YBX1 mediates persistence of JAK2-mutated neoplasms. *588*, 157-163. 10.1038/s41586-020-2968-3.
45. Kato, M., Wang, L., Putta, S., Wang, M., Yuan, H., Sun, G., Lanting, L., Todorov, I., Rossi, J.J., and Natarajan, R. (2010). Post-transcriptional up-regulation of Tsc-22 by Ybx1, a target of miR-216a, mediates TGF- β -induced collagen expression in kidney cells. *The Journal of biological chemistry* 285, 34004-34015. 10.1074/jbc.M110.165027.
46. Hanssen, L., Alidousty, C., Djudjaj, S., Frye, B.C., Rauen, T., Boor, P., Mertens, P.R., van Roeyen, C.R., Tacke, F., Heymann, F., et al. (2013). YB-1 is an early and central mediator of bacterial and sterile inflammation in vivo. *Journal of immunology (Baltimore, Md. : 1950)* 191, 2604-2613. 10.4049/jimmunol.1300416.
47. Gibbert, L., Hermert, D., Wang, J., D, M.B., Alidousty, C., Neusser, M., Cohen, C.D., Gröne, E., Macheleidt, I., Rauen, T., et al. (2018). YB-1 increases glomerular, but decreases interstitial fibrosis in CNI-induced nephropathy. *Clinical immunology (Orlando, Fla.)* 194, 67-74. 10.1016/j.clim.2018.07.002.

48. Hanssen, L., Frye, B.C., Ostendorf, T., Alidousty, C., Djudjaj, S., Boor, P., Rauen, T., Floege, J., Mertens, P.R., and Raffetseder, U. (2011). Y-box binding protein-1 mediates profibrotic effects of calcineurin inhibitors in the kidney. *J Immunol* 187, 298-308. 10.4049/jimmunol.1100382.
49. Zhu, X., Ye, Y., Xu, C., Gao, C., Zhang, Y., Zhou, J., Lin, W., and Mao, J. (2019). Protein phosphatase 2A modulates podocyte maturation and glomerular functional integrity in mice. *Cell Commun Signal* 17, 91. 10.1186/s12964-019-0402-y.
50. van Roeyen, C.R., Eitner, F., Martinkus, S., Thielges, S.R., Ostendorf, T., Bokemeyer, D., Lüscher, B., Lüscher-Firzlaff, J.M., Floege, J., and Mertens, P.R. (2005). Y-box protein 1 mediates PDGF-B effects in mesangioproliferative glomerular disease. *J Am Soc Nephrol* 16, 2985-2996. 10.1681/asn.2004111009.
51. Raffetseder, U., Rauen, T., Boor, P., Ostendorf, T., Hanssen, L., Floege, J., En-Nia, A., Djudjaj, S., Frye, B.C., and Mertens, P.R. (2011). Extracellular YB-1 blockade in experimental nephritis upregulates Notch-3 receptor expression and signaling. *Nephron Exp Nephrol* 118, e100-108. 10.1159/000324209.
52. Wang, J., Liu, X., Gu, Y., Gao, Y., Jankowski, V., Was, N., Leitz, A., Reiss, L.K., Shi, Y., Cai, J., et al. (2023). DNA binding protein YB-1 is a part of the neutrophil extracellular trap mediation of kidney damage and cross-organ effects. *Kidney Int.* 10.1016/j.kint.2023.02.032.
53. Dong, W., Wang, H., Shahzad, K., Bock, F., Al-Dabet, M.M., Ranjan, S., Wolter, J., Kohli, S., Hoffmann, J., Dhople, V.M., et al. (2015). Activated Protein C Ameliorates Renal Ischemia-Reperfusion Injury by Restricting Y-Box Binding Protein-1 Ubiquitination. *J Am Soc Nephrol* 26, 2789-2799. 10.1681/asn.2014080846.
54. Tacke, F., Kanig, N., En-Nia, A., Kaehne, T., Eberhardt, C.S., Shpacovitch, V., Trautwein, C., and Mertens, P.R. (2011). Y-box protein-1/p18 fragment identifies malignancies in patients with chronic liver disease. *BMC Cancer* 11, 185. 10.1186/1471-2407-11-185.
55. Tacke, F., Galm, O., Kanig, N., Yagmur, E., Brandt, S., Lindquist, J.A., Eberhardt, C.S., Raffetseder, U., and Mertens, P.R. (2014). High prevalence of Y-box protein-1/p18 fragment in plasma of patients with malignancies of different origin. *BMC Cancer* 14, 33. 10.1186/1471-2407-14-33.

56. Rohr, I., Braicu, E.I., En-Nia, A., Heinrich, M., Richter, R., Chekerov, R., Dechend, R., Heidecke, H., Dragun, D., Schäfer, R., et al. (2016). Y-box protein-1/p18 as novel serum marker for ovarian cancer diagnosis: A study by the Tumor Bank Ovarian Cancer (TOC). *Cytokine* 85, 157-164. 10.1016/j.cyto.2016.06.021.
57. Higashi, K., Tomigahara, Y., Shiraki, H., Miyata, K., Mikami, T., Kimura, T., Moro, T., Inagaki, Y., and Kaneko, H. (2011). A novel small compound that promotes nuclear translocation of YB-1 ameliorates experimental hepatic fibrosis in mice. *J Biol Chem* 286, 4485-4492. 10.1074/jbc.M110.151936.
58. Imai, J., Hozumi, K., Sumiyoshi, H., Yazawa, M., Hirano, K., Abe, J., Higashi, K., Inagaki, Y., and Mine, T. (2015). Anti-fibrotic effects of a novel small compound on the regulation of cytokine production in a mouse model of colorectal fibrosis. *Biochem Biophys Res Commun* 468, 554-560. 10.1016/j.bbrc.2015.10.123.
59. Khan, M.I., Adhami, V.M., Lall, R.K., Sechi, M., Joshi, D.C., Haidar, O.M., Syed, D.N., Siddiqui, I.A., Chiu, S.Y., and Mukhtar, H. (2014). YB-1 expression promotes epithelial-to-mesenchymal transition in prostate cancer that is inhibited by a small molecule fisetin. *Oncotarget* 5, 2462-2474. 10.18632/oncotarget.1790.
60. Ciani, F., Tafuri, S., Troiano, A., Cimmino, A., Fioretto, B.S., Guarino, A.M., Pollice, A., Vivo, M., Evidente, A., Carotenuto, D., and Calabrò, V. (2018). Anti-proliferative and pro-apoptotic effects of *Uncaria tomentosa* aqueous extract in squamous carcinoma cells. *J Ethnopharmacol* 211, 285-294. 10.1016/j.jep.2017.09.031.
61. Gunasekaran, V.P., Nishi, K., Sivakumar, D., Sivaraman, T., and Mathan, G. (2018). Identification of 2,4-dihydroxy-5-pyrimidinyl imidothiocarbamate as a novel inhibitor to Y box binding protein-1 (YB-1) and its therapeutic actions against breast cancer. *Eur J Pharm Sci* 116, 2-14. 10.1016/j.ejps.2017.09.019.
62. Zhu, C., Sauter, E., Schreiter, A., van Roeyen, C.R., Ostendorf, T., Floege, J., Gembardt, F., Hugo, C.P., Isermann, B., Lindquist, J.A., and Mertens, P.R. (2016). Cold Shock Proteins Mediate GN with Mesangioproliferation. *J Am Soc Nephrol* 27, 3678-3689. 10.1681/asn.2015121367.
63. Festa, B.P., Chen, Z., Berquez, M., Debaix, H., Tokonami, N., Prange, J.A., Hoek, G.V., Alessio, C., Raimondi, A., Nevo, N., et al. (2018). Impaired autophagy bridges lysosomal storage disease and epithelial dysfunction in the kidney. *Nat Commun* 9, 161. 10.1038/s41467-017-02536-7.

64. Raggi, C., Luciani, A., Nevo, N., Antignac, C., Terry, S., and Devuyst, O. (2014). Dedifferentiation and aberrations of the endolysosomal compartment characterize the early stage of nephropathic cystinosis. *Hum Mol Genet* 23, 2266-2278. 10.1093/hmg/ddt617.
65. Sun, H., Li, H., Yan, J., Wang, X., Xu, M., Wang, M., Fan, B., Liu, J., Lin, N., Wang, X., et al. (2022). Loss of CLDN5 in podocytes deregulates WIF1 to activate WNT signaling and contributes to kidney disease. *Nat Commun* 13, 1600. 10.1038/s41467-022-29277-6.
66. Lindquist, J.A., Bernhardt, A., Reichardt, C., Sauter, E., Brandt, S., Rana, R., Lindenmeyer, M.T., Philipsen, L., Isermann, B., Zhu, C., and Mertens, P.R. (2023). Cold Shock Domain Protein DbpA Orchestrates Tubular Cell Damage and Interstitial Fibrosis in Inflammatory Kidney Disease. *Cells* 12. 10.3390/cells12101426.
67. Duann, P., and Lin, P.H. (2017). Mitochondria Damage and Kidney Disease. *Adv Exp Med Biol* 982, 529-551. 10.1007/978-3-319-55330-6_27.
68. Scott, R.P., and Quaggin, S.E. (2015). Review series: The cell biology of renal filtration. *J Cell Biol* 209, 199-210. 10.1083/jcb.201410017.
69. Puelles, V.G., Hoy, W.E., Hughson, M.D., Diouf, B., Douglas-Denton, R.N., and Bertram, J.F. (2011). Glomerular number and size variability and risk for kidney disease. *Curr Opin Nephrol Hypertens* 20, 7-15. 10.1097/MNH.0b013e3283410a7d.
70. Huen, S.C., and Cantley, L.G. (2017). Macrophages in Renal Injury and Repair. *Annu Rev Physiol* 79, 449-469. 10.1146/annurev-physiol-022516-034219.
71. Wang, Z., and Zhang, C. (2022). From AKI to CKD: Maladaptive Repair and the Underlying Mechanisms. *Int J Mol Sci* 23. 10.3390/ijms231810880.
72. Makris, K., and Spanou, L. (2016). Acute Kidney Injury: Definition, Pathophysiology and Clinical Phenotypes. *Clin Biochem Rev* 37, 85-98.
73. Finlay, S., Bray, B., Lewington, A.J., Hunter-Rowe, C.T., Banerjee, A., Atkinson, J.M., and Jones, M.C. (2013). Identification of risk factors associated with acute kidney injury in patients admitted to acute medical units. *Clin Med (Lond)* 13, 233-238. 10.7861/clinmedicine.13-3-233.

-
74. An, J.N., Hwang, J.H., Kim, D.K., Lee, H., Ahn, S.Y., Kim, S., Park, J.T., Kang, S.W., Oh, Y.K., Kim, Y.S., et al. (2017). Chronic Kidney Disease After Acute Kidney Injury Requiring Continuous Renal Replacement Therapy and Its Impact on Long-Term Outcomes: A Multicenter Retrospective Cohort Study in Korea. *Crit Care Med* 45, 47-57. 10.1097/ccm.0000000000002012.
 75. Mehta, R.L., Cerdá, J., Burdmann, E.A., Tonelli, M., García-García, G., Jha, V., Susantitaphong, P., Rocco, M., Vanholder, R., Sever, M.S., et al. (2015). International Society of Nephrology's Oby25 initiative for acute kidney injury (zero preventable deaths by 2025): a human rights case for nephrology. *Lancet* 385, 2616-2643. 10.1016/s0140-6736(15)60126-x.
 76. Hoste, E.A., Clermont, G., Kersten, A., Venkataraman, R., Angus, D.C., De Bacquer, D., and Kellum, J.A. (2006). RIFLE criteria for acute kidney injury are associated with hospital mortality in critically ill patients: a cohort analysis. *Crit Care* 10, R73. 10.1186/cc4915.
 77. Zuk, A., and Bonventre, J.V. (2016). Acute Kidney Injury. *Annu Rev Med* 67, 293-307. 10.1146/annurev-med-050214-013407.
 78. Coca, S.G., Yusuf, B., Shlipak, M.G., Garg, A.X., and Parikh, C.R. (2009). Long-term risk of mortality and other adverse outcomes after acute kidney injury: a systematic review and meta-analysis. *Am J Kidney Dis* 53, 961-973. 10.1053/j.ajkd.2008.11.034.
 79. Coca, S.G., Singanamala, S., and Parikh, C.R. (2012). Chronic kidney disease after acute kidney injury: a systematic review and meta-analysis. *Kidney Int* 81, 442-448. 10.1038/ki.2011.379.
 80. Cerdá, J., Bagga, A., Kher, V., and Chakravarthi, R.M. (2008). The contrasting characteristics of acute kidney injury in developed and developing countries. *Nat Clin Pract Nephrol* 4, 138-153. 10.1038/ncpneph0722.
 81. Kirita, Y., Wu, H., Uchimura, K., Wilson, P.C., and Humphreys, B.D. (2020). Cell profiling of mouse acute kidney injury reveals conserved cellular responses to injury. *Proc Natl Acad Sci U S A* 117, 15874-15883. 10.1073/pnas.2005477117.
 82. Dixon, E.E., Wu, H., Muto, Y., Wilson, P.C., and Humphreys, B.D. (2022). Spatially Resolved Transcriptomic Analysis of Acute Kidney Injury in a Female Murine Model. *J Am Soc Nephrol* 33, 279-289. 10.1681/asn.2021081150.

83. Hinze, C., Kocks, C., Leiz, J., Karaiskos, N., Boltengagen, A., Cao, S., Skopnik, C.M., Klocke, J., Hardenberg, J.H., Stockmann, H., et al. (2022). Single-cell transcriptomics reveals common epithelial response patterns in human acute kidney injury. *Genome Med* 14, 103. 10.1186/s13073-022-01108-9.
84. Khwaja, A. (2012). KDIGO clinical practice guidelines for acute kidney injury. *Nephron Clin Pract* 120, c179-184. 10.1159/000339789.
85. Yoon, S.Y., Kim, J.S., Jeong, K.H., and Kim, S.K. (2022). Acute Kidney Injury: Biomarker-Guided Diagnosis and Management. *Medicina (Kaunas)* 58. 10.3390/medicina58030340.
86. Ostermann, M., Zarbock, A., Goldstein, S., Kashani, K., Macedo, E., Murugan, R., Bell, M., Forni, L., Guzzi, L., Joannidis, M., et al. (2020). Recommendations on Acute Kidney Injury Biomarkers From the Acute Disease Quality Initiative Consensus Conference: A Consensus Statement. *JAMA Netw Open* 3, e2019209. 10.1001/jamanetworkopen.2020.19209.
87. Hinze, C., and Schmidt-Ott, K.M. (2022). Acute kidney injury biomarkers in the single-cell transcriptomic era. *Am J Physiol Cell Physiol* 323, C1430-c1443. 10.1152/ajpcell.00079.2022.
88. Mercado, M.G., Smith, D.K., and Guard, E.L. (2019). Acute Kidney Injury: Diagnosis and Management. *Am Fam Physician* 100, 687-694.
89. Chanchaoenthana, W., and Leelahavanichkul, A. (2019). Acute kidney injury spectrum in patients with chronic liver disease: Where do we stand? *World J Gastroenterol* 25, 3684-3703. 10.3748/wjg.v25.i28.3684.
90. Holgado, J.L., Lopez, C., Fernandez, A., Sauri, I., Uso, R., Trillo, J.L., Vela, S., Nuñez, J., Redon, J., and Ruiz, A. (2020). Acute kidney injury in heart failure: a population study. *ESC Heart Fail* 7, 415-422. 10.1002/ehf2.12595.
91. Chevet, B., Cornec, D., Casal Moura, M., Cornec-Le Gall, E., Fervenza, F.C., Warrington, K.J., Specks, U., and Berti, A. (2023). Diagnosing and treating ANCA-associated vasculitis: an updated review for clinical practice. *Rheumatology (Oxford)* 62, 1787-1803. 10.1093/rheumatology/keac623.
92. Zhang, X., Agborbesong, E., and Li, X. (2021). The Role of Mitochondria in Acute Kidney Injury and Chronic Kidney Disease and Its Therapeutic Potential. *Int J Mol Sci* 22. 10.3390/ijms222011253.

93. Ferenbach, D.A., and Bonventre, J.V. (2015). Mechanisms of maladaptive repair after AKI leading to accelerated kidney ageing and CKD. *Nat Rev Nephrol* 11, 264-276. 10.1038/nrneph.2015.3.
94. Guzzi, F., Cirillo, L., Roperto, R.M., Romagnani, P., and Lazzeri, E. (2019). Molecular Mechanisms of the Acute Kidney Injury to Chronic Kidney Disease Transition: An Updated View. *Int J Mol Sci* 20. 10.3390/ijms20194941.
95. Klomjit, N., and Ungprasert, P. (2022). Acute kidney injury associated with non-steroidal anti-inflammatory drugs. *European journal of internal medicine* 101, 21-28. 10.1016/j.ejim.2022.05.003.
96. Thongprayoon, C., Hansrivijit, P., Kovvuru, K., Kanduri, S.R., Torres-Ortiz, A., Acharya, P., Gonzalez-Suarez, M.L., Kaewput, W., Bathini, T., and Cheungpasitporn, W. (2020). Diagnostics, Risk Factors, Treatment and Outcomes of Acute Kidney Injury in a New Paradigm. *J Clin Med* 9. 10.3390/jcm9041104.
97. Verma, S.K., and Molitoris, B.A. (2015). Renal endothelial injury and microvascular dysfunction in acute kidney injury. *Semin Nephrol* 35, 96-107. 10.1016/j.semnephrol.2015.01.010.
98. Bonventre, J.V., and Yang, L. (2011). Cellular pathophysiology of ischemic acute kidney injury. *J Clin Invest* 121, 4210-4221. 10.1172/jci45161.
99. Malek, M., and Nematbakhsh, M. (2015). Renal ischemia/reperfusion injury; from pathophysiology to treatment. *Journal of renal injury prevention* 4, 20-27. 10.12861/jrip.2015.06.
100. Molitoris, B.A. (2014). Therapeutic translation in acute kidney injury: the epithelial/endothelial axis. *J Clin Invest* 124, 2355-2363. 10.1172/jci72269.
101. Peired, A.J., and Melica, M.E. (2021). Molecular Mechanisms of Renal Progenitor Regulation: How Many Pieces in the Puzzle? *10*. 10.3390/cells10010059.
102. De Chiara, L., Conte, C., Semeraro, R., Diaz-Bulnes, P., Angelotti, M.L., Mazzinghi, B., Molli, A., Antonelli, G., Landini, S., Melica, M.E., et al. (2022). Tubular cell polyploidy protects from lethal acute kidney injury but promotes consequent chronic kidney disease. *Nat Commun* 13, 5805. 10.1038/s41467-022-33110-5.
103. Forbes, J.M. (2016). Mitochondria-Power Players in Kidney Function? *Trends Endocrinol Metab* 27, 441-442. 10.1016/j.tem.2016.05.002.

104. Pujalte-Martin, M., Belaïd, A., Bost, S., Kahi, M., Peraldi, P., Rouleau, M., Mazure, N.M., and Bost, F. (2024). Targeting cancer and immune cell metabolism with the complex I inhibitors metformin and IACS-010759. *Mol Oncol.* 10.1002/1878-0261.13583.
105. Zhang, S., Lv, K., Liu, Z., Zhao, R., and Li, F. (2024). Fatty acid metabolism of immune cells: a new target of tumour immunotherapy. *Cell Death Discov* 10, 39. 10.1038/s41420-024-01807-9.
106. Yan, P., Liu, J., Li, Z., Wang, J., Zhu, Z., Wang, L., and Yu, G. (2023). Glycolysis Reprogramming in Idiopathic Pulmonary Fibrosis: Unveiling the Mystery of Lactate in the Lung. *Int J Mol Sci* 25. 10.3390/ijms25010315.
107. Kao, T.W., Chuang, Y.C., Lee, H.L., Kuo, C.C., and Shen, Y.A. (2022). Therapeutic Targeting of Glutaminolysis as a Novel Strategy to Combat Cancer Stem Cells. *Int J Mol Sci* 23. 10.3390/ijms232315296.
108. MacLean, A., Legendre, F., and Appanna, V.D. (2023). The tricarboxylic acid (TCA) cycle: a malleable metabolic network to counter cellular stress. *Crit Rev Biochem Mol Biol* 58, 81-97. 10.1080/10409238.2023.2201945.
109. Germano, J.F., Huang, C., Sin, J., Song, Y., Tucker, K.C., Taylor, D.J.R., Saadaeijahromi, H., Stotland, A., Piplani, H., Gottlieb, R.A., et al. (2020). Intermittent Use of a Short-Course Glucagon-like Peptide-1 Receptor Agonist Therapy Limits Adverse Cardiac Remodeling via Parkin-dependent Mitochondrial Turnover. *Sci Rep* 10, 8284. 10.1038/s41598-020-64924-2.
110. Qin, N., Cai, T., Ke, Q., Yuan, Q., Luo, J., Mao, X., Jiang, L., Cao, H., Wen, P., Zen, K., et al. (2019). UCP2-dependent improvement of mitochondrial dynamics protects against acute kidney injury. *J Pathol* 247, 392-405. 10.1002/path.5198.
111. Hall, A.M., Unwin, R.J., Parker, N., and Duchon, M.R. (2009). Multiphoton imaging reveals differences in mitochondrial function between nephron segments. *J Am Soc Nephrol* 20, 1293-1302. 10.1681/asn.2008070759.
112. Wang, Y., Quan, F., Cao, Q., Lin, Y., Yue, C., Bi, R., Cui, X., Yang, H., Yang, Y., Birnbaumer, L., et al. (2021). Quercetin alleviates acute kidney injury by inhibiting ferroptosis. *J Adv Res* 28, 231-243. 10.1016/j.jare.2020.07.007.

113. Müller-Deile, J., and Schiffer, M. (2014). The podocyte power-plant disaster and its contribution to glomerulopathy. *Front Endocrinol (Lausanne)* 5, 209. 10.3389/fendo.2014.00209.
114. Stieger, N., Worthmann, K., Teng, B., Engeli, S., Das, A.M., Haller, H., and Schiffer, M. (2012). Impact of high glucose and transforming growth factor- β on bioenergetic profiles in podocytes. *Metabolism* 61, 1073-1086. 10.1016/j.metabol.2011.12.003.
115. Duann, P., Lianos, E.A., Ma, J., and Lin, P.H. (2016). Autophagy, Innate Immunity and Tissue Repair in Acute Kidney Injury. *Int J Mol Sci* 17. 10.3390/ijms17050662.
116. Eiyama, A., and Okamoto, K. (2015). PINK1/Parkin-mediated mitophagy in mammalian cells. *Curr Opin Cell Biol* 33, 95-101. 10.1016/j.ceb.2015.01.002.
117. Stotland, A., and Gottlieb, R.A. (2015). Mitochondrial quality control: Easy come, easy go. *Biochim Biophys Acta* 1853, 2802-2811. 10.1016/j.bbamcr.2014.12.041.
118. Ashrafi, G., and Schwarz, T.L. (2013). The pathways of mitophagy for quality control and clearance of mitochondria. *Cell Death Differ* 20, 31-42. 10.1038/cdd.2012.81.
119. Onishi, M., Yamano, K., Sato, M., Matsuda, N., and Okamoto, K. (2021). Molecular mechanisms and physiological functions of mitophagy. *Embo j* 40, e104705. 10.15252/emj.2020104705.
120. Youle, R.J., and Narendra, D.P. (2011). Mechanisms of mitophagy. *Nat Rev Mol Cell Biol* 12, 9-14. 10.1038/nrm3028.
121. Popov, L.D. (2020). Mitochondrial biogenesis: An update. *J Cell Mol Med* 24, 4892-4899. 10.1111/jcmm.15194.
122. Scarpulla, R.C. (2011). Metabolic control of mitochondrial biogenesis through the PGC-1 family regulatory network. *Biochim Biophys Acta* 1813, 1269-1278. 10.1016/j.bbamcr.2010.09.019.
123. Hardie, D.G., Ross, F.A., and Hawley, S.A. (2012). AMPK: a nutrient and energy sensor that maintains energy homeostasis. *Nat Rev Mol Cell Biol* 13, 251-262. 10.1038/nrm3311.
124. Steinberg, G.R., and Hardie, D.G. (2023). New insights into activation and function of the AMPK. *Nat Rev Mol Cell Biol* 24, 255-272. 10.1038/s41580-022-00547-x.

125. Willows, R., Sanders, M.J., Xiao, B., Patel, B.R., Martin, S.R., Read, J., Wilson, J.R., Hubbard, J., Gamblin, S.J., and Carling, D. (2017). Phosphorylation of AMPK by upstream kinases is required for activity in mammalian cells. *Biochem J* 474, 3059-3073. 10.1042/bcj20170458.
126. Darisipudi, M.N., and Knauf, F. (2016). An update on the role of the inflammasomes in the pathogenesis of kidney diseases. *Pediatr Nephrol* 31, 535-544. 10.1007/s00467-015-3153-z.
127. Funk, J.A., and Schnellmann, R.G. (2012). Persistent disruption of mitochondrial homeostasis after acute kidney injury. *Am J Physiol Renal Physiol* 302, F853-864. 10.1152/ajprenal.00035.2011.
128. Stallons, L.J., Funk, J.A., and Schnellmann, R.G. (2013). Mitochondrial Homeostasis in Acute Organ Failure. *Curr Pathobiol Rep* 1. 10.1007/s40139-013-0023-x.
129. Rolfe, D.F., and Brown, G.C. (1997). Cellular energy utilization and molecular origin of standard metabolic rate in mammals. *Physiol Rev* 77, 731-758. 10.1152/physrev.1997.77.3.731.
130. Quadri, M.M., Fatima, S.S., Che, R.C., and Zhang, A.H. (2019). Mitochondria and Renal Fibrosis. *Adv Exp Med Biol* 1165, 501-524. 10.1007/978-981-13-8871-2_25.
131. Nolfi-Donagan, D., Braganza, A., and Shiva, S. (2020). Mitochondrial electron transport chain: Oxidative phosphorylation, oxidant production, and methods of measurement. *Redox Biol* 37, 101674. 10.1016/j.redox.2020.101674.
132. Martínez-Reyes, I., and Chandel, N.S. (2020). Mitochondrial TCA cycle metabolites control physiology and disease. *Nat Commun* 11, 102. 10.1038/s41467-019-13668-3.
133. Zhao, R.Z., Jiang, S., Zhang, L., and Yu, Z.B. (2019). Mitochondrial electron transport chain, ROS generation and uncoupling (Review). *Int J Mol Med* 44, 3-15. 10.3892/ijmm.2019.4188.
134. Tan, P., Feng, Z., Zhang, L., Hou, T., and Li, Y. (2015). The mechanism of proton translocation in respiratory complex I from molecular dynamics. *J Recept Signal Transduct Res* 35, 170-179. 10.3109/10799893.2014.942464.
135. Bezawork-Geleta, A., Rohlena, J., Dong, L., Pacak, K., and Neuzil, J. (2017). Mitochondrial Complex II: At the Crossroads. *Trends Biochem Sci* 42, 312-325. 10.1016/j.tibs.2017.01.003.

136. Shimada, S., Shinzawa-Itoh, K., Baba, J., Aoe, S., Shimada, A., Yamashita, E., Kang, J., Tateno, M., Yoshikawa, S., and Tsukihara, T. (2017). Complex structure of cytochrome c-cytochrome c oxidase reveals a novel protein-protein interaction mode. *Embo j* 36, 291-300. 10.15252/embj.201695021.
137. Jonckheere, A.I., Smeitink, J.A., and Rodenburg, R.J. (2012). Mitochondrial ATP synthase: architecture, function and pathology. *J Inherit Metab Dis* 35, 211-225. 10.1007/s10545-011-9382-9.
138. Dröse, S., and Brandt, U. (2012). Molecular mechanisms of superoxide production by the mitochondrial respiratory chain. *Adv Exp Med Biol* 748, 145-169. 10.1007/978-1-4614-3573-0_6.
139. Kroemer, G., Galluzzi, L., and Brenner, C. (2007). Mitochondrial membrane permeabilization in cell death. *Physiol Rev* 87, 99-163. 10.1152/physrev.00013.2006.
140. Matsuyama, S., and Reed, J.C. (2000). Mitochondria-dependent apoptosis and cellular pH regulation. *Cell Death Differ* 7, 1155-1165. 10.1038/sj.cdd.4400779.
141. Pernas, L., and Scorrano, L. (2016). Mito-Morphosis: Mitochondrial Fusion, Fission, and Cristae Remodeling as Key Mediators of Cellular Function. *Annu Rev Physiol* 78, 505-531. 10.1146/annurev-physiol-021115-105011.
142. Morigi, M., Perico, L., Rota, C., Longaretti, L., Conti, S., Rottoli, D., Novelli, R., Remuzzi, G., and Benigni, A. (2015). Sirtuin 3-dependent mitochondrial dynamic improvements protect against acute kidney injury. *J Clin Invest* 125, 715-726. 10.1172/jci77632.
143. Benigni, A., Perico, L., and Macconi, D. (2016). Mitochondrial Dynamics Is Linked to Longevity and Protects from End-Organ Injury: The Emerging Role of Sirtuin 3. *Antioxid Redox Signal* 25, 185-199. 10.1089/ars.2016.6682.
144. Tang, C., and Dong, Z. (2016). Mitochondria in Kidney Injury: When the Power Plant Fails. *J Am Soc Nephrol* 27, 1869-1872. 10.1681/asn.2015111277.
145. Linkermann, A., Chen, G., Dong, G., Kunzendorf, U., Krautwald, S., and Dong, Z. (2014). Regulated cell death in AKI. *J Am Soc Nephrol* 25, 2689-2701. 10.1681/asn.2014030262.

146. Suzuki, T., Yamaguchi, H., Kikusato, M., Hashizume, O., Nagatoishi, S., Matsuo, A., Sato, T., Kudo, T., Matsubashi, T., Murayama, K., et al. (2016). Mitochondrial Acid 5 Binds Mitochondria and Ameliorates Renal Tubular and Cardiac Myocyte Damage. *J Am Soc Nephrol* 27, 1925-1932. 10.1681/asn.2015060623.
147. Tsuji, N., Tsuji, T., Ohashi, N., Kato, A., Fujigaki, Y., and Yasuda, H. (2016). Role of Mitochondrial DNA in Septic AKI via Toll-Like Receptor 9. *J Am Soc Nephrol* 27, 2009-2020. 10.1681/asn.2015040376.
148. Reichold, M., Klootwijk, E.D., Reinders, J., Otto, E.A., Milani, M., Broeker, C., Laing, C., Wiesner, J., Devi, S., Zhou, W., et al. (2018). Glycine Amidinotransferase (GATM), Renal Fanconi Syndrome, and Kidney Failure. *J Am Soc Nephrol* 29, 1849-1858. 10.1681/asn.2017111179.
149. Birk, A.V., Liu, S., Soong, Y., Mills, W., Singh, P., Warren, J.D., Seshan, S.V., Pardee, J.D., and Szeto, H.H. (2013). The mitochondrial-targeted compound SS-31 re-energizes ischemic mitochondria by interacting with cardiolipin. *J Am Soc Nephrol* 24, 1250-1261. 10.1681/asn.2012121216.
150. Szeto, H.H., Liu, S., Soong, Y., Wu, D., Darrah, S.F., Cheng, F.Y., Zhao, Z., Ganger, M., Tow, C.Y., and Seshan, S.V. (2011). Mitochondria-targeted peptide accelerates ATP recovery and reduces ischemic kidney injury. *J Am Soc Nephrol* 22, 1041-1052. 10.1681/asn.2010080808.
151. Liu, S., Soong, Y., Seshan, S.V., and Szeto, H.H. (2014). Novel cardiolipin therapeutic protects endothelial mitochondria during renal ischemia and mitigates microvascular rarefaction, inflammation, and fibrosis. *Am J Physiol Renal Physiol* 306, F970-980. 10.1152/ajprenal.00697.2013.
152. Liu, Z.R., Chen, S.Q., Zou, Y.W., Wu, X.Y., Li, H.Y., Wang, X.Q., Shi, Y., and Niu, H.X. (2018). Hypochlorite modified albumins promote cell death in the tubule interstitium in rats via mitochondrial damage in obstructive nephropathy and the protective effects of antioxidant peptides. *Free Radic Res* 52, 616-628. 10.1080/10715762.2018.1457789.
153. Sun, M., Ma, J., Ye, J., Fan, H., Le, J., and Zhu, J. (2021). [Protective effect of mitochondria-targeted antioxidant peptide SS-31 in sepsis-induced acute kidney injury]. *Zhonghua Wei Zhong Bing Ji Jiu Yi Xue* 33, 1418-1422. 10.3760/cma.j.cn121430-20210719-01063.

154. Miyamoto, S., Zhang, G., Hall, D., Oates, P.J., Maity, S., Madesh, M., Han, X., and Sharma, K. (2020). Restoring mitochondrial superoxide levels with elamipretide (MTP-131) protects db/db mice against progression of diabetic kidney disease. *J Biol Chem* 295, 7249-7260. 10.1074/jbc.RA119.011110.
155. Hou, Y., Li, S., Wu, M., Wei, J., Ren, Y., Du, C., Wu, H., Han, C., Duan, H., and Shi, Y. (2016). Mitochondria-targeted peptide SS-31 attenuates renal injury via an antioxidant effect in diabetic nephropathy. *Am J Physiol Renal Physiol* 310, F547-559. 10.1152/ajprenal.00574.2014.
156. Eirin, A., Hedayat, A.F., Ferguson, C.M., Textor, S.C., Lerman, A., and Lerman, L.O. (2018). Mitoprotection preserves the renal vasculature in porcine metabolic syndrome. *Exp Physiol* 103, 1020-1029. 10.1113/ep086988.
157. Szeto, H.H., Liu, S., Soong, Y., Alam, N., Prusky, G.T., and Seshan, S.V. (2016). Protection of mitochondria prevents high-fat diet-induced glomerulopathy and proximal tubular injury. *Kidney Int* 90, 997-1011. 10.1016/j.kint.2016.06.013.
158. Fosgerau, K., and Hoffmann, T. (2015). Peptide therapeutics: current status and future directions. *Drug Discov Today* 20, 122-128. 10.1016/j.drudis.2014.10.003.
159. Tanriover, C., Copur, S., Ucku, D., Cakir, A.B., Hasbal, N.B., Soler, M.J., and Kanbay, M. (2023). The Mitochondrion: A Promising Target for Kidney Disease. *Pharmaceutics* 15. 10.3390/pharmaceutics15020570.
160. Kitada, M., Kume, S., Imaizumi, N., and Koya, D. (2011). Resveratrol improves oxidative stress and protects against diabetic nephropathy through normalization of Mn-SOD dysfunction in AMPK/SIRT1-independent pathway. *Diabetes* 60, 634-643. 10.2337/db10-0386.
161. Wang, H., Guan, Y., Karamercan, M.A., Ye, L., Bhatti, T., Becker, L.B., Baur, J.A., and Sims, C.A. (2015). Resveratrol Rescues Kidney Mitochondrial Function Following Hemorrhagic Shock. *Shock* 44, 173-180. 10.1097/shk.0000000000000390.
162. Sattarinezhad, A., Roozbeh, J., Shirazi Yeganeh, B., Omrani, G.R., and Shams, M. (2019). Resveratrol reduces albuminuria in diabetic nephropathy: A randomized double-blind placebo-controlled clinical trial. *Diabetes Metab* 45, 53-59. 10.1016/j.diabet.2018.05.010.

163. Pan, W., Wang, L., Zhang, X.F., Zhang, H., and Zhang, J. (2019). Hypoxia-induced microRNA-191 contributes to hepatic ischemia/reperfusion injury through the ZONAB/Cyclin D1 axis. *26*, 291-305. 10.1038/s41418-018-0120-9.
164. Bernhardt, A., Krause, A., Reichardt, C., Steffen, H., Isermann, B., Völker, U., Hammer, E., Geffers, R., Phillipsen, L., Dhjamandi, K., et al. (2023). Excessive sodium chloride ingestion promotes inflammation and kidney fibrosis in aging mice. *Am J Physiol Cell Physiol*. 10.1152/ajpcell.00230.2023.
165. Brandt, S., Bernhardt, A., Häberer, S., Wolters, K., Gehringer, F., Reichardt, C., Krause, A., Geffers, R., Kahlfuß, S., Jeron, A., et al. (2024). Comparative Analysis of Acute Kidney Injury Models and Related Fibrogenic Responses: Convergence on Methylation Patterns Regulated by Cold Shock Protein. *Cells* *13*. 10.3390/cells13050367.
166. Lindquist, A.B., Charlotte Reichardt, Eva Sauter, Sabine Brandt, Rajiv Rana, Maja T. Lindenmeyer, Lars Philipsen, Berend Isermann, Cheng Zhu and Peter R. Mertens (2023). Cold Shock Domain Protein DbpA Orchestrates Tubular Cell Damage and Interstitial Fibrosis in Inflammatory Kidney Disease. *Cells*. 10.3390/cells12101426.
167. Bernhardt, A., Fehr, A., Brandt, S., Jerchel, S., Ballhause, T.M., Philipsen, L., Stolze, S., Geffers, R., Weng, H., Fischer, K.D., et al. (2017). Inflammatory cell infiltration and resolution of kidney inflammation is orchestrated by the cold-shock protein Y-box binding protein-1. *Kidney Int* *92*, 1157-1177. 10.1016/j.kint.2017.03.035.
168. Schock-Kusch, D., Sadick, M., Henninger, N., Kraenzlin, B., Claus, G., Kloetzer, H.M., Weiss, C., Pill, J., and Gretz, N. (2009). Transcutaneous measurement of glomerular filtration rate using FITC-sinistrin in rats. *Nephrology, dialysis, transplantation : official publication of the European Dialysis and Transplant Association - European Renal Association* *24*, 2997-3001. 10.1093/ndt/gfp225.
169. Schreiber, A., Shulhevich, Y., Geraci, S., Hesser, J., Stsepankou, D., Neudecker, S., Koenig, S., Heinrich, R., Hoecklin, F., Pill, J., et al. (2012). Transcutaneous measurement of renal function in conscious mice. *Am J Physiol Renal Physiol* *303*, F783-788. 10.1152/ajprenal.00279.2012.
170. Zhao, M., Wang, Y., Li, L., Liu, S., Wang, C., Yuan, Y., Yang, G., Chen, Y., Cheng, J., Lu, Y., and Liu, J. (2021). Mitochondrial ROS promote mitochondrial dysfunction and inflammation in ischemic acute kidney injury by disrupting TFAM-mediated mtDNA maintenance. *Theranostics* *11*, 1845-1863. 10.7150/thno.50905.

171. Brandt, S., Ballhause, T.M., Bernhardt, A., Becker, A., Salaru, D., Le-Deffge, H.M., Fehr, A., Fu, Y., Philipsen, L., Djudjaj, S., et al. (2020). Fibrosis and Immune Cell Infiltration Are Separate Events Regulated by Cell-Specific Receptor Notch3 Expression. *J Am Soc Nephrol* 31, 2589-2608. 10.1681/asn.2019121289.
172. Miller, F.J., Rosenfeldt, F.L., Zhang, C., Linnane, A.W., and Nagley, P. (2003). Precise determination of mitochondrial DNA copy number in human skeletal and cardiac muscle by a PCR-based assay: lack of change of copy number with age. *Nucleic acids research* 31, e61. 10.1093/nar/gng060.
173. Kim, M.J., Hwang, J.W., Yun, C.K., Lee, Y., and Choi, Y.S. (2018). Delivery of exogenous mitochondria via centrifugation enhances cellular metabolic function. *Sci Rep* 8, 3330. 10.1038/s41598-018-21539-y.
174. Clough, E., and Barrett, T. (2016). The Gene Expression Omnibus Database. *Methods Mol Biol* 1418, 93-110. 10.1007/978-1-4939-3578-9_5.
175. Famulski, K.S., de Freitas, D.G., Kreepala, C., Chang, J., Sellares, J., Sis, B., Einecke, G., Mengel, M., Reeve, J., and Halloran, P.F. (2012). Molecular phenotypes of acute kidney injury in kidney transplants. *J Am Soc Nephrol* 23, 948-958. 10.1681/asn.2011090887.
176. Wu, H., Kirita, Y., Donnelly, E.L., and Humphreys, B.D. (2019). Advantages of Single-Nucleus over Single-Cell RNA Sequencing of Adult Kidney: Rare Cell Types and Novel Cell States Revealed in Fibrosis. *J Am Soc Nephrol* 30, 23-32. 10.1681/asn.2018090912.
177. Mukherjee, M., deRiso, J., Otterpohl, K., Ratnayake, I., Kota, D., Ahrenkiel, P., Chandrasekar, I., and Surendran, K. (2019). Endogenous Notch Signaling in Adult Kidneys Maintains Segment-Specific Epithelial Cell Types of the Distal Tubules and Collecting Ducts to Ensure Water Homeostasis. *J Am Soc Nephrol* 30, 110-126. 10.1681/asn.2018040440.
178. Liu, D., Gao, Y., Liu, J., Huang, Y., Yin, J., Feng, Y., Shi, L., Meloni, B.P., Zhang, C., Zheng, M., and Gao, J. (2021). Intercellular mitochondrial transfer as a means of tissue revitalization. *Signal Transduct Target Ther* 6, 65. 10.1038/s41392-020-00440-z.
179. Liu, Y., Fu, T., Li, G., Li, B., Luo, G., Li, N., and Geng, Q. (2023). Mitochondrial transfer between cell crosstalk - An emerging role in mitochondrial quality control. *Ageing Res Rev* 91, 102038. 10.1016/j.arr.2023.102038.

-
180. Soliman, A.M., and Barreda, D.R. (2022). Acute Inflammation in Tissue Healing. *Int J Mol Sci* 24. 10.3390/ijms24010641.
181. Martínez-Klimova, E., Aparicio-Trejo, O.E., Gómez-Sierra, T., Jiménez-Urbe, A.P., Bellido, B., and Pedraza-Chaverri, J. (2020). Mitochondrial dysfunction and endoplasmic reticulum stress in the promotion of fibrosis in obstructive nephropathy induced by unilateral ureteral obstruction. *46*, 716-733. 10.1002/biof.1673.
182. Chiang, C.K., Hsu, S.P., Wu, C.T., Huang, J.W., Cheng, H.T., Chang, Y.W., Hung, K.Y., Wu, K.D., and Liu, S.H. (2011). Endoplasmic reticulum stress implicated in the development of renal fibrosis. *Mol Med* 17, 1295-1305. 10.2119/molmed.2011.00131.
183. Guo, R., Duan, J., Pan, S., Cheng, F., Qiao, Y., Feng, Q., Liu, D., and Liu, Z. (2023). The Road from AKI to CKD: Molecular Mechanisms and Therapeutic Targets of Ferroptosis. *Cell Death Dis* 14, 426. 10.1038/s41419-023-05969-9.
184. Ruan, Y.C., Wang, Y., Da Silva, N., Kim, B., Diao, R.Y., Hill, E., Brown, D., Chan, H.C., and Breton, S. (2014). CFTR interacts with ZO-1 to regulate tight junction assembly and epithelial differentiation through the ZONAB pathway. *J Cell Sci* 127, 4396-4408. 10.1242/jcs.148098.
185. Park, K.M., Kim, J.I., Ahn, Y., Bonventre, A.J., and Bonventre, J.V. (2004). Testosterone is responsible for enhanced susceptibility of males to ischemic renal injury. *J Biol Chem* 279, 52282-52292. 10.1074/jbc.M407629200.
186. Rojas-Morales, P., León-Contreras, J.C., Granados-Pineda, J., Hernández-Pando, R., Gonzaga, G., Sánchez-Lozada, L.G., Osorio-Alonso, H., Pedraza-Chaverri, J., and Tapia, E. (2020). Protection against renal ischemia and reperfusion injury by short-term time-restricted feeding involves the mitochondrial unfolded protein response. *Free Radic Biol Med* 154, 75-83. 10.1016/j.freeradbiomed.2020.04.025.
187. Chiba, T., Peasley, K.D., Cargill, K.R., Maringer, K.V., Bharathi, S.S., Mukherjee, E., Zhang, Y., Holtz, A., Basisty, N., Yagobian, S.D., et al. (2019). Sirtuin 5 Regulates Proximal Tubule Fatty Acid Oxidation to Protect against AKI. *J Am Soc Nephrol* 30, 2384-2398. 10.1681/asn.2019020163.
188. Miguel, V., Tituaña, J., Herrero, J.I., Herrero, L., Serra, D., Cuevas, P., Barbas, C., Puyol, D.R., Márquez-Expósito, L., Ruiz-Ortega, M., et al. (2021). Renal tubule Cpt1a overexpression protects from kidney fibrosis by restoring mitochondrial homeostasis. *J Clin Invest* 131. 10.1172/jci140695.

-
189. Cooke, A., Schwarzl, T., Huppertz, I., Kramer, G., Mantas, P., Alleaume, A.M., Huber, W., Krijgsveld, J., and Hentze, M.W. (2019). The RNA-Binding Protein YBX3 Controls Amino Acid Levels by Regulating SLC mRNA Abundance. *Cell Rep* 27, 3097-3106.e3095. 10.1016/j.celrep.2019.05.039.
190. Awad, S., Skipper, W., Vostrejs, W., Ozorowski, K., Min, K., Pfuhler, L., Mehta, D., and Cooke, A. (2023). The YBX3 RNA-binding protein posttranscriptionally controls SLC1A5 mRNA in proliferating and differentiating skeletal muscle cells. *J Biol Chem* 300, 105602. 10.1016/j.jbc.2023.105602.
191. Ni, L., and Yuan, C. (2021). The Mitochondrial-Associated Endoplasmic Reticulum Membrane and Its Role in Diabetic Nephropathy. *Oxid Med Cell Longev* 2021, 8054817. 10.1155/2021/8054817.
192. Guariento, A., Piekarski, B.L., Doulamis, I.P., Blitzer, D., Ferraro, A.M., Harrild, D.M., Zurakowski, D., Del Nido, P.J., McCully, J.D., and Emani, S.M. (2021). Autologous mitochondrial transplantation for cardiogenic shock in pediatric patients following ischemia-reperfusion injury. *The Journal of thoracic and cardiovascular surgery* 162, 992-1001. 10.1016/j.jtcvs.2020.10.151.
193. Konari, N., Nagaishi, K., Kikuchi, S., and Fujimiya, M. (2019). Mitochondria transfer from mesenchymal stem cells structurally and functionally repairs renal proximal tubular epithelial cells in diabetic nephropathy in vivo. *Scientific reports* 9, 5184. 10.1038/s41598-019-40163-y.
194. Doulamis, I.P., Guariento, A., Duignan, T., Kido, T., Orfany, A., Saeed, M.Y., Weixler, V.H., Blitzer, D., Shin, B., Snay, E.R., et al. (2020). Mitochondrial transplantation by intra-arterial injection for acute kidney injury. *American journal of physiology. Renal physiology* 319, F403-f413. 10.1152/ajprenal.00255.2020.
195. Kubat, G.B., Ozler, M., Ulger, O., Ekinci, O., Atalay, O., Celik, E., Safali, M., and Budak, M.T. (2021). The effects of mesenchymal stem cell mitochondrial transplantation on doxorubicin-mediated nephrotoxicity in rats. *J Biochem Mol Toxicol* 35, e22612. 10.1002/jbt.22612.
196. Tonnus, W., Meyer, C., Steinebach, C., Belavgeni, A., von Mässenhausen, A., Gonzalez, N.Z., Maremonti, F., Gembardt, F., Himmerkus, N., Latk, M., et al. (2021). Dysfunction of the key ferroptosis-surveilling systems hypersensitizes mice to tubular necrosis during acute kidney injury. *Nat Commun* 12, 4402. 10.1038/s41467-021-24712-6.

197. Tao, W., Liu, F., Zhang, J., Fu, S., Zhan, H., and Qian, K. (2021). miR-3587 Inhibitor Attenuates Ferroptosis Following Renal Ischemia-Reperfusion Through HO-1. *Front Mol Biosci* 8, 789927. 10.3389/fmolb.2021.789927.
198. Shi, L., Song, Z., Li, Y., Huang, J., Zhao, F., Luo, Y., Wang, J., Deng, F., Shadekejiang, H., Zhang, M., et al. (2023). MiR-20a-5p alleviates kidney ischemia/reperfusion injury by targeting ACSL4-dependent ferroptosis. *Am J Transplant* 23, 11-25. 10.1016/j.ajt.2022.09.003.
199. Sun, Z., Wu, J., Bi, Q., and Wang, W. (2022). Exosomal lncRNA TUG1 derived from human urine-derived stem cells attenuates renal ischemia/reperfusion injury by interacting with SRSF1 to regulate ASCL4-mediated ferroptosis. *Stem Cell Res Ther* 13, 297. 10.1186/s13287-022-02986-x.
200. Sun, X., Huang, N., Li, P., Dong, X., Yang, J., Zhang, X., Zong, W.X., Gao, S., and Xin, H. (2023). TRIM21 ubiquitylates GPX4 and promotes ferroptosis to aggravate ischemia/reperfusion-induced acute kidney injury. *Life Sci* 321, 121608. 10.1016/j.lfs.2023.121608.
201. Ostermann, M., Bellomo, R., Burdmann, E.A., Doi, K., Endre, Z.H., Goldstein, S.L., Kane-Gill, S.L., Liu, K.D., Prowle, J.R., Shaw, A.D., et al. (2020). Controversies in acute kidney injury: conclusions from a Kidney Disease: Improving Global Outcomes (KDIGO) Conference. *Kidney Int* 98, 294-309. 10.1016/j.kint.2020.04.020.
202. Rovin, B.H., Adler, S.G., Barratt, J., Bridoux, F., Burdige, K.A., Chan, T.M., Cook, H.T., Fervenza, F.C., Gibson, K.L., Glassock, R.J., et al. (2021). Executive summary of the KDIGO 2021 Guideline for the Management of Glomerular Diseases. *Kidney Int* 100, 753-779. 10.1016/j.kint.2021.05.015.
203. National Clinical Guideline, C. (2013). National Institute for Health and Clinical Excellence: Guidance. In *Acute Kidney Injury: Prevention, Detection and Management Up to the Point of Renal Replacement Therapy*, (Royal College of Physicians (UK)
204. Kaucsár, T., Róka, B., Tod, P., Do, P.T., Hegedűs, Z., Szénási, G., and Hamar, P. (2022). Divergent regulation of lncRNA expression by ischemia in adult and aging mice. *Geroscience* 44, 429-445. 10.1007/s11357-021-00460-9.
205. Peng, J., Li, X., Zhang, D., Chen, J.K., Su, Y., Smith, S.B., and Dong, Z. (2015). Hyperglycemia, p53, and mitochondrial pathway of apoptosis are involved in the susceptibility of diabetic models to ischemic acute kidney injury. *Kidney Int* 87, 137-150. 10.1038/ki.2014.226.

206. Polichnowski, A.J., Lan, R., Geng, H., Griffin, K.A., Venkatachalam, M.A., and Bidani, A.K. (2014). Severe renal mass reduction impairs recovery and promotes fibrosis after AKI. *J Am Soc Nephrol* 25, 1496-1507. 10.1681/asn.2013040359.

Declaration of Honor

„I hereby declare that I prepared this thesis without impermissible help of third parties and that none other than the indicated tools have been used; all sources of information are clearly marked, including my own publications.

In particular I have not consciously:

- Fabricated data or rejected undesired results
- Misused statistical methods with the aim of drawing other conclusions than those warranted by the available data
- Plagiarized external data or publications
- Presented the results of other researchers in a distorted way

I am aware that violations of copyright may lead to injunction and damage claims of the author and also to prosecution by the law enforcement authorities.

I hereby agree that the thesis may be reviewed for plagiarism by mean of electronic data processing.

This work has not yet been submitted as a doctoral thesis in the same or a similar form in Germany or in any other country. It has not yet been published as a whole.”

Magdeburg, August 16, 2024

Charlotte Reichardt